

Journal of Advanced Transportation

Integrated Sensing and Communications in Intelligent Internet of Vehicle Systems

Lead Guest Editor: Lingwei Xu

Guest Editors: Li Feng and Thomas Aaron Gulliver





Integrated Sensing and Communications in Intelligent Internet of Vehicle Systems

Journal of Advanced Transportation

**Integrated Sensing and
Communications in Intelligent Internet
of Vehicle Systems**

Lead Guest Editor: Lingwei Xu





Guest Editors: Li Feng and Thomas Aaron Gulliver



Copyright © 2024 Hindawi Limited. All rights reserved.







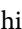


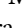
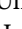











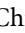
This is a special issue published in "Journal of Advanced Transportation." All articles are open access articles distributed under the Creative Commons Attribution License, which permits unrestricted use, distribution, and reproduction in any medium, provided the original work is properly cited.

Associate Editors

Juan C. Cano , Spain
Steven I. Chien , USA
Antonio Comi , Italy
Zhi-Chun Li, China
Jinjun Tang , China

Academic Editors

Kun An, China
Shriniwas Arkatkar, India
José M. Armingol , Spain
Socrates Basbas , Greece
Francesco Bella , Italy
Abdelaziz Bensrhair, France
Hui Bi, China
María Calderon, Spain
Tiziana Campisi , Italy
Giulio E. Cantarella , Italy
Maria Castro , Spain
Mei Chen , USA
Maria Vittoria Corazza , Italy
Andrea D'Ariano, Italy
Stefano De Luca , Italy
Rocío De Oña , Spain
Luigi Dell'Olio , Spain
Cédric Demonceaux , France
Sunder Lall Dhingra, India
Roberta Di Pace , Italy
Dilum Dissanayake , United Kingdom
Jing Dong , USA
Yuchuan Du , China
Juan-Antonio Escareno, France
Domokos Esztergár-Kiss , Hungary
Saber Fallah , United Kingdom
Gianfranco Fancello , Italy
Zhixiang Fang , China
Francesco Galante , Italy
Yuan Gao , China
Laura Garach, Spain
Indrajit Ghosh , India
Rosa G. González-Ramírez, Chile
Ren-Yong Guo , China

Yanyong Guo , China
Jérôme Ha#rri, France
Hocine Imine, France
Umar Iqbal , Canada
Rui Jiang , China
Peter J. Jin, USA
Sheng Jin , China
Victor L. Knoop , The Netherlands
Eduardo Lalla , The Netherlands
Michela Le Pira , Italy
Jaeyoung Lee , USA
Seungjae Lee, Republic of Korea
Ruimin Li , China
Zhenning Li , China
Christian Liebchen , Germany
Tao Liu, China
Chung-Cheng Lu , Taiwan
Filomena Mauriello , Italy
Luis Miranda-Moreno, Canada
Rakesh Mishra, United Kingdom
Tomio Miwa , Japan
Andrea Monteriù , Italy
Sara Moridpour , Australia
Giuseppe Musolino , Italy
Jose E. Naranjo , Spain
Mehdi Nourinejad , Canada
Eneko Osaba , Spain
Dongjoo Park , Republic of Korea
Luca Pugi , Italy
Alessandro Severino , Italy
Nirajan Shiwakoti , Australia
Michele D. Simoni, Sweden
Ziqi Song , USA
Amanda Stathopoulos , USA
Daxin Tian , China
Alejandro Tirachini, Chile
Long Truong , Australia
Avinash Unnikrishnan , USA
Pascal Vasseur , France
Antonino Vitetta , Italy
S. Travis Waller, Australia
Bohui Wang, China
Jianbin Xin , China



Hongtai Yang , China
Vincent F. Yu , Taiwan
Mustafa Zeybek, Turkey
Jing Zhao, China
Ming Zhong , China
Yajie Zou , China

Contents

Retracted: Research on Urban Traffic Industrial Management under Big Data: Taking Traffic Congestion as an Example

Journal of Advanced Transportation

Retraction (1 page), Article ID 9838979, Volume 2024 (2024)

Retracted: Statistical Characteristics and Security Analysis over Multi-Cascade κ - μ Shadowed Channels

Journal of Advanced Transportation

Retraction (1 page), Article ID 9895680, Volume 2023 (2023)

Retracted: Deep Learning-Based Crack Monitoring for Ultra-High Performance Concrete (UHPC)

Journal of Advanced Transportation

Retraction (1 page), Article ID 9863586, Volume 2023 (2023)

Retracted: Power Allocation Intelligent Optimization for Mobile NOMA Communication System

Journal of Advanced Transportation

Retraction (1 page), Article ID 9842715, Volume 2023 (2023)

Retracted: Research on the Style of Art Works Based on Deep Learning

Journal of Advanced Transportation

Retraction (1 page), Article ID 9824764, Volume 2023 (2023)

Retracted: Integration and Application of Online Sports Resources Based on Multidimensional Intelligent Technology and Resource Optimization Architecture

Journal of Advanced Transportation

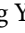
Retraction (1 page), Article ID 9795267, Volume 2023 (2023)

[Retracted] Statistical Characteristics and Security Analysis over Multi-Cascade κ - μ Shadowed Channels

Xiaohong Wang , Ming Ren , Yiwei Fang , Xinji Tian , and Yanyang Zeng 


Research Article (10 pages), Article ID 5342655, Volume 2022 (2022)

[Retracted] Deep Learning-Based Crack Monitoring for Ultra-High Performance Concrete (UHPC)

Dongling Wu, Hongxiang Zhang , and Yiyang Yang


Research Article (10 pages), Article ID 4117957, Volume 2022 (2022)

[Retracted] Research on the Style of Art Works based on Deep Learning

Shulin Liu 


Research Article (8 pages), Article ID 5433623, Volume 2022 (2022)

[Retracted] Research on Urban Traffic Industrial Management under Big Data: Taking Traffic Congestion as an Example

Yi Zhang , Shuwang Yang, and Hang Zhang

Research Article (8 pages), Article ID 1615482, Volume 2022 (2022)

[Retracted] Integration and Application of Online Sports Resources Based on Multidimensional Intelligent Technology and Resource Optimization Architecture

Ting Chu 

Research Article (9 pages), Article ID 2333497, Volume 2022 (2022)

[Retracted] Power Allocation Intelligent Optimization for Mobile NOMA Communication System

Xiaobin Fu , Zhen Tang , and Pingping Xiao 

Research Article (6 pages), Article ID 5838186, Volume 2022 (2022)

Retraction

Retracted: Research on Urban Traffic Industrial Management under Big Data: Taking Traffic Congestion as an Example

Journal of Advanced Transportation

Received 23 January 2024; Accepted 23 January 2024; Published 24 January 2024

Copyright © 2024 Journal of Advanced Transportation. This is an open access article distributed under the Creative Commons Attribution License, which permits unrestricted use, distribution, and reproduction in any medium, provided the original work is properly cited.

This article has been retracted by Hindawi following an investigation undertaken by the publisher [1]. This investigation has uncovered evidence of one or more of the following indicators of systematic manipulation of the publication process:

- (1) Discrepancies in scope
- (2) Discrepancies in the description of the research reported
- (3) Discrepancies between the availability of data and the research described
- (4) Inappropriate citations
- (5) Incoherent, meaningless and/or irrelevant content included in the article
- (6) Manipulated or compromised peer review

The presence of these indicators undermines our confidence in the integrity of the article's content and we cannot, therefore, vouch for its reliability. Please note that this notice is intended solely to alert readers that the content of this article is unreliable. We have not investigated whether authors were aware of or involved in the systematic manipulation of the publication process.

Wiley and Hindawi regrets that the usual quality checks did not identify these issues before publication and have since put additional measures in place to safeguard research integrity.

We wish to credit our own Research Integrity and Research Publishing teams and anonymous and named external researchers and research integrity experts for contributing to this investigation.

The corresponding author, as the representative of all authors, has been given the opportunity to register their agreement or disagreement to this retraction. We have kept a record of any response received.

References

- [1] Y. Zhang, S. Yang, and H. Zhang, "Research on Urban Traffic Industrial Management under Big Data: Taking Traffic Congestion as an Example," *Journal of Advanced Transportation*, vol. 2022, Article ID 1615482, 8 pages, 2022.

Retraction

Retracted: Statistical Characteristics and Security Analysis over Multi-Cascade κ - μ Shadowed Channels

Journal of Advanced Transportation

Received 19 December 2023; Accepted 19 December 2023; Published 20 December 2023

Copyright © 2023 Journal of Advanced Transportation. This is an open access article distributed under the Creative Commons Attribution License, which permits unrestricted use, distribution, and reproduction in any medium, provided the original work is properly cited.

This article has been retracted by Hindawi following an investigation undertaken by the publisher [1]. This investigation has uncovered evidence of one or more of the following indicators of systematic manipulation of the publication process:

- (1) Discrepancies in scope
- (2) Discrepancies in the description of the research reported
- (3) Discrepancies between the availability of data and the research described
- (4) Inappropriate citations
- (5) Incoherent, meaningless and/or irrelevant content included in the article
- (6) Manipulated or compromised peer review

The presence of these indicators undermines our confidence in the integrity of the article's content and we cannot, therefore, vouch for its reliability. Please note that this notice is intended solely to alert readers that the content of this article is unreliable. We have not investigated whether authors were aware of or involved in the systematic manipulation of the publication process.

Wiley and Hindawi regrets that the usual quality checks did not identify these issues before publication and have since put additional measures in place to safeguard research integrity.

We wish to credit our own Research Integrity and Research Publishing teams and anonymous and named external researchers and research integrity experts for contributing to this investigation.

The corresponding author, as the representative of all authors, has been given the opportunity to register their agreement or disagreement to this retraction. We have kept a record of any response received.

References

- [1] X. Wang, M. Ren, Y. Fang, X. Tian, and Y. Zeng, "Statistical Characteristics and Security Analysis over Multi-Cascade κ - μ Shadowed Channels," *Journal of Advanced Transportation*, vol. 2022, Article ID 5342655, 10 pages, 2022.

Retraction

Retracted: Deep Learning-Based Crack Monitoring for Ultra-High Performance Concrete (UHPC)

Journal of Advanced Transportation

Received 8 August 2023; Accepted 8 August 2023; Published 9 August 2023

Copyright © 2023 Journal of Advanced Transportation. This is an open access article distributed under the Creative Commons Attribution License, which permits unrestricted use, distribution, and reproduction in any medium, provided the original work is properly cited.

This article has been retracted by Hindawi following an investigation undertaken by the publisher [1]. This investigation has uncovered evidence of one or more of the following indicators of systematic manipulation of the publication process:

- (1) Discrepancies in scope
- (2) Discrepancies in the description of the research reported
- (3) Discrepancies between the availability of data and the research described
- (4) Inappropriate citations
- (5) Incoherent, meaningless and/or irrelevant content included in the article
- (6) Peer-review manipulation

The presence of these indicators undermines our confidence in the integrity of the article's content and we cannot, therefore, vouch for its reliability. Please note that this notice is intended solely to alert readers that the content of this article is unreliable. We have not investigated whether authors were aware of or involved in the systematic manipulation of the publication process.

Wiley and Hindawi regrets that the usual quality checks did not identify these issues before publication and have since put additional measures in place to safeguard research integrity.

We wish to credit our own Research Integrity and Research Publishing teams and anonymous and named external researchers and research integrity experts for contributing to this investigation.

The corresponding author, as the representative of all authors, has been given the opportunity to register their agreement or disagreement to this retraction. We have kept a record of any response received.

References

- [1] D. Wu, H. Zhang, and Y. Yang, "Deep Learning-Based Crack Monitoring for Ultra-High Performance Concrete (UHPC)," *Journal of Advanced Transportation*, vol. 2022, Article ID 4117957, 10 pages, 2022.

Retraction

Retracted: Power Allocation Intelligent Optimization for Mobile NOMA Communication System

Journal of Advanced Transportation

Received 8 August 2023; Accepted 8 August 2023; Published 9 August 2023

Copyright © 2023 Journal of Advanced Transportation. This is an open access article distributed under the Creative Commons Attribution License, which permits unrestricted use, distribution, and reproduction in any medium, provided the original work is properly cited.

This article has been retracted by Hindawi following an investigation undertaken by the publisher [1]. This investigation has uncovered evidence of one or more of the following indicators of systematic manipulation of the publication process:

- (1) Discrepancies in scope
- (2) Discrepancies in the description of the research reported
- (3) Discrepancies between the availability of data and the research described
- (4) Inappropriate citations
- (5) Incoherent, meaningless and/or irrelevant content included in the article
- (6) Peer-review manipulation

The presence of these indicators undermines our confidence in the integrity of the article's content and we cannot, therefore, vouch for its reliability. Please note that this notice is intended solely to alert readers that the content of this article is unreliable. We have not investigated whether authors were aware of or involved in the systematic manipulation of the publication process.

Wiley and Hindawi regrets that the usual quality checks did not identify these issues before publication and have since put additional measures in place to safeguard research integrity.

We wish to credit our own Research Integrity and Research Publishing teams and anonymous and named external researchers and research integrity experts for contributing to this investigation.

The corresponding author, as the representative of all authors, has been given the opportunity to register their agreement or disagreement to this retraction. We have kept a record of any response received.

References

- [1] X. Fu, Z. Tang, and P. Xiao, "Power Allocation Intelligent Optimization for Mobile NOMA Communication System," *Journal of Advanced Transportation*, vol. 2022, Article ID 5838186, 6 pages, 2022.

Retraction

Retracted: Research on the Style of Art Works Based on Deep Learning

Journal of Advanced Transportation

Received 8 August 2023; Accepted 8 August 2023; Published 9 August 2023

Copyright © 2023 Journal of Advanced Transportation. This is an open access article distributed under the Creative Commons Attribution License, which permits unrestricted use, distribution, and reproduction in any medium, provided the original work is properly cited.

This article has been retracted by Hindawi following an investigation undertaken by the publisher [1]. This investigation has uncovered evidence of one or more of the following indicators of systematic manipulation of the publication process:

- (1) Discrepancies in scope
- (2) Discrepancies in the description of the research reported
- (3) Discrepancies between the availability of data and the research described
- (4) Inappropriate citations
- (5) Incoherent, meaningless and/or irrelevant content included in the article
- (6) Peer-review manipulation

The presence of these indicators undermines our confidence in the integrity of the article's content and we cannot, therefore, vouch for its reliability. Please note that this notice is intended solely to alert readers that the content of this article is unreliable. We have not investigated whether authors were aware of or involved in the systematic manipulation of the publication process.

Wiley and Hindawi regrets that the usual quality checks did not identify these issues before publication and have since put additional measures in place to safeguard research integrity.

We wish to credit our own Research Integrity and Research Publishing teams and anonymous and named external researchers and research integrity experts for contributing to this investigation.

The corresponding author, as the representative of all authors, has been given the opportunity to register their agreement or disagreement to this retraction. We have kept a record of any response received.

References

- [1] S. Liu, "Research on the Style of Art Works Based on Deep Learning," *Journal of Advanced Transportation*, vol. 2022, Article ID 5433623, 8 pages, 2022.

Retraction

Retracted: Integration and Application of Online Sports Resources Based on Multidimensional Intelligent Technology and Resource Optimization Architecture

Journal of Advanced Transportation

Received 8 August 2023; Accepted 8 August 2023; Published 9 August 2023

Copyright © 2023 Journal of Advanced Transportation. This is an open access article distributed under the Creative Commons Attribution License, which permits unrestricted use, distribution, and reproduction in any medium, provided the original work is properly cited.

This article has been retracted by Hindawi following an investigation undertaken by the publisher [1]. This investigation has uncovered evidence of one or more of the following indicators of systematic manipulation of the publication process:

- (1) Discrepancies in scope
- (2) Discrepancies in the description of the research reported
- (3) Discrepancies between the availability of data and the research described
- (4) Inappropriate citations
- (5) Incoherent, meaningless and/or irrelevant content included in the article
- (6) Peer-review manipulation

The presence of these indicators undermines our confidence in the integrity of the article's content and we cannot, therefore, vouch for its reliability. Please note that this notice is intended solely to alert readers that the content of this article is unreliable. We have not investigated whether authors were aware of or involved in the systematic manipulation of the publication process.

Wiley and Hindawi regrets that the usual quality checks did not identify these issues before publication and have since put additional measures in place to safeguard research integrity.

We wish to credit our own Research Integrity and Research Publishing teams and anonymous and named external researchers and research integrity experts for contributing to this investigation.

The corresponding author, as the representative of all authors, has been given the opportunity to register their agreement or disagreement to this retraction. We have kept a record of any response received.

References

- [1] T. Chu, "Integration and Application of Online Sports Resources Based on Multidimensional Intelligent Technology and Resource Optimization Architecture," *Journal of Advanced Transportation*, vol. 2022, Article ID 2333497, 9 pages, 2022.

Retraction

Retracted: Statistical Characteristics and Security Analysis over Multi-Cascade κ - μ Shadowed Channels

Journal of Advanced Transportation

Received 19 December 2023; Accepted 19 December 2023; Published 20 December 2023

Copyright © 2023 Journal of Advanced Transportation. This is an open access article distributed under the Creative Commons Attribution License, which permits unrestricted use, distribution, and reproduction in any medium, provided the original work is properly cited.

This article has been retracted by Hindawi following an investigation undertaken by the publisher [1]. This investigation has uncovered evidence of one or more of the following indicators of systematic manipulation of the publication process:

- (1) Discrepancies in scope
- (2) Discrepancies in the description of the research reported
- (3) Discrepancies between the availability of data and the research described
- (4) Inappropriate citations
- (5) Incoherent, meaningless and/or irrelevant content included in the article
- (6) Manipulated or compromised peer review

The presence of these indicators undermines our confidence in the integrity of the article's content and we cannot, therefore, vouch for its reliability. Please note that this notice is intended solely to alert readers that the content of this article is unreliable. We have not investigated whether authors were aware of or involved in the systematic manipulation of the publication process.

Wiley and Hindawi regrets that the usual quality checks did not identify these issues before publication and have since put additional measures in place to safeguard research integrity.

We wish to credit our own Research Integrity and Research Publishing teams and anonymous and named external researchers and research integrity experts for contributing to this investigation.

The corresponding author, as the representative of all authors, has been given the opportunity to register their agreement or disagreement to this retraction. We have kept a record of any response received.

References

- [1] X. Wang, M. Ren, Y. Fang, X. Tian, and Y. Zeng, "Statistical Characteristics and Security Analysis over Multi-Cascade κ - μ Shadowed Channels," *Journal of Advanced Transportation*, vol. 2022, Article ID 5342655, 10 pages, 2022.

Research Article

Statistical Characteristics and Security Analysis over Multi-Cascade κ - μ Shadowed Channels

Xiaohong Wang ¹, Ming Ren ², Yiwei Fang ³, Xinji Tian ¹ and Yanyang Zeng ⁴

¹The College of Physics and Electronic Information Engineering, Henan Polytechnic University, Jiaozuo 454003, China

²The Department of Mathematics and Physics Education, Luoyang Institute of Science and Technology, Luoyang 471023, China

³The Wuhan Maritime Communication Research Institute, Wuhan 430079, China

⁴The College of Computer Science and Technology, Henan Polytechnic University, Jiaozuo 454003, China

Correspondence should be addressed to Ming Ren; renming926@163.com

Received 24 March 2022; Revised 10 May 2022; Accepted 16 May 2022; Published 20 June 2022

Academic Editor: Li Feng

Copyright © 2022 Xiaohong Wang et al. This is an open access article distributed under the Creative Commons Attribution License, which permits unrestricted use, distribution, and reproduction in any medium, provided the original work is properly cited.

In this paper, the statistical characteristics of the multi-cascade κ - μ shadowed fading channels are investigated and analyzed under the classic Wyner's eavesdropping model. In particular, the general accurate expressions of the probability density function and the cumulative distribution function for amplitude and signal-to-noise ratio (SNR) are derived for the first time. Moreover, we further utilize the two performance evaluation metrics including outage probability and intercept probability to investigate the impacts of cascade number and channel parameters on reliability and security. Finally, the theoretical results are consistent with the simulations, proving the correctness of the derivation. The interesting conclusion is that when the average SNR is greater than 2 dB, the reliability of the multi-cascade model will decrease as the number of cascade increases; on the contrary, more cascading can lead to stronger anti-eavesdropping ability.

1. Introduction

With the wide application of wireless networks, people have higher demands on the transmission performance and security of the communication system. Secure and reliable wireless communication systems have become an important support for providing reliable services, transmitting confidential information, ensuring social stability, and maintaining national security. Different from traditional encryption and decryption algorithms, physical layer security (PLS) utilizes its fading properties to improve the system's anti-eavesdropping ability by increasing the security capacity. Many scholars are committed to the security performance analysis of communication networks and have obtained some research results [1–8]. Wyner et al. in [1] proposed the security matter of the physical layer. The most crucial feature of physical security was to use the characteristics of its own channel to evaluate and improve the anti-eavesdropping capabilities of the system [2]. The authors in

[3] utilized the collaborative automatic repeat request technology to improve the security performance. Cao et al. in [4] studied the PLS of the collaborative non-orthogonal multiple access (NOMA) system. The authors in [5] evaluated the confidentiality of cognitive radio networks. Song et al. in [6] investigated the optimal confidentiality capabilities of two different schemes of amplified forwarding and coordinated interference based on cooperative communication. The basic metrics on physical layer performance over fading distributions were defined and researched in [7, 8], such as the strictly positive secrecy capacity (SPSC), the security outage probability (SOP), and the average secrecy capacity (ASC).

In practical wireless communication systems, wireless fading channels are susceptible to noise, interference, and other channel factors, which can lead to serious challenges for reliable communication. Therefore, research on fading channels is of great practical significance. The statistical characteristics of the channel are crucial to the analysis of

system performance [9]. In recent years, with the emergence of complex communication environments, many fading channels have been explored by scholars [10–18]. When there is no line-of-sight component in the transmitted signal, the fading channel can be modeled as Rayleigh distribution [10]. Mason et al. in [11] put forward the Rician fading, which is also called Nakagami- n distribution. The Nakagami- m fading was first studied in [12], and its statistical properties were investigated in [13]. The η - μ fading can characterize small-scale changes of fading signals [14], and the accurate expression of the level crossing rate was investigated. Michel et al. in [15] proposed the α - μ distribution and deduced the principal characteristic function of the channels. The authors in [16] applied α - μ fading to the NOMA system and analyzed the effect of residual transceiver hardware impairments on the communication networks. The κ - μ fading considers the propagation of signal in a non-uniform scene, and the authors in [17] gave the characteristics of κ - μ fading distribution and important attributes. Imperfect Weibull channels and their applications were researched in [18].

The above-mentioned channels are all single-fading channels, but in practice, many scenarios are more complex and need to be simulated by complicated models. For example, since the mobile-to-mobile communication model experienced more severe channel fading, the cascaded Nakagami- m distribution model was used to simulate this scenario [19]. The cascaded fading channel can also be applied to satellite communications systems [20], ultra-high frequency identification systems [21], multiple-input multiple-output correspondence [22], and vehicle-to-vehicle communication networks [23]. Therefore, more and more research on n -level cascaded fading channels has been conducted in recent years [24–26]. The precise expressions of the probability density function (PDF) and cumulative distribution function (CDF) for the SNR of the $N *$ Nakagami random variables were first investigated in [24]. The cascaded Weibull distribution was composed of multiple random variables, and its statistical properties were derived in [25]. Tashman et al. in [26] studied the expressions of PDF and CDF of the receivers' SNR of the multi-cascade κ - μ distribution and deduced security performance of the channels when there are multiple eavesdroppers.

The κ - μ fading is a general composite distribution, which can be simplified to Rician, Nakagami- m , and Rayleigh models by changing the parameters [17] where as the channel assumes that the components in each cluster are deterministic. For the limitation of κ - μ distribution, the κ - μ shadowed distribution was first investigated in [27], which is the physical extension of the κ - μ fading. The channel can simulate that the deterministic components of all clusters fluctuate stochastically. Also, the accurate expressions of PDF and CDF of SNR over the κ - μ shadowed distribution have been obtained, which makes it easier to carry out mathematical operations and analyses. The security of κ - μ shadowed fading was analyzed in [28], and the precise expressions of SPSC and the lower limit of SOP were investigated. The authors in [29] gave the capacity analysis of the multiple-input multiple-output communication system over

κ - μ shadowed distribution. The security performance of downlink NOMA networks over κ - μ shadowed fading was researched in [30]. Bhatnagar in [31] studied the statistical properties of correlated squared κ - μ shadowed fading by deriving theoretical expressions for PDF and moment-generating function. In [32], the outage probability (OP) of amplify-and-forward relay communication system over κ - μ shadowed distribution and the expression of ASC were studied; moreover, the effect of beamforming and shaping arguments on system property was analyzed. Sun et al. in [33] deduced the new expression of SOP for single-input multi-output system based on the κ - μ shadowed random variables. In [34], the authors investigated the effective rate of communication networks under κ - μ shadowed random variables. The authors in [35] deduced the theoretical formulas of the channel capacity over κ - μ shadowed fading and investigated the performance of the spectrum aggregation system based on composite fading channels.

References [1–8] describe the research on wireless communication network security by scholars, references [9–18] mainly list the investigation status of several common fading channels, references [19–26] aim to present the cascaded wireless related investigations and applications of fading channels, and references [19–34] specifically introduce the characteristics and research status of the κ - μ shadowed random variables. Combining the above analysis, to the authors' knowledge, no relevant literature exploring multi-cascaded κ - μ shadowed distribution has appeared in the current database. Therefore, we carried out this work. Furthermore, the outstanding contributions of the paper are summarized as follows:

- (1) Through the statistical analysis, the accurate expression of PDF and CDF of SNR over a multi-cascaded model is deduced mainly by deriving the unified closed expression of PDF and CDF of the amplitude of n -level κ - μ shadowed distribution.
- (2) Based on the derived expressions of PDF and CDF of SNR, the theoretical analytic equations of OP and intercept probability (IP) are derived, and the security performance of the system is analyzed. Finally, the theoretical results and Monte Carlo simulations are used for comparison and verification. Moreover, the impacts of its parameters on the systems' performance are discussed.

The content of the paper is arranged as follows. Section 2 depicts the system model and statistical features. Section 3 derives the universal formulas for PDF and CDF of amplitude and SNR under the multi-cascade κ - μ shadowed distribution. The theoretical expressions of OP and IP are presented in Section 4. The influences of each parameter are provided in Section 5. The conclusions of this paper are given in Section 6.

2. System Model and Channel Characteristics

2.1. System Model. In Figure 1, the paper considers Wyner's eavesdropping model under multi-cascade κ - μ shadowed fading. The model mainly includes an emission source (S), a

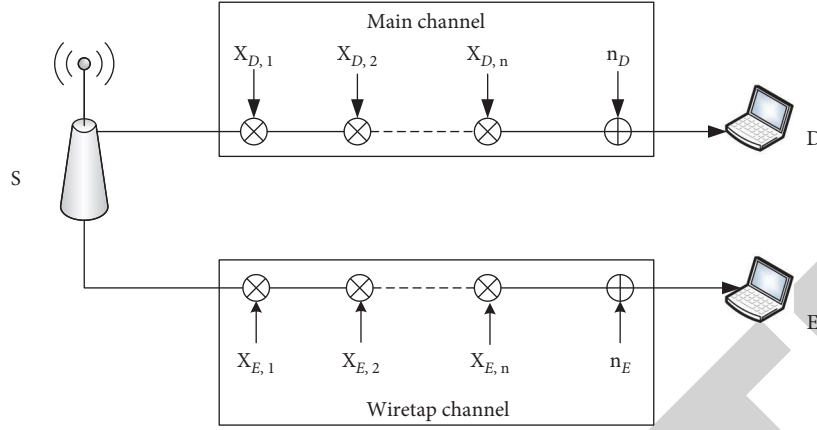


FIGURE 1: The system model.

legitimate user (D), and an illegal user (E). We suppose that confidential information is transmitted through the main channel (S to D), but the eavesdropper will intercept the information through the eavesdropping channel (S to E). The fading of both the main (S to D) and wiretap (S to E) channels experiences multi-cascade κ - μ shadowed distribution, where $X_{D,i}$ and $X_{E,i}$, $i \in \{1, n\}$ represent the i -th cascade channel gain of the main channel and the eavesdropping channel, respectively.

The signal received by the receiving terminals (D or E) can be expressed as

$$y_w = h_w x + n_w \quad w \in \{D, E\}, \quad (1)$$

where x denotes the transmitting signal and n_w represents the additive white Gaussian noise (AWGN) with an average value of zero and fixed variance σ_n^2 . In addition, h_w represents multi-cascade κ - μ shadowed distributions between S and w , which can be expressed as

$$h_w = \prod_{i=1}^n h_{w,i}, \quad (2)$$

where $h_w = \prod_{i=1}^n h_{w,i}$ is the product of amplitudes representing κ - μ shadowed fading with the independent non-identical distribution.

2.2. Statistical Features. We presume that both the main and eavesdropper channels are submissive to i.n.i.d. over κ - μ shadowed random variables, and the PDF of the SNR over the channel was presented as [27]

$$f_\gamma(\gamma) = \frac{m^m (1 + \kappa)^\mu \mu^\mu}{\Gamma(\mu)(m + \kappa\mu)^m \bar{\gamma}} \left(\frac{\gamma}{\bar{\gamma}}\right)^{\mu-1} e^{-\gamma(1+\kappa)\mu/\bar{\gamma}} \times {}_1F_1\left(m; \mu; \frac{\mu^2 \kappa (1 + \kappa) \gamma}{\bar{\gamma}(m + \kappa\mu)}\right), \quad (3)$$

where $\kappa = d^2/2\sigma^2\mu$, d^2 indicates total power of primary ingredients, $2\sigma^2\mu$ represents the general power of scattered waves, $\kappa > 0$ represents the ratio of aggregate power of the primary ingredients to the overall power of the dispersive

waves, and $\mu > 0$ is an attenuation parameter whose value is correlative to the quantity N of cluster groups in the received signal. M is the shaping parameter of Nakagami- m distribution. Besides, $\bar{\gamma} = E[\cdot]$ and $E[\cdot]$ represent the average SNR and the expectation operator, respectively. $\Gamma(\cdot)$ is defined in [36, eq. (8.310.1)] and ${}_1F_1(\cdot)$ is contained in [36, eq. (9.210.1)].

The PDF of the amplitude for single κ - μ shadowed random variable was deduced as [37]

$$f_x(x) = \frac{2m^m (1 + \kappa)^\mu \mu^\mu}{\Gamma(\mu)(m + \kappa\mu)^m} \frac{x^{2\mu-1}}{\Omega^\mu} e^{-x^2(1+\kappa)\mu/\Omega} \times {}_1F_1\left(m; \mu; \frac{\mu^2 \kappa (1 + \kappa) x^2}{\Omega(m + \kappa\mu)}\right), \quad (4)$$

where $\Omega = E[R^2]$ represents the mean power and $E[R^2] = 2\mu\sigma^2 + d^2$ is the average signal power.

3. System Model and Channel Characteristics

This section mainly deduces the theoretical expressions of the PDF and CDF for amplitude and SNR over multi-cascade κ - μ shadowed fading.

3.1. Analysis of Channel Amplitude Characteristics. The amplitude of κ - μ shadowed fading with cascade degree n is expressed as

$$Y_n = \prod_{i=1}^n X_i, \quad (5)$$

where $Y_n = \prod_{i=1}^n X_i$ is the transformation of (2). Since the derivation process of the main and the eavesdropping channels is similar, only the main channel is considered in the analysis. Also, we denote the product of the magnitude of the cascade by $\{X_i\}_{i=1}^n$.

We first consider the condition of the two-level cascade. Let $Y_2 = X_1 X_2$; these two random variables are considered the product of the PDF of X_1 and X_2 of κ - μ shadowed fading. Employing substitution of random variables, the PDF of Y_2 is represented by the following equation:

$$f_{Y_2}(y) = \int_{-\infty}^{\infty} \frac{1}{|t|} f_{X_1}\left(\frac{y}{t}\right) f_{X_2}(t) dt. \quad (6)$$

Substituting (4) into (6),(6) can be rewritten as

$$f_{Y_2}(y) = \Phi_1 y^{2\mu_1-1} \int_0^{\infty} t^{-2\mu_1+2\mu_2-1} \times \exp\left(-\frac{(y/t)^2(1+\kappa_1)\mu_1}{\Omega_1}\right) \times \exp\left(-\frac{(t)^2(1+\kappa_2)\mu_2}{\Omega_2}\right) \\ \times {}_1F_1\left(m_1; \mu_1; \frac{\mu_1^2 \kappa_1 (1+\kappa_1)(y/t)^2}{\Omega_1(m_1+\kappa_1\mu_1)}\right) \times {}_1F_1\left(m_2; \mu_2; \frac{\mu_2^2 \kappa_2 (1+\kappa_2)(t)^2}{\Omega_2(m_2+\kappa_2\mu_2)}\right) dt, \quad (7)$$

where Φ_1 is given as

$$\Phi_1 = \frac{2m_1^{m_1}(1+\kappa_1)^{\mu_1}\mu_1^{\mu_1}}{\Gamma(\mu_1)(m_1+\kappa_1\mu_1)^{m_1}} \frac{1}{\Omega_1^{\mu_1}} \times \frac{2m_2^{m_2}(1+\kappa_2)^{\mu_2}\mu_2^{\mu_2}}{\Gamma(\mu_2)(m_2+\kappa_2\mu_2)^{m_2}} \frac{1}{\Omega_2^{\mu_2}}. \quad (8)$$

After some mathematical operations, (7) can be re-written as

$$f_{Y_2}(y) = \sum_{g_1=0}^{\infty} \sum_{g_2=0}^{\infty} \frac{\Phi_1 \Phi_2}{2} y^{2\mu_1+2g_1-1} \times \left[\frac{(1+\kappa_2)\mu_2}{\Omega_2}\right]^{\mu_1-\mu_2+g_1-g_2} \\ \times G_{2,0}^{0,2} \left[\frac{\Omega_1 \Omega_2}{(1+\kappa_1)\mu_1(1+\kappa_2)\mu_2 y^2} \middle| \begin{matrix} 1, 1+\mu_1-\mu_2+g_1-g_2 \\ - \end{matrix} \right], \quad (9)$$

where

$$\Phi_x = 2 \prod_{i=1}^n \frac{m_i^{m_i}(1+\kappa_i)^{\mu_i}\mu_i^{\mu_i}}{\Gamma(\mu_i)(m_i+\kappa_i\mu_i)^{m_i}} \left(\frac{1}{\Omega_i}\right)^{\mu_1+g_1} \times \prod_{i=1}^n [(1+\kappa_i)\mu_i]^{\mu_1-\mu_i+g_1-g_i} \\ \times \prod_{i=1}^n \frac{(m_i)_{g_i}}{(\mu_i)_{g_i} g_i!} \left[\frac{\mu_i^2 \kappa_i (1+\kappa_i)}{(m_i+\kappa_i\mu_i)}\right]^{g_i}. \quad (12)$$

After some operations, the CDF of amplitude can be obtained as

$$F_{Y_n}(y) = \sum_{g_1=0}^{\infty} \sum_{g_2=0}^{\infty} \dots \sum_{g_n=0}^{\infty} \Phi_x \int_0^y x^{2\mu_1+2g_1-1} \times G_{n,0}^{0,n} \left[\frac{\prod_{i=1}^n \Omega_i}{x^2 \prod_{i=1}^n (1+\kappa_i)\mu_i} \middle| \begin{matrix} \Psi \\ - \end{matrix} \right] dx. \quad (13)$$

According to [38], we have

$$\int_0^y x^{\alpha-1} G_{u,v}^{s,t} \left[\omega x \middle| \begin{matrix} (a_u) \\ (b_v) \end{matrix} \right] dx = y^{\alpha} G_{u+1,v+1}^{s,t+1} \left[\omega y \middle| \begin{matrix} a_1, \dots, a_t, 1-\alpha, a_t, \dots, a_u \\ b_1, \dots, b_s, -\alpha, b_{s+1}, \dots, b_v \end{matrix} \right], \quad (14)$$

Through mathematical induction, the PDF of multi-cascade κ - μ shadowed distribution can be written as

$$f_{Y_n}(y) = \sum_{g_1=0}^{\infty} \sum_{g_2=0}^{\infty} \dots \sum_{g_n=0}^{\infty} \Phi_x y^{2\mu_1+2g_1-1} \\ \times G_{n,0}^{0,n} \left[\frac{\prod_{i=1}^n \Omega_i}{y^2 \prod_{i=1}^n (1+\kappa_i)\mu_i} \middle| \begin{matrix} \Psi \\ - \end{matrix} \right], \quad (11)$$

where $\psi = 1, 1+\mu_1-\mu_2+g_1-g_2, \dots, 1+\mu_1-\mu_n+g_1-g_n$ and

and using (A.5) and (14), formula (13) can be converted to

$$F_{Y_n}(y) = \sum_{g_1=0}^{\infty} \sum_{g_2=0}^{\infty} \cdots \sum_{g_n=0}^{\infty} \frac{\Phi_x}{2} y^{2(\mu_1+g_1)} \times G_{1,n+1}^{n,1} \left[\frac{\prod_{i=1}^n (1+\kappa_i)\mu_i}{\prod_{i=1}^n \Omega_i} y^2 \middle| \begin{matrix} 1-\mu_1-g_1 \\ \zeta \end{matrix} \right], \quad (15)$$

where.

$$\zeta = 0, -\mu_1 + \mu_2 - g_1 + g_2, \dots, -\mu_1 + \mu_n - g_1 + g_n, -\mu_1 - g_1.$$

Proof. See Appendix. \square

3.2. Characteristics Analysis of SNR. This section will give the PDF and CDF of the SNR. We utilize the variate γ to represent the SNR at the import of the receiving terminal. The received average SNR ($\bar{\gamma}$) is expressed as

$$\bar{\gamma} = E[Y_n^2] \frac{P}{N_0}, \quad (16)$$

where Y_n is the product vector of the multi-cascade κ - μ shadowed fading, N_0 is the power spectral density of AWGN, and P is the transmitted power. Using (5) and (16), we can obtain

$$\bar{\gamma} = \frac{P}{N_0} \prod_{i=0}^n E[X_i^2]. \quad (17)$$

According to [10, eq. (2.3)], the PDF of the SNR at receiver terminal can be written as

$$f_{\gamma}(y) = \frac{f_{Y_n}(\sqrt{\prod_{i=0}^n \Omega_i \gamma / \bar{\gamma}})}{2\sqrt{\gamma \bar{\gamma}} / \prod_{i=0}^n \Omega_i}. \quad (18)$$

Substituting (11) into (18),

$$f_{\gamma}(y) = \sum_{g_1=0}^{\infty} \sum_{g_2=0}^{\infty} \cdots \sum_{g_n=0}^{\infty} \frac{\Lambda_x}{2} \left(\frac{1}{\bar{\gamma}}\right)^{\mu_1+g_1} \times G_{n,0}^{0,n} \left[\frac{\bar{\gamma}}{\gamma \prod_{i=1}^n (1+\kappa_i)\mu_i} \middle| \begin{matrix} \Psi \\ - \end{matrix} \right] \gamma^{\mu_1+g_1-1}. \quad (19)$$

By using (A.5) and (14), the CDF of SNR can be gained as

$$F_{\gamma}(y) = \sum_{g_1=0}^{\infty} \sum_{g_2=0}^{\infty} \cdots \sum_{g_n=0}^{\infty} \frac{\Lambda_x}{2} \left(\frac{y}{\bar{\gamma}}\right)^{\mu_1+g_1} \times G_{1,n+1}^{n,1} \left[\frac{\prod_{i=1}^n (1+\kappa_i)\mu_i}{\bar{\gamma}} y \middle| \begin{matrix} 1-\mu_1-g_1 \\ \zeta \end{matrix} \right], \quad (20)$$

where

$$\Lambda_x = 2 \prod_{i=1}^n \frac{m_i^{m_i} (1+\kappa_i)^{\mu_i} \mu_i^{\mu_i}}{\Gamma(\mu_i) (m_i + \kappa_i \mu_i)^{m_i}} \times \prod_{i=1}^n [(1+\kappa_i)\mu_i]^{\mu_1-\mu_i+g_1-g_i} \times \prod_{i=1}^n \frac{(m_i)_{g_i}}{(\mu_i)_{g_i} g_i!} \left[\frac{\mu_i^2 \kappa_i (1+\kappa_i)}{(m_i + \kappa_i \mu_i)} \right]^{g_i}. \quad (21)$$

The meanings of the parameters in formulas (20) and (21) mentioned above are as follows. m_i , μ_i , and κ_i are all parameters of the κ - μ shadowed distribution. m_i are the shaping parameters of Nakagami- m random variables, μ_i are non-negative natural numbers, representing the number of clusters, and κ_i are non-negative real numbers, expressing the ratio of overall power of the primary ingredients to aggregate power of the dispersive waves. In addition, g_i means loop variables, n represents the number of cascade, and $G_{p,q}^{m,n}[\cdot]$ is Meijer's G function [39].

4. Analysis of OP and IP

In this section, we mainly research the accurate expressions of OP and IP based on the above channel model and statistical properties of multi-cascade κ - μ shadowed fading.

4.1. Outage Probability. OP is the probability that the instantaneous SNR of the system output is lower than a fixed threshold; the threshold is γ_{th} ; then, the expression of OP is

$$P_{out} = P_{\gamma}(\gamma \leq \gamma_{th}) = F_{\gamma}(\gamma_{th}). \quad (22)$$

Substituting (20) into (22),

$$P_{out} = \sum_{g_1=0}^{\infty} \sum_{g_2=0}^{\infty} \cdots \sum_{g_n=0}^{\infty} \frac{\Lambda_x}{2} \left(\frac{\gamma_{th}}{\bar{\gamma}}\right)^{\mu_1+g_1} \times G_{1,n+1}^{n,1} \left[\frac{\prod_{i=1}^n (1+\kappa_i)\mu_i}{\bar{\gamma}} \gamma_{th} \middle| \begin{matrix} 1-\mu_1-g_1 \\ \zeta \end{matrix} \right]. \quad (23)$$

4.2. Intercept Probability. IP is expressed as the probability that the eavesdropping channel capacity is greater than the target secrecy rate, which is the probability of the system being eavesdropped. Then, the IP can be presented as

$$P_{int} = P(C_E > R_S) = 1 - P(C_E \leq R_S) = 1 - F_{\gamma}(e^{R_S} - 1), \quad (24)$$

where we suppose that C_E represents the channel capacity of the eavesdropping and R_S is the target secrecy rate; substituting (20) into (24),

$$P_{int} = 1 - \sum_{g_1=0}^{\infty} \sum_{g_2=0}^{\infty} \cdots \sum_{g_n=0}^{\infty} \frac{\Phi_x}{2} \left(\frac{e^{R_S} - 1}{\bar{\gamma}}\right)^{\mu_1+g_1} \times G_{1,n+1}^{n,1} \left[\frac{\prod_{i=1}^n (1+\kappa_i)\mu_i}{\bar{\gamma}} (e^{R_S} - 1) \middle| \begin{matrix} 1-\mu_1-g_1 \\ \zeta \end{matrix} \right]. \quad (25)$$

5. Numerical Analysis

In this section, some comparisons between numerical simulation results and Monte Carlo trials are provided. All experimental figures show that the theoretical results are consistent with the simulation trials. In Figures 2–6, unless otherwise mentioned, we used the following parameter settings: $m_1 = m_2 = 1$, $\kappa_1 = \kappa_2 = 2$, $\mu_1 = \mu_2 = 2$, $C_{th} = 1$, and $n = 2$. It is worth noting that although the derived formulas contain infinite series, it has been verified by simulation that the expressions of OP and IP have converged when the number of simulation cycles reaches 50.

Figure 2 demonstrates the OP and IP versus the average SNR in different cascade numbers ($n = 1, 2, 3$). It can be observed that the influence of the cascade degree n on the value of IP varies with the change of the average SNR. When $\bar{\gamma} > 2$ dB, as n increases, the IP gradually decreases. Also, when the SNR is large, increase in n will enhance its security. The value of OP becomes bigger with the increase of n , which may be due to the increase in the number of scatterers between the transmitter and the receiver, which reduces the possibility of successful transmission.

Figure 3 presents the impact of OP and IP with average SNR in different parameters ($\kappa = 1, 2, 3$). We clearly see that the Monte Carlo simulations and theoretical curves coincide very well. Comparing Figures 3 and 2, it can be concluded that the trends of their diagrams are similar, and the influences of cascade degree n and the parameter κ on OP and IP are analogical. However, the change amplitude of OP and IP caused by different n values is more significant than that caused by different κ .

Figure 4 plots the variation of OP and IP with average SNR in different thresholds ($C_{th} = 1, 2, 3$). We can note that in the entire range of the abscissa, as the SNR rises, the reliability of the system increases while the security decreases. Furthermore, as the value of C_{th} increases, OP rises and IP reduces. Therefore, the reliability of the channel will decrease by increasing the threshold, and the anti-eavesdropping capability of the channel will be improved.

Figure 5 depicts the OP and IP versus the average SNR when m is different. The figure presents that when $\bar{\gamma} > 2$ dB, OP reduces and IP increases with the increase of m , which shows that when $\bar{\gamma} > 2$ dB, the increase of parameter m will strengthen the reliability of the multi-cascade network, and its security will gradually worsen with the increase of m . When $\bar{\gamma} < 2$ dB, the change of m has little impact on the reliability, and the security improves with the increase of the value of m .

Figure 6 illustrates the OP and IP versus average SNR in different parameters ($\mu = 1, 2, 3$). The figure shows that as the average SNR increases, OP decreases and IP rises. It means that increasing the average SNR can improve the reliability and weaken its security. Through the analysis of Figures 6 and 5, we discover that the various tendencies of

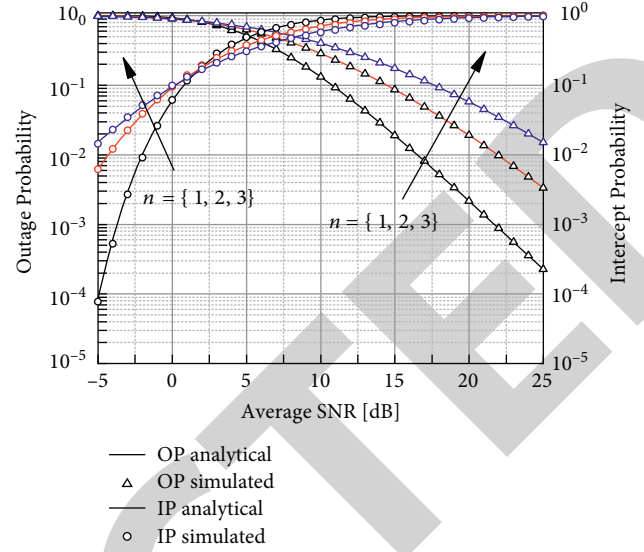


FIGURE 2: OP and IP versus average SNR for various values of n .

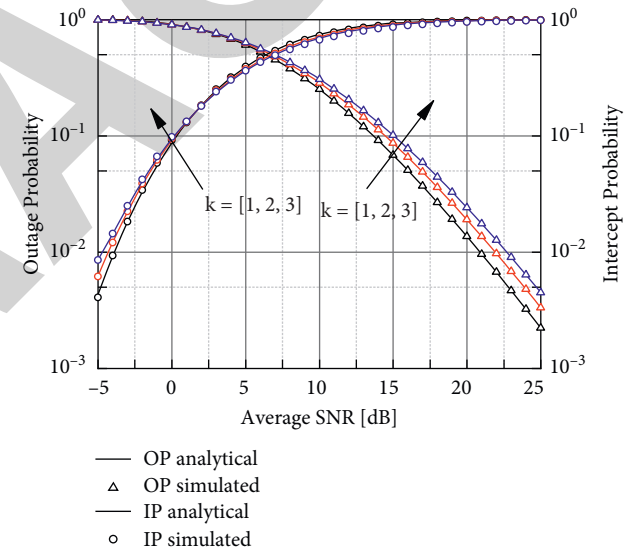


FIGURE 3: OP and IP versus average SNR for various values of κ .

the two figures are similar, which shows that the changes of the parameters m and μ of the system have similar effects on the communication process of the multi-cascaded κ - μ shadowed fading channels.

In summary, the parameters of the channel and the environmental parameters in the model determine the transmission and security performance. Utilizing Figures 2–6, we can obtain the settings for enhanced security performance as smaller cascade degree n , small SNR, large threshold C_{th} , and small κ and m and the environmental settings for improving the transmission performance as larger SNR, small threshold, small cascade degree, and large m and μ at low SNR.

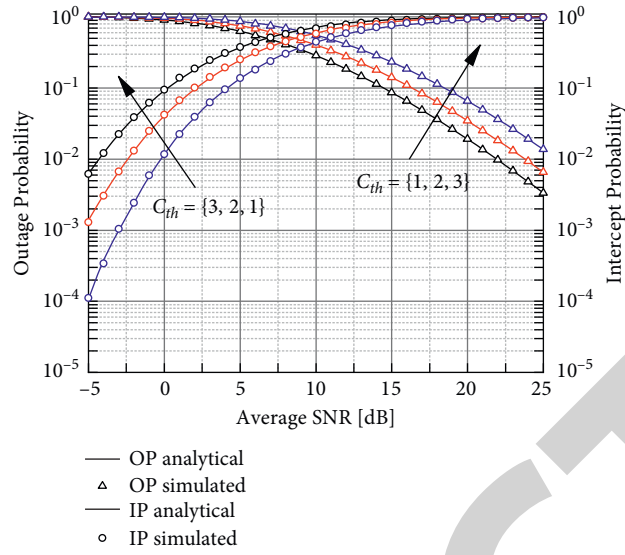


FIGURE 4: OP and IP versus average SNR for various values of C_{th} .

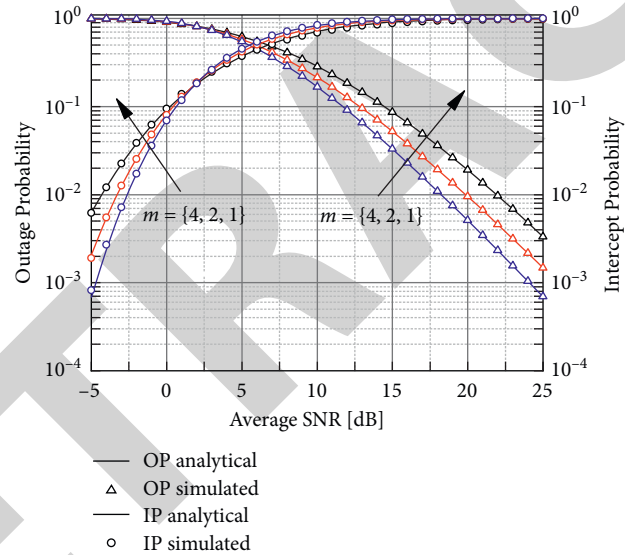


FIGURE 5: OP and IP versus average SNR for various values of m .

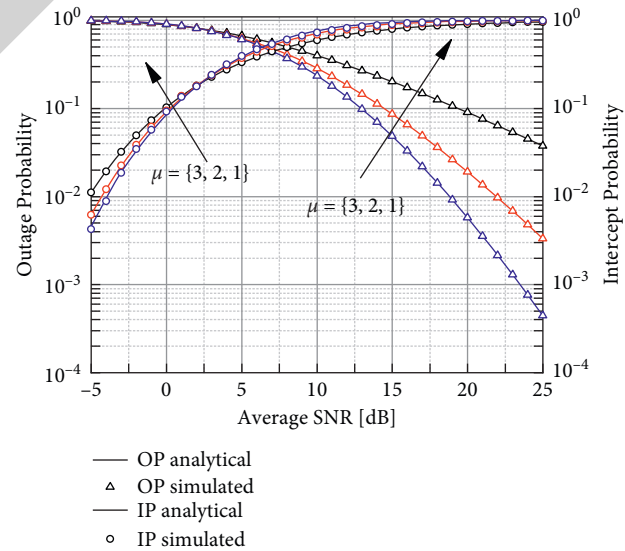


FIGURE 6: SOP OP and IP versus average SNR for various values of μ .

6. Conclusion

This paper mainly studies the n -level cascade situation of the κ - μ shadowed fading under Wyner's eavesdropping model. In particular, the statistical characteristics including the PDF and CDF of the amplitude and SNR are investigated. Then, the evaluation indicators (OP and IP) are obtained. Finally, we conduct theoretical simulations and Monte Carlo trials, respectively. According to the simulation results, we analyze the factors that affect the reliability and security. In addition, the multi-cascade system studied in this article can provide a

theoretical basis for vehicle-to-vehicle communication and satellite communication systems.

Appendix

Utilizing the formula [30]

$${}_1F_1(a; b; x) = \sum_{n=0}^{\infty} \frac{(a)_n}{(b)_n n!} x^n, \quad (\text{A.1})$$

we can obtain

$${}_1F_1\left(m_1; \mu_1; \frac{\mu_1^2 \kappa_1 (1 + \kappa_1) (y/t)^2}{\Omega_1 (m_1 + \kappa_1 \mu_1)}\right) = \sum_{g_1=0}^{\infty} y^{2g_1} t^{-2g_1} \frac{(m_1)_{g_1}}{(\mu_1)_{g_1} g_1!} \left[\frac{\mu_1^2 \kappa_1 (1 + \kappa_1)}{\Omega_1 (m_1 + \kappa_1 \mu_1)} \right]^{g_1}, \quad (\text{A.2})$$

and

$${}_1F_1\left(m_2; \mu_2; \frac{\mu_2^2 \kappa_2 (1 + \kappa_2) (t)^2}{\Omega_2 (m_2 + \kappa_2 \mu_2)}\right) = \sum_{g_2=0}^{\infty} t^{2g_2} \frac{(m_2)_{g_2}}{(\mu_2)_{g_2} g_2!} \left[\frac{\mu_2^2 \kappa_2 (1 + \kappa_2)}{\Omega_2 (m_2 + \kappa_2 \mu_2)} \right]^{g_2}. \quad (\text{A.3})$$

According to [37, 39], we have

$$\exp(-px) = G_{0,1}^{1,0} \left[px \middle| \begin{matrix} - \\ 0 \end{matrix} \right], \quad (\text{A.4})$$

$$G_{u,v}^{s,t} \left[x^{-1} \middle| \begin{matrix} c_p \\ d_q \end{matrix} \right] = G_{v,u}^{t,s} \left[x \middle| \begin{matrix} 1-d_q \\ 1-c_p \end{matrix} \right]. \quad (\text{A.5})$$

Using (A.4) and (A.5), we get

$$\exp\left[-\frac{(1 + \kappa_1) \mu_1 y^2 \eta^{-1}}{\Omega_1}\right] = G_{0,1}^{1,0} \left[\frac{(1 + \kappa_1) \mu_1 y^2 \eta^{-1}}{\Omega_1} \middle| \begin{matrix} - \\ 0 \end{matrix} \right] = G_{1,0}^{0,1} \left[\frac{\Omega_1}{(1 + \kappa_1) \mu_1 y^2} \eta \middle| \begin{matrix} 1 \\ - \end{matrix} \right], \quad (\text{A.6})$$

and

$$\exp\left[-\frac{(1 + \kappa_2) \mu_2 \eta}{\Omega_2}\right] = G_{0,1}^{1,0} \left[\frac{(1 + \kappa_2) \mu_2 \eta}{\Omega_2} \middle| \begin{matrix} - \\ 0 \end{matrix} \right]. \quad (\text{A.7})$$

Substituting (A.2), (A.3), (A.6), and (A.7) into (7) and using variable substitution, the following formula can be obtained:

$$\begin{aligned} f_{Y_2}(y) &= \sum_{g_1=0}^{\infty} \sum_{g_2=0}^{\infty} \frac{\Phi_1 \Phi_2}{2} y^{2\mu_1 + 2g_1 - 1} \times \int_0^{\infty} \eta^{-\mu_1 + \mu_2 - g_1 + g_2 - 1} \\ &\quad \times G_{0,1}^{1,0} \left[\frac{(1 + \kappa_2) \mu_2 \eta}{\Omega_2} \middle| \begin{matrix} - \\ 0 \end{matrix} \right] \times G_{1,0}^{0,1} \left[\frac{\Omega_1}{(1 + \kappa_1) \mu_1 y^2} \eta \middle| \begin{matrix} 1 \\ - \end{matrix} \right] d\eta. \end{aligned} \quad (\text{A.8})$$

Then, use the classical integrals of the two Meijer's G functions given in [39]:

$$\int_0^{\infty} \tau^{\alpha-1} G_{u,v}^{s,t} \left[w\tau \left| \begin{matrix} a_1, \dots, a_t, a_{t+1}, \dots, a_u \\ \kappa_1, \dots, \kappa_s, \kappa_{s+1}, \dots, \kappa_v \end{matrix} \right. G_{p,q}^{m,m} \left[\sigma\tau \left| \begin{matrix} e_1, \dots, e_n, e_{n+1}, \dots, e_p \\ f_1, \dots, f_m, f_{m+1}, \dots, f_q \end{matrix} \right. \right] d\tau \right. \\ \left. = w^{-\alpha} G_{v+p, u+q}^{m+t, n+s} \left[\frac{\sigma}{w} \left| \begin{matrix} e_1, \dots, e_n, 1-\alpha-\kappa_1, \dots, 1-\alpha-\kappa_s, 1-\alpha-\kappa_{s+1}, \dots, 1-\alpha-\kappa_v, e_{n+1}, \dots, e_p \\ f_1, \dots, f_m, 1-\alpha-a_1, \dots, 1-\alpha-a_t, 1-\alpha-a_{t+1}, \dots, 1-\alpha-a_u, f_{m+1}, \dots, f_q \end{matrix} \right. \right] \right. \quad (\text{A.9})$$

Substitute (A.8) into (A.9) to obtain (9).

Data Availability

The data supporting the results of this study can be obtained from the corresponding author upon request.

Conflicts of Interest

The authors declare that they have no conflicts of interest to report regarding the present study.

Acknowledgments

This study was supported in part by the Key Scientific Research Projects of Higher Education Institutions in Henan Province under grant no. 20A510007 and in part by the Doctoral Fund of Henan Polytechnic University under grant no. B2022-13.

References

- [1] A. D. Wyner, "The wire-tap channel," *Bell System Technical Journal*, vol. 54, no. 8, pp. 1355–1387, 1975.
- [2] J.-H. Lee, "Full-duplex relay for enhancing physical layer security in multi-hop relaying systems," *IEEE Communications Letters*, vol. 19, no. 4, pp. 525–528, Apr 2015.
- [3] H. He and P. Ren, "Secure ARQ protocol for wireless communications: performance analysis and packet coding design," *IEEE Transactions on Vehicular Technology*, vol. 67, no. 8, pp. 7158–7169, 2018.
- [4] K. Cao, B. Wang, H. Ding, L. Lv, J. Tian, and F. Gong, "On the security enhancement of uplink NOMA systems with jammer selection," *IEEE Transactions on Communications*, vol. 68, no. 9, pp. 5747–5763, 2020.
- [5] A. Yener and S. Ulukus, "Wireless physical-layer security: lessons learned from information theory," *Proceedings of the IEEE*, vol. 103, no. 10, pp. 1814–1825, 2015.
- [6] S. Wenbo, "Research on physical layer security schemes based on cooperative wireless communication," in *Proceedings of the 2015 Seventh International Conference on Measuring Technology and Mechatronics Automation*, pp. 888–891, IEEE, Nanchang, China, 13 June 2015.
- [7] J. Barros and M. R. D. Rodrigues, "Secrecy capacity of wireless channels," in *Proceedings of the 2006 IEEE International Symposium on Information Theory*, pp. 356–360, IEEE, Washington, USA, 9 July 2006.
- [8] M. Bloch, J. Barros, M. R. D. Rodrigues, and S. W. McLaughlin, "Wireless information-theoretic security," *IEEE Transactions on Information Theory*, vol. 54, no. 6, pp. 2515–2534, 2008.
- [9] A. Goldsmith, *Wireless Communications*, Vol. 10, Cambridge University Press, Cambridge, UK, Aug 2005.
- [10] M. K. Simon and M.-S. Alouini, *Digital Communication over Fading Channels*, Vol. 95, Wiley, Hoboken, NJ, USA, 2005.
- [11] L. Mason, "Error probability evaluation for systems employing differential detection in a Rician fast fading environment and Gaussian noise," *IEEE Transactions on Communications*, vol. 35, no. 1, pp. 39–46, Jan 1987.
- [12] S. O. Rice, "Statistical properties of a sine wave plus random noise," *Bell System Technical Journal*, vol. 27, no. 1, pp. 109–157, Jan 1948.
- [13] H. Popovic, D. Stefanovic, A. Mitic, I. Stefanovic, and D. Stefanovic, "Some statistical characteristics of Nakagami- m distribution," in *Proceedings of the 2007 8th International Conference on Telecommunications in Modern Satellite, Cable and Broadcasting Services*, pp. 509–512, IEEE, Serbia, Nis, 26 September 2007.
- [14] M. Yacoub, "The η - μ distribution: a general fading distribution," in *Proceedings of the Vehicular Technology Conference Fall 2000. IEEE VTS Fall VTC2000. 52nd Vehicular Technology Conference*, vol. 2, pp. 872–877, IEEE, Boston, MA, USA, 24 September 2000.
- [15] M. Daoud Yacoub, "The α - μ distribution: a general fading distribution," *The 13th IEEE International Symposium on Personal Indoor and Mobile Radio Communications*, vol. 2, pp. 629–633, 2002.
- [16] X. Li, J. Li, Y. Liu, Z. Ding, and A. Nallanathan, "Residual transceiver hardware impairments on cooperative NOMA networks," *IEEE Transactions on Wireless Communications*, vol. 19, no. 1, pp. 680–695, Jan 2020.
- [17] M. Yacoub, "The κ - μ distribution: a general fading distribution," vol. 3, pp. 1427–1431, in *Proceedings of the IEEE 54th Vehicular Technology Conference. VTC Fall 2001*, vol. 3, pp. 1427–1431, IEEE, Atlantic City, NJ, USA, 7 October 2001.
- [18] X. Li, J. Li, and L. Li, "Performance analysis of impaired swipt NOMA relaying networks over imperfect Weibull channels," *IEEE Systems Journal*, vol. 14, no. 1, pp. 669–672, Mar 2020.
- [19] F. Gong, J. Ge, and N. Zhang, "SER analysis of the Mobile-Relay-Based M2M communication over double Nakagami- m fading channels," *IEEE Communications Letters*, vol. 15, no. 1, pp. 34–36, Jan 2011.
- [20] N. Hajri, N. Youssef, and M. Patzold, "A study on the statistical properties of double Hoyt fading channels," in *Proceedings of the 2009 6th International Symposium on Wireless*

Retraction

Retracted: Deep Learning-Based Crack Monitoring for Ultra-High Performance Concrete (UHPC)

Journal of Advanced Transportation

Received 8 August 2023; Accepted 8 August 2023; Published 9 August 2023

Copyright © 2023 Journal of Advanced Transportation. This is an open access article distributed under the Creative Commons Attribution License, which permits unrestricted use, distribution, and reproduction in any medium, provided the original work is properly cited.

This article has been retracted by Hindawi following an investigation undertaken by the publisher [1]. This investigation has uncovered evidence of one or more of the following indicators of systematic manipulation of the publication process:

- (1) Discrepancies in scope
- (2) Discrepancies in the description of the research reported
- (3) Discrepancies between the availability of data and the research described
- (4) Inappropriate citations
- (5) Incoherent, meaningless and/or irrelevant content included in the article
- (6) Peer-review manipulation

The presence of these indicators undermines our confidence in the integrity of the article's content and we cannot, therefore, vouch for its reliability. Please note that this notice is intended solely to alert readers that the content of this article is unreliable. We have not investigated whether authors were aware of or involved in the systematic manipulation of the publication process.

Wiley and Hindawi regrets that the usual quality checks did not identify these issues before publication and have since put additional measures in place to safeguard research integrity.

We wish to credit our own Research Integrity and Research Publishing teams and anonymous and named external researchers and research integrity experts for contributing to this investigation.

The corresponding author, as the representative of all authors, has been given the opportunity to register their agreement or disagreement to this retraction. We have kept a record of any response received.

References

- [1] D. Wu, H. Zhang, and Y. Yang, "Deep Learning-Based Crack Monitoring for Ultra-High Performance Concrete (UHPC)," *Journal of Advanced Transportation*, vol. 2022, Article ID 4117957, 10 pages, 2022.

Research Article

Deep Learning-Based Crack Monitoring for Ultra-High Performance Concrete (UHPC)

Dongling Wu,¹ Hongxiang Zhang ,¹ and Yiying Yang²

¹School of Civil Engineering, Northeast Forestry University, Harbin 150040, China

²School of Business Administration, Harbin Cambridge University, Harbin 150069, China

Correspondence should be addressed to Hongxiang Zhang; ldzhldzhx@163.com

Received 9 March 2022; Revised 12 April 2022; Accepted 30 April 2022; Published 15 June 2022

Academic Editor: Lingwei Xu

Copyright © 2022 Dongling Wu et al. This is an open access article distributed under the Creative Commons Attribution License, which permits unrestricted use, distribution, and reproduction in any medium, provided the original work is properly cited.

In civil engineering, image recognition technology in artificial intelligence is widely used in structural damage detection. Traditional crack monitoring based on concrete images uses image processing, which requires high image preprocessing techniques, and the results of detection are vulnerable to factors, such as lighting and noise. In this study, the full convolutional neural networks FCN-8s, FCN-16s, and FCN-32s are applied to monitoring of concrete apparent cracks and according to the image characteristics of concrete cracks and experimental results. The FCN-8s model was tested with a correct crack monitoring rate of 0.6721, while the new network model had a correct crack detection rate of 0.7585, a significant improvement in the correct crack detection rate.

1. Introduction

Concrete is an important infrastructure for the development of the national economy, the development of concrete to strengthen the links between various cities, thus promoting the economic development of all walks of life, and with the economic development of the country, there will be a large number of construction of roads. Although road construction has been developing, but cannot just focus on the constant construction of new roads and not focus on road maintenance, road maintenance and repair and road construction are equally important [1].

With the construction of a large number of roads and the increase in road density, the health of roads requires even more close attention. With the spread of the automobile, many old roads are experiencing increasing traffic volumes that have long exceeded the standards for which they were designed. Because of the road surface in the long-term load and frequent natural disasters, damage, and the emergence of cracks, structural strength continues to decline, affecting the safety of traffic; even if the cracks are left less serious, the presence of too many will not only affect the comfort of driving and affect the aesthetics but also the potential safety risks, so for the location of the road damage, certain

measures should be taken to extend the life of the structure [2, 3] and to prevent road accidents from occurring [4, 5]. However, with the large number of roads and the changing condition of the pavement, it is not realistic to perfectly and strictly control the integrity of each road, and it is important to take appropriate measures to regularly record the health of each road and provide recommendations for its repair based on the actual condition of each road. Therefore, for pavement works, a proper assessment of the health of the road is essential for the rehabilitation of the road.

Assessing the health of a road is not an easy task, as the complexity of the road surface makes it difficult to collect information on the road surface, but with the development of technology, today's camera equipment can now take real-time pictures of the road surface at certain moving speeds, so we can both use the massive amount of photos taken by a car with the ability to take pictures of a section of the road surface and use them as statistical data in the form of big data [6]. However, for a large amount of photo data, it is obviously not appropriate to take manual statistics, so machine learning can be used to train a learner capable of recognizing cracks through a large number of crack samples to recognize and count the large amount of photos, while the learner can also be used for real-time inspection by inspecting vehicles;

the recognition accuracy of the learner is crucial to be able to correctly assess the health of the road. The study of road crack recognition algorithms is of great significance [7].

2. Related Work

With the development of computer technology, researchers at home and abroad have come up with their own crack extraction solutions. With the development of pavement photography technology, CCD cameras are commonly used to capture images of pavement cracks [8]. With traditional digital image crack detection algorithms, the captured crack images can be processed to analyze the location where they are located in the image. Wang et al. [9] combined feature extraction of cracks by Sobel's operator combined with the iterative threshold segmentation method and morphology [10]. Yang et al. [11] proposed an improved Sobel operator to do feature extraction of pavement cracks with remarkable results. In addition, many researchers have used the Sobel operator for crack feature extraction [12]. In [13], an improved Canny operator was proposed for feature extraction of pavement cracks, and it was demonstrated that the improved Canny operator was more effective in denoising cracks than the improved one before [14]. In [15], an application was designed to detect the width of cracks by processing images with the Canny operator in conjunction with Android development [16]. In addition to this, many researchers have used the Canny operator for crack feature extraction [17].

Crack detection based on SVM is usually performed by manually tagging the cracked and noncracked images after image processing with classification labels and training the trained model for crack recognition by the SVM algorithm. Wang Yixin segmented the image by an improved DBC algorithm, extracted cracks by a threshold detection algorithm, and then recognized the cracks by the traditional SVM algorithm [18]. Wang et al. [19] designed feature images of different scales to identify noise, cracks, and background pavement by training a classifier through SVM. In addition to this, a number of researchers have used SVM algorithms for crack recognition [20].

Similar to SVM, BP neural network-based crack detection also requires a model trained on a large number of images to identify cracks, except that the BP neural network simulates a computational model defined by the human brain. In [21], unprocessed native images were used to train a BP neural network, which did not work well. Garcia et al. [10] proposed an improved median filter algorithm combined with an area contrast algorithm for crack feature extraction, classification, and recognition using a BP neural network. In [11], cracks were extracted by median filtering and noise reduction through Sobel's operator, and finally, a BP neural network was constructed to identify these cracks. In addition, many researchers have used BP neural networks for crack recognition [12].

The deep learning-based convolutional neural network is also a type of the neural network, which is able to learn deeper features in images compared to shallow neural networks. Kou Xiao used a grey-scale feature algorithm to extract crack features and used a convolutional neural network for crack training recognition via the deep learning

framework Caffe [13]. In [14], the image was binarized by threshold segmentation of the crack image, and then, the binarized image was flagged with a connected domain, and the rectangular parameters of the connected domain were denoised to extract features, which were then trained for recognition by the convolutional neural network AlexNet [15]. Due to the rapid development of computer technology in recent years, convolutional neural networks have been used in large numbers for image recognition in recent years, so there are also many researchers using convolutional neural networks for crack recognition [16].

3. Dataset Creation

One hundred and twenty-five (3120×4160) images of cracked concrete were taken as the original dataset, of which 35 images were taken as the test set and the remaining 90 images were used for training and validation of the convolutional neural network. The network used in this study has a fixed size requirement for input images, so the samples need to be sliced and deflated, and this process is carried out through a MATLAB program.

Before the network is trained, all training samples need to be labelled, i.e., the class of each training sample needs to be determined. One method of labelling is to first slice the original image collection into smaller samples and then label each sample. This method has many drawbacks, such as the number of samples needed for network training is huge, and manually classifying the samples one by one is undoubtedly a tedious and time-consuming task; for some images with obscure image features, different people may have different classification results for the same sample, and the manual classification method is highly subjective. As crack images are cut into small samples, people lose other reference information in the original images for sample labelling, and it causes people to classify the samples inaccurately. Therefore, this study applies a semiautomatic labelling method [17] to circumvent these drawbacks.

Cracked samples can be broadly classified into three categories according to the learning difficulty of the network: the first category of cracks are in the central region of the sample, such samples have obvious features and are easy for the network to learn, as shown in Figure 1(a); the second category of cracks are at the edges of the sample, but have sufficient length to make it easier for the network to learn their features, as shown in Figure 1(b); the third category is when cracks exist at the edges of the sample and have a short length, it is difficult for the network to learn and detect such samples, as shown in Figure 1(b). These samples are referred to as fuzzy samples, as shown in Figures 1(c) and 1(d). In traditional crack detection methods, fuzzy samples are often discarded from training samples because they are prone to misclassification. In this study, two classification criteria are used to compare the effect of sample discard on crack detection.

4. Full Convolutional Neural Network Crack Detection

4.1. Improved FCN-8s Crack Detection Model Based on Cavity Convolution. FCN-8s performed best in crack detection, but its crack accuracy (CA) was only 67.21%, leaving much room

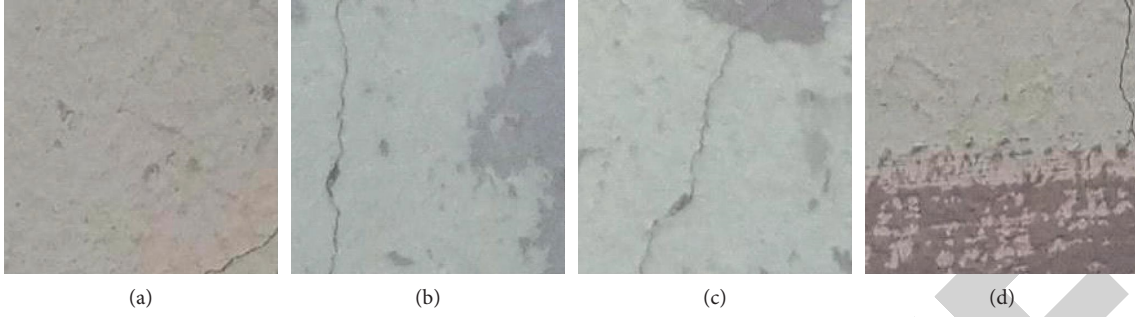


FIGURE 1: Sample cracks. (a) Short cracks at edges. (b) Central cracks. (c) Short cracks at corners. (d) Long cracks at edges.

for improvement. 53.05%, 46.86%, and 67.21% were achieved by FCN-32s, FCN-16s, and FCN-8s, respectively, with FCN-16s being the worst performer. FCN-16s added more front-end feature map information to the network than FCN-32s, i.e., the inclusion of the feature map extracted by convolution module 4 (conv4) did not contribute to crack detection. This is due to the fact that the front-end convolution of the network has a smaller field of perception and some of the features extracted from the concrete surface are partially similar to the feature information of the cracks. This part of information can interfere with the network learning crack features, so the perception of convolution module 4 should be expanded appropriately. In this way, the convolutional module 4 can extract a larger range of information, allowing the network to better learn the difference between the crack and its similar parts.

The cost function of the warp network is

$$J(w, b) = \frac{1}{m} \sum_{i=1}^m J(w, b; x^{(i)}, y^{(i)}), \quad (1)$$

$$J(w, b; x^{(i)}, y^{(i)}) = \frac{1}{2} (y^{(i)} - h_{w,b}(x^{(i)}))^2.$$

The overall cost of the network is the average cost of all training samples.

We are trying to find the best w, b that minimizes the value of $J(w, b)$ and the cost function, so J is a function on w, b , where w, b is also not a scalar, but a set of many w_{ij}, b_{ij} s. The expression for w, b is not explicitly seen in the cost function because it is replaced by the concise $h_{w,b}(x^{(i)})$. Therefore, it is important to emphasize that only w, b is a variable in the expanded expression of J (assuming it can be expanded), and the rest is known. Therefore, according to the idea of gradient descent, for each $w_{ij}^{(l)}, b_{ij}^{(l)}$, we simply update in the direction of the negative gradient, i.e.,

$$w_{ij}^{(l)} := w_{ij}^{(l)} - \alpha \frac{\partial J}{\partial w_{ij}^{(l)}}, \quad (2)$$

$$b_{ij}^{(l)} := b_{ij}^{(l)} - \alpha \frac{\partial J}{\partial b_{ij}^{(l)}}.$$

The vectorized expression is

$$\begin{aligned} w^{(l)} &:= w^{(l)} - \alpha \frac{\partial J}{\partial w^{(l)}}, \\ b^{(l)} &:= b^{(l)} - \alpha \frac{\partial J}{\partial b^{(l)}}, \end{aligned} \quad (3)$$

where α is the learning rate.

Therefore, as long as the partial derivative of w, b can be obtained, it can be updated iteratively, so as to complete the whole algorithm. It seems simple, but it is difficult. Because $J(w, b)$ is difficult to write an explicit expression, it is difficult to find the partial derivative for each w_{ij}, b_{ij} . The main reason is that the network is layered, and then, w, b is layered, which leads to the difficulty of finding the partial derivative and back propagation.

Since w, b is hierarchical, it is natural to find the partial derivatives of w, b in a hierarchical way. Then, it is natural to find a recursive structure to express the bias. Observing the structure $z^{(l+1)} = w^{(l+1)}a^{(l)} + b^{(l+1)}$ in forward conduction, it is natural to find the bias of $w^{(l+1)}, b^{(l+1)}$, by simply asking for the bias of $z^{(l+1)}$ (matrices and vectors are derived in a scalar-like form, $a^{(l)}$ considered as constants).

Considering the case of a single sample, when is the output layer ($l=3$), we have

$$\begin{aligned} \delta^{(3)} &= \frac{\partial J}{\partial z^{(3)}} \\ &= \frac{\partial}{\partial z^{(3)}} \frac{1}{2} (y - h(x))^2 \\ &= \frac{\partial}{\partial z^{(3)}} \frac{1}{2} (y - a^{(3)})^2 \\ &= \frac{\partial}{\partial z^{(3)}} \frac{1}{2} (y - f(z^{(3)}))^2 \\ &= (y - h(x)) \text{of}'(z^{(3)}). \end{aligned} \quad (4)$$

When l is a nonoutput layer (hidden layer) ($l=2$), we have

$$\begin{aligned}
\delta^{(2)} &= \frac{\partial J}{\partial z^{(2)}} \\
&= \frac{\partial J}{\partial z^{(3)}} \cdot \frac{\partial z^{(3)}}{\partial z^{(2)}} \\
&= \delta^{(3)} \cdot \frac{\partial z^{(3)}}{\partial z^{(2)}} \\
&= \delta^{(3)} \cdot \frac{\partial}{\partial z^{(2)}} [w^{(2)} f(z^{(2)}) + b^{(2)}] \\
&= w^{(2)} f'(z^{(2)}) \circ \delta^{(3)}.
\end{aligned} \tag{5}$$

So,

$$\begin{aligned}
\delta^{(L)} &= (y - h(x)) \cdot a^{(L)} \\
\delta^{(l)} &= w^{(l)} a^{(l)} \cdot \delta^{(l+1)}, \quad (l = 2, \dots, L-1) \\
\frac{\partial J}{\partial w^{(l)}} &= \frac{\partial J}{\partial z^{(l)}} \cdot \frac{\partial z^{(l)}}{\partial w^{(l)}} = \delta^{(l)} \cdot (a^{(l-1)})^T \\
\frac{\partial J}{\partial b^{(l)}} &= \frac{\partial J}{\partial z^{(l)}} \cdot \frac{\partial z^{(l)}}{\partial b^{(l)}} = \delta^{(l)}, \quad (l = 2, \dots, L).
\end{aligned} \tag{6}$$

4.2. Null Convolution. The first is to increase the number of convolutions, e.g., 2 layers of 3×3 convolutions can be combined to obtain a 5×5 field of perception, and the second is to use pooling layers, where pooling operation reduces the feature map to make the field of perception of subsequent convolutions relatively larger. The first method increases network parameters less than using 5×5 convolution directly, but the number of convolutions per layer in convolution module 4 is 512, and each additional layer of 3×3 convolution increases the number of parameters by $3 \times 3 \times 512$, which is still a significant increase. The second method does not increase the number of parameters, but loses some of the image information. These cracks themselves have a low number of pixels, and this loss of information may have a detrimental effect on the detection of cracks.

Dilated convolution [18] is a data sampling method that can increase the convolution field while avoiding the problems mentioned above. Figures 2(a) and 2(b) show the size of the convolution field for a convolution kernel size of 3×3 and an expansion factor of 1, 2, and 3, respectively. The field size of null convolution can be calculated from equation (7), where k is the conventional convolution field edge length, r is the expansion factor, and k' is the corresponding null convolution field edge length. Null convolution can make the receptive field grow rapidly with the same number of convolution parameters involved in the calculation, e.g., when three-layer convolution in Figure 2 is coupled, a receptive field of size 13×13 can be obtained, whereas a normal three-layer 3×3 convolution can only obtain a receptive field of size 7×7 .

$$k' = (k - 1)(r - 1) + k. \tag{7}$$

The use of null convolution requires the following rules. (1) The maximum convention of the expansion coefficients of superimposed null convolution cannot be greater than 1. (2) The expansion coefficients of null convolution need to be designed in a sawtooth shape. (3) The expansion coefficients the null convolution need to satisfy equation (8), where M_i is the maximum expansion coefficient of the i^{th} layer and r_i is the expansion coefficient of the i^{th} layer. When the edge length of the convolution kernel is k , we need to let $M_i \leq k$.

$$M_i = \text{Max}[M_{i+1} - 2r_i, M_{i+1} - 2(M_{i+1} - r_i), r_i]. \tag{8}$$

The jagged expansion coefficients help the network to detect information about objects of different sizes in the image, and the other two rules ensure that null convolution utilizes the full pixel value of the image. Figures 3 and 4 show the utilization of this part of the input layer feature map eigenvalues when 3×3 convolution with expansion coefficients of $[2 \ 2 \ 2]$ and $[1 \ 2 \ 9]$ is coupled, respectively. The utilization of the eigenvalues in the layer 2 convolution output, the layer 1 convolution output, and the layer 1 convolution input eigenmap by layer 3 convolution is shown in Figures 3 and 4 in (a), (b), and (c), respectively. These two combinations of null convolution do not conform to rules 1 and 2, respectively, and their convolution operations on the input feature map are discontinuous and do not utilize all the eigenvalues of the input feature map.

4.3. New Network Architecture. From the previous section, it is clear that FCN-8s have the best detection of cracks among the three full convolutional networks, and the extracted feature map of convolutional module 4 is not helpful for crack detection. Therefore, the new network will be based on FCN-8s with modifications to convolutional module 4. Null convolution is used to replace normal convolution in the original convolution module 4, so that the convolution can extract a larger range of information and avoid the network being too sensitive to the detailed information of the image and confusing the cracks with the parts of the concrete background that are similar to it [22].

The size of the feature map output from convolution module 4 is reduced due to the use of null convolution instead of normal convolution in the original convolution module 4. To prevent the feature map size from being too small at the back end of the network, the padding parameter of first convolution in convolution module 1 (conv1) changed from 100 to 150. The detailed parameters of new convolution module 4 are given in Table 1, where the initial input image size is 256×256 pixels when training the network and the feature map size is 69×69 when input to convolution module 4, with a depth of 512. In the following, the improved FCN-8s crack detection model based on null convolution is referred to as the new network.

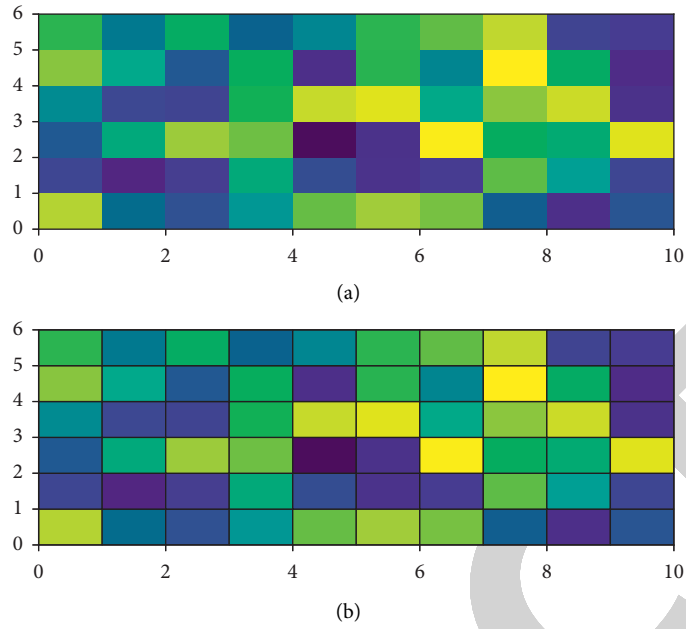


FIGURE 2: Schematic diagram of the convolution field of a cavity. (a) Normal convolution. (b) Convolution with an expansion factor of 2.

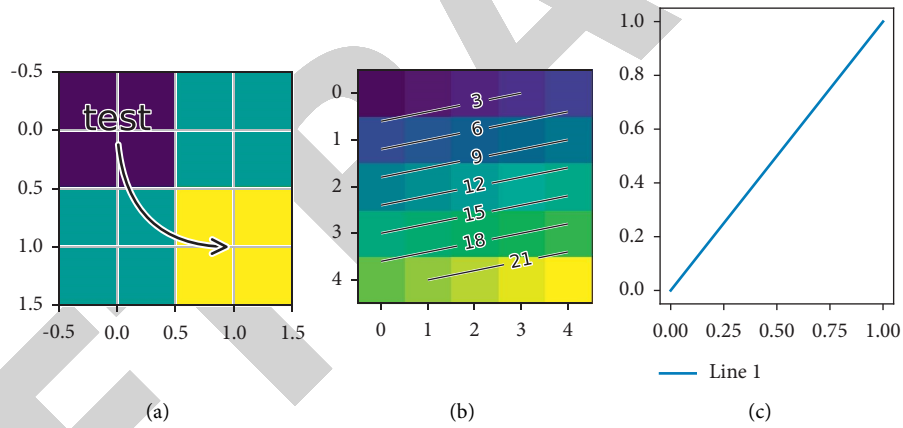


FIGURE 3: Convolutional combination of voids with expansion factor [2 2 2]. (a) Layer 2 convolution output feature map. (b) Layer 1 convolution output feature map. (c) Input feature map.

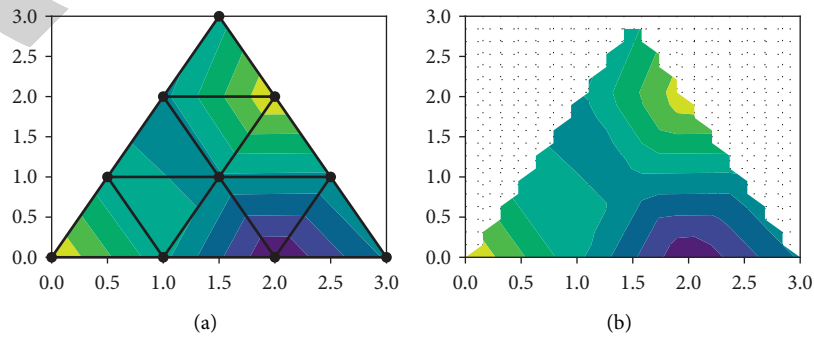


FIGURE 4: Continued.

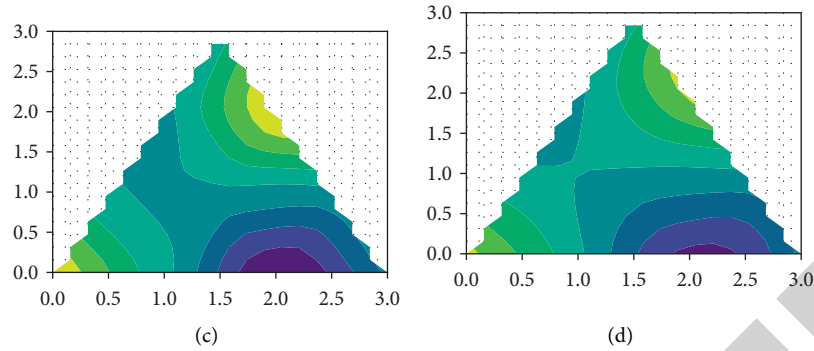


FIGURE 4: Convolutional combination of voids with expansion factor [1 2 9]. (a) Layer 2 convolution output feature map. (b) Layer 1 convolution output feature map. (c) Input feature map. (d) Input feature map.

TABLE 1: Parameters of convolutional module 4 in the new network.

Layer	Operator	Rate	Stride	Padding	Output size
Input	—	—	—	—	$69 \times 69 \times 512$
Conv4_1	[3, 3, 256, 512] conv ReLU	1 —	1 —	1 —	$69 \times 69 \times 512$
Conv4_2	[3, 3, 512, 512] conv ReLU	3 —	1 —	1 —	$65 \times 65 \times 512$
Conv4_3	[3, 3, 512, 512] conv ReLU	5 —	1 —	1 —	$57 \times 57 \times 512$
Pool4	[2] max pool	—	2	0	$28 \times 28 \times 512$

5. Crack Identification Experiments

5.1. Experimental Results and Analysis. The new network was tested using the same test set and the results were compared with those of FCN-8s, as given in Table 2.

As given in Table 2, the new network has a reduced correct rate compared to the FCN-8s background, while the correct rate for cracks has increased by 8.64%, which shows that the improvement to convolution module 4 is effective. By expanding the field of perception of the convolution in convolution module 4, the network is able to extract more complete information about these cracks and better distinguish between cracks and their similarities. Figure 5 shows a picture of cracks detected by FCN-8s and the new network, and Figure 5 shows a zoomed-in view of boxed section in Figure 6.

The reduction in correctness of the new network compared to the FCN-8s background, as given in Table 2, is due to the convolution of a larger field of perception, which can cause some loss of detailed information. When the image background is more complex, the impact caused by this part of information will likely become apparent. As shown in Figure 7, the folded parts present in their images are detected as cracks on a large scale.

It was also found that the new network performed better than FCN-8s for interference on rough concrete surfaces, as shown in Figure 8. FCN-8s detected more uneven parts of rough concrete surfaces as cracks. This is due to the fact that the unevenness of the concrete surface is more uniform, and some of the image detail information lost due to the larger receptive field do not affect the network's learning, while the

TABLE 2: Results of various types of detection for FCN-8s and the new network model.

Type	FCN-8s	New network
Pixel accuracy	0.9815	0.9716
Mean accuracy	0.8247	0.8654
Crack accuracy	0.6721	0.7587
Background accuracy	0.9258	0.9174

larger convolutional receptive field allows the network to better learn the difference between rough concrete surfaces and cracks.

In summary, the new network built by expanding the convolution field in convolution module 4 by means of cavity convolution can effectively improve the detection accuracy of cracks and has a good effect on rough concrete surfaces, but is not suitable for the detection of complex parts such as folds and smears in the background. Cracks are a concern to us and we want to improve the detection of cracks as much as possible, so the new network meets our needs to a certain extent.

5.2. Test Results. The test results of FCN-8s and the new network are given in Table 3. As the new dataset is from a different region than the training set of the network, the correct crack rate in the test results of both FCN-8s and the new network has decreased compared to the previous one. As this test set was not adjusted for difficulty and concrete surfaces in most of the images were more uniform and flat, the new network's detection of the background improved

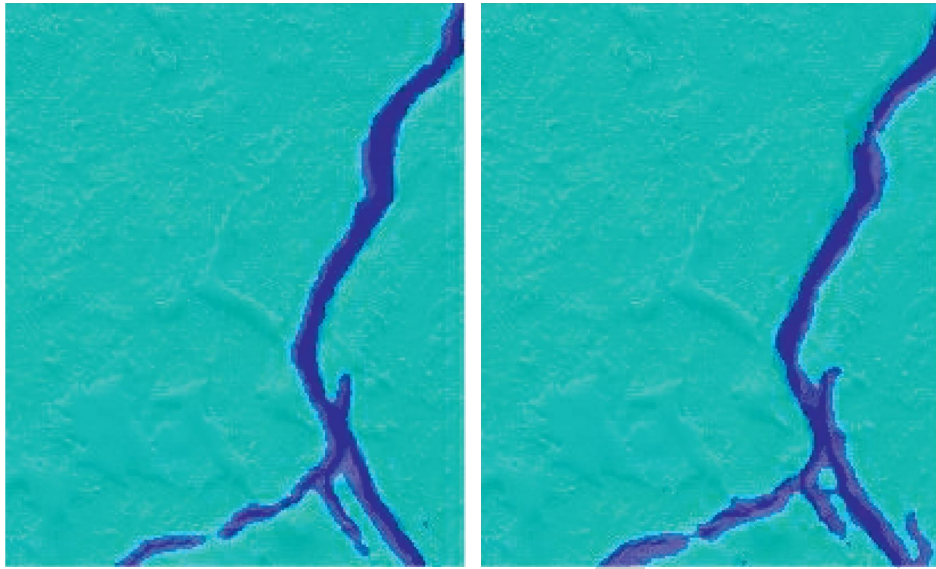


FIGURE 5: Partial enlargement of FCN-8s and new network fracture detection results.

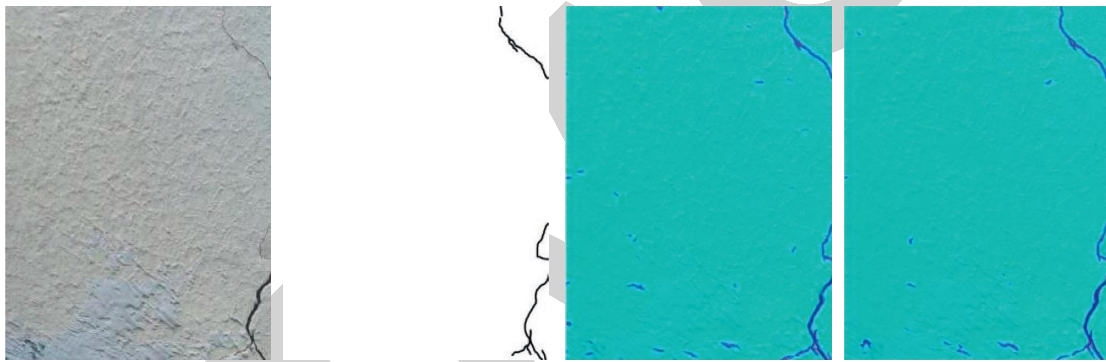


FIGURE 6: Crack detection results of FCN-8s and the new network.



FIGURE 7: FCN-8s and new network concrete crease detection results.

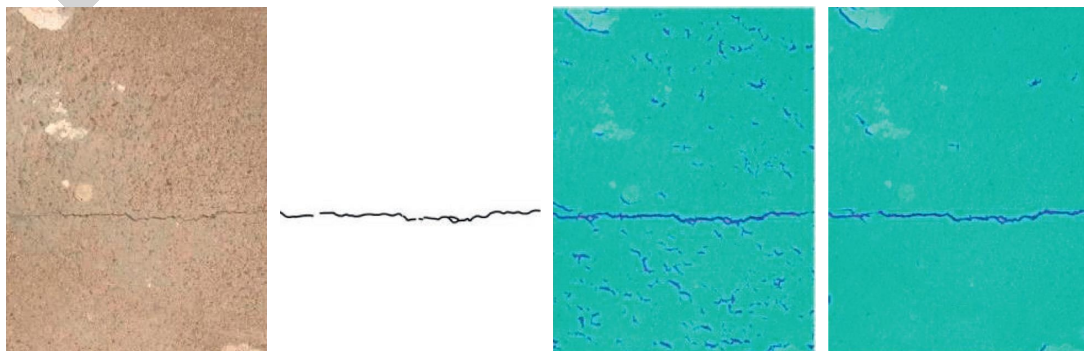


FIGURE 8: FCN-8s and new network coagulation rough surface inspection results.

TABLE 3: Results of various types of detection for FCN-8s and the new network model.

Type	FCN-8s	New network
Pixel accuracy	0.9875	0.9816
Mean accuracy	0.7247	0.8154
Crack accuracy	0.5721	0.6587
Background accuracy	0.98258	0.9874



FIGURE 9: FCN-8s and new network detection results.

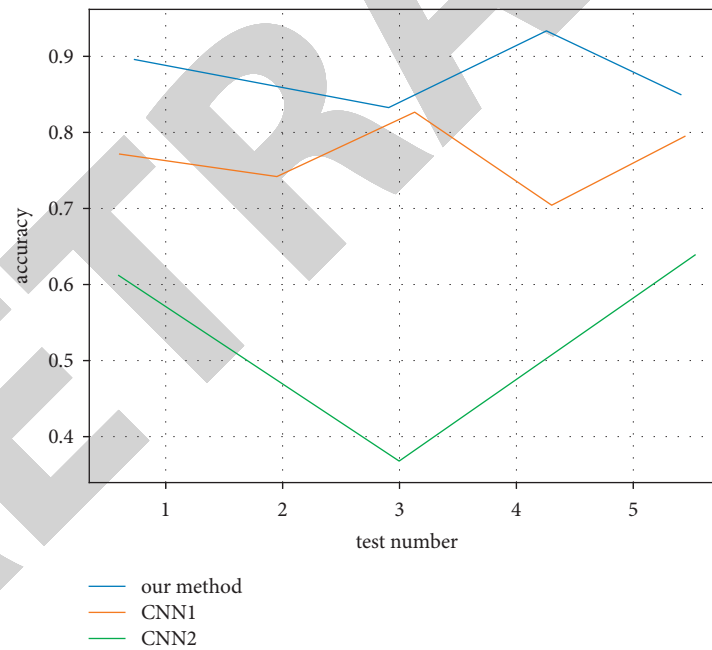


FIGURE 10: Classification accuracy of different models.

significantly from the previous results, and the difference between the new network and FCN-8s in the correct background rate was reduced from 1.02% to 0.33%. On the new dataset, the new network improved the crack correctness metric by 13.09% compared to FCN-8s, and the difference between the two was greater than the test results on the original dataset. This means that the new network performs better on normal cracked images (those with a

more homogeneous concrete surface). The test images in the new dataset are shown in Figure 9, where the new network is more effective in detecting cracks in normal concrete with a flat surface.

The results of the three types of convolutional neural networks are shown in Figure 10. The relationship between the mean square error and the number of iterations for the first group of experiments is shown in Figure 11.

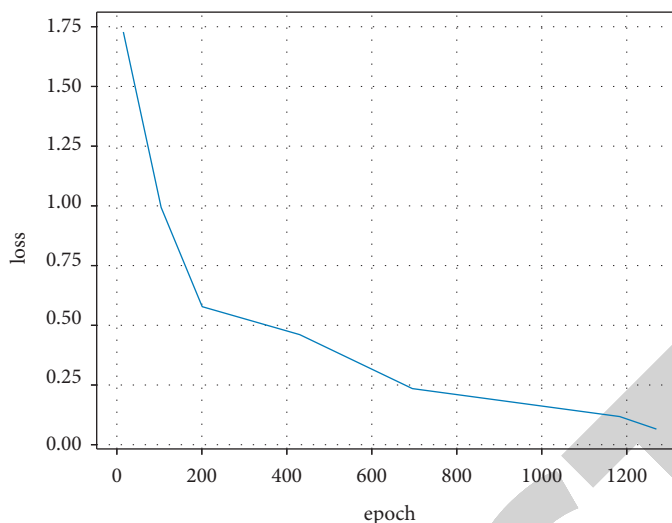


FIGURE 11: Variation of mean squared error.

6. Conclusion

Traditional concrete image-based crack detection uses image processing, which requires high image preprocessing techniques, and the results are susceptible to factors, such as illumination and noise. In this paper, full convolutional neural networks FCN-8s, FCN-16s, and FCN-32s are applied to the detection of apparent cracks in concrete. The correct crack detection rate of the FCN-8s model was 0.6721 when tested, while the new network model had a correct crack detection rate of 0.7585, a significant improvement in the correct crack detection rate.

Data Availability

The data used to support the findings of this study are available from the corresponding author upon request.

Conflicts of Interest

The authors declare that they have no conflicts of interest.

Acknowledgments

This study was sponsored in part by the Fundamental Research Funds for the Central Universities (DL12CB03).

References

- [1] P. Guo, W. Meng, and Y. Bao, "Automatic identification and quantification of dense microcracks in high-performance fiber-reinforced cementitious composites through deep learning-based computer vision," *Cement and Concrete Research*, vol. 148, Article ID 106532, 2021.
- [2] R. Kravchuk and E. N. Landis, "Acoustic emission-based classification of energy dissipation mechanisms during fracture of fiber-reinforced ultra-high-performance concrete," *Construction and Building Materials*, vol. 176, pp. 531–538, 2018.
- [3] A. I. B. Farouk and Z. Jinsong, "Prediction of Interface Bond strength between ultra-high-performance concrete (UHPC) and normal strength concrete (NSC) using a machine learning approach," *Arabian Journal for Science and Engineering*, vol. 47, no. 4, pp. 5337–5363, 2022.
- [4] P. R. Prem, M. Verma, A. R. Murthy, and P. S. Ambily, "Smart monitoring of strengthened beams made of ultrahigh performance concrete using integrated and nonintegrated acoustic emission approach," *Structural Control and Health Monitoring*, vol. 28, no. 5, 2021.
- [5] S. Mahjoubi, W. Meng, and Y. Bao, "Auto-tune learning framework for prediction of flowability, mechanical properties, and porosity of ultra-high-performance concrete (UHPC)," *Applied Soft Computing*, vol. 115, Article ID 108182, 2022.
- [6] J. Wang, C. Liu, and Y. J. Kim, "Artificial Intelligence for Real-Time Crack Detection of Ultra-high-performance Concrete," *Special Publication*, vol. 350, pp. 153–166, 2021.
- [7] R. Solhmirzaei, H. Salehi, V. Kodur, and M. Z. Naser, "Machine learning framework for predicting failure mode and shear capacity of ultra high performance concrete beams," *Engineering Structures*, vol. 224, Article ID 111221, 2020.
- [8] Y. Jiao, Y. Zhang, M. Guo, L. Zhang, H. Ning, and S. Liu, "Mechanical and fracture properties of ultra-high performance concrete (UHPC) containing waste glass sand as partial replacement material," *Journal of Cleaner Production*, vol. 277, Article ID 123501, 2020.
- [9] J. Y. Wang, Z. Z. Chen, and K. Wu, "Properties of calcium sulfoaluminate cement made ultra-high performance concrete: tensile performance, acoustic emission monitoring of damage evolution and microstructure," *Construction and Building Materials*, vol. 208, pp. 767–779, 2019.
- [10] J. A. García, J. F. Gómez, and N. T. Castellanos, "Properties prediction of environmentally friendly ultra-high-performance concrete using artificial neural networks," *European Journal of Environmental and Civil Engineering*, vol. 26, no. 6, pp. 2319–2343, 2020.
- [11] I. H. Yang, C. Joh, and B. S. Kim, "Flexural strength of large-scale ultra high performance concrete prestressed T-beams," *Canadian Journal of Civil Engineering*, vol. 38, no. 11, pp. 1185–1195, 2011.
- [12] J. A. García, "Artificial neural network model for strength prediction of ultra-high-performance concrete," *ACI Materials Journal*, vol. 118, no. 4, pp. 3–14, 2021.

Retraction

Retracted: Research on the Style of Art Works Based on Deep Learning

Journal of Advanced Transportation

Received 8 August 2023; Accepted 8 August 2023; Published 9 August 2023

Copyright © 2023 Journal of Advanced Transportation. This is an open access article distributed under the Creative Commons Attribution License, which permits unrestricted use, distribution, and reproduction in any medium, provided the original work is properly cited.

This article has been retracted by Hindawi following an investigation undertaken by the publisher [1]. This investigation has uncovered evidence of one or more of the following indicators of systematic manipulation of the publication process:

- (1) Discrepancies in scope
- (2) Discrepancies in the description of the research reported
- (3) Discrepancies between the availability of data and the research described
- (4) Inappropriate citations
- (5) Incoherent, meaningless and/or irrelevant content included in the article
- (6) Peer-review manipulation

The presence of these indicators undermines our confidence in the integrity of the article's content and we cannot, therefore, vouch for its reliability. Please note that this notice is intended solely to alert readers that the content of this article is unreliable. We have not investigated whether authors were aware of or involved in the systematic manipulation of the publication process.

Wiley and Hindawi regrets that the usual quality checks did not identify these issues before publication and have since put additional measures in place to safeguard research integrity.

We wish to credit our own Research Integrity and Research Publishing teams and anonymous and named external researchers and research integrity experts for contributing to this investigation.

The corresponding author, as the representative of all authors, has been given the opportunity to register their agreement or disagreement to this retraction. We have kept a record of any response received.

References

- [1] S. Liu, "Research on the Style of Art Works Based on Deep Learning," *Journal of Advanced Transportation*, vol. 2022, Article ID 5433623, 8 pages, 2022.

Research Article

Research on the Style of Art Works based on Deep Learning

Shulin Liu 

Department of Fine Arts, Science and Technology College Gannan Normal University, Ganzhou 341000, Jiangxi, China

Correspondence should be addressed to Shulin Liu; 2012012@gnnu.edu.cn

Received 8 March 2022; Revised 24 April 2022; Accepted 9 May 2022; Published 11 June 2022

Academic Editor: Lingwei Xu

Copyright © 2022 Shulin Liu. This is an open access article distributed under the Creative Commons Attribution License, which permits unrestricted use, distribution, and reproduction in any medium, provided the original work is properly cited.

In view of the unsatisfactory effect and major limitations of the style transfer of art works, this paper takes Chinese ink painting for the research subject. The obvious texture characteristics of Chinese ink painting are selected as the input of the Cycle Generative Adversarial Network (CycleGAN) model builder, and the relativistic evaluator is employed to improve the model loss function and the adversarial loss function. An improved art style transfer method of the CycleGAN model is proposed. The experiment shows that the improved CycleGAN model is efficient and feasible for style transfer. Compared with the traditional CycleGAN model, the proposed model performs better in GAN train and GAN test, with a higher average pass rate, which is an increase of nearly 10%. At the same time, with the increase of the number of iterations, the training time of the improved model is close to that of the original model, but the image of the improved model training is larger, which shows that it has more advantages.

1. Introduction

Art works are products of human culture, embodying the spirit of humanism and reflecting the cultural characteristics of the times. Research on the style transfer of art works is conducive to spreading art more widely. However, the current studies of art style mainly focus on image analogy, image preprocessing, and feature extraction. For instance, Hahn et al. extracted image features from multiple art works with the same style by preprocessing images and image analogy, and carried out art style transformation, thus realized the style transfer learning of art works [1, 2]. Wang et al., for the purpose of objectively calculating the artistic style of Xin An Art School, tried to put forward digital features such as redundancy, order degree, and intricacy to represent the art style of painting algorithm based on Shannon entropy in information theory. To some extent, it reflects the artistic styles of Xin'an School of Painting in different times and the diversity of different artists. Over the years, the progression and application of deep learning have brought new opportunities for the study of art works style [3, 4]. Yang, and Ghani and Md Azahar put forward an image art classification method on the basis of the VGGNET model for the classification of various painting artistic styles in contemporary society. Convolutional neural network

(CNN) was employed to complete the classification of various painting art styles, which lays a foundation for the transfer learning of art works [5, 6]. Chen et al. applied deep learning in different artistic contexts, discussing to which extent the space induced by deep learning CNN can capture the progress of works in music and visual art. Based on the main path algorithm, the evolution analysis of the vector space induced by CNN was carried out, and the reasonable connection between visual art works and songs of different styles was found, which provides interesting insights for extracting evolutionary information in any high-dimensional spaces [7, 8]. Kang et al. proposed a texture migration method for video stream, which can stylize the perception-enhanced video [9]. Ruder et al. proposed a style transfer method of deep learning, which can stylize videos of any length [10]. Zhu et al. proposed the saliency algorithm to guide style transfer, showing good performance [11]. Cui et al. proposed visual smooth bilateral convolution block (B-block) and feature fusion strategy (f-block) to improve the image quality in style conversion [12]. According to the above research, it can be found that the neural network has certain advantages in the style classification and transfer learning of art works. The style transfer image can be obtained by reorganizing the features of rented images through the network and then using the decoder to generate synthetic

images. However, the transfer effect of the model based on the above neural network has to be improved. For solving this problem, this paper takes Chinese ink painting as the research object. Based on the CycleGAN, which is currently ideal style transfer model, the obvious texture features of Chinese ink painting are used as the input of CycleGAN model generator. The loss function and adversarial loss function are improved by relativistic discriminator, and an improved CycleGAN art style transfer model is proposed.

2. Basic Methods

2.1. Introduction to CycleGAN Style Transfer Model. CycleGAN style transfer model is an unsupervised style transfer method for transforming in different image fields without requiring specific image pairs. It is often used in language translation and image conversion tasks in daily life [13]. When the CycleGAN model is applied to the image conversion task, its specific operations are as follows.

$$\begin{aligned} L_{\text{GAN}}(G, D_Y, X, Y) &= E_{y \sim p_{\text{data}}(y)} [\log D_Y(y)] + E_{x \sim p_{\text{data}}(x)} [\log(1 - D_Y(G(x)))], \\ L_{\text{cyc}}(G, F) &= E_{x \sim p_{\text{data}}(x)} [\|F(G(x)) - x\|_1] + E_{y \sim p_{\text{data}}(y)} [\|G(F(y)) - y\|_1]. \end{aligned} \quad (2)$$

In the formula, L_{GAN} is the confrontation loss, while L_{cyc} represents the cyclic consistency loss and $\|\cdot\|_1$ represents the L1 loss.

$$L_{\text{GAN}}(G, F, D_x, D_Y) = L_{\text{GAN}}(G, D_Y, X, Y) + L_{\text{GAN}}(F, D_x, X, Y) + \lambda_1 L_{\text{cyc}}(G, F) + \lambda_2 L_{\text{idt}}(G, F). \quad (3)$$

In the formula, L_{idt} stands for the identity mapping loss; λ_1 and λ_2 stand for the weighting coefficients.

Figure 1 shows the framework of the CycleGAN model.

2.2. Improvement of CycleGAN Style Transfer Model

2.2.1. Improvement of Discriminator. This paper argues that the missing key characteristics of the CycleGAN model are the increased probability of fake data becoming real ($D(xf)$) and the decreased probability of real data becoming real ($D(xr)$). In the standard CycleGAN model, the identifier can be defined as follows, according to the non-transformation layer $C(x)$ [16]:

$$D(x) = \text{Sigmoid}(C(x)). \quad (4)$$

Relativistic discriminator is adopted to improve model discriminator and generator loss function, that is, to sample A from real/false data, then formula (4) can be rewritten to [17]:

$$D(x) = \text{sigmoid}(C(xf)). \quad (5)$$

The probability that the given true data are more real than the fake data which are randomly sampled can be

Given images X and Y of two different domains, construct generators G and F , respectively:

$$\begin{aligned} G: X &\longrightarrow Y, \\ F: Y &\longrightarrow X. \end{aligned} \quad (1)$$

In other words, the real image I_A in source domain A is transformed into the false image I_B in target domain B through generator G . Then, I_B is reconstructed through generator F to obtain reconstructed image I_{RA} so that the original image information can be saved. Finally, I_B and its real image I_B are put into the discriminator D to judge the authenticity, and the complete one-way GAN network is obtained. Combining the two one-way GAN networks, a consistent loss supervision training network can be obtained. The related formulas of the whole process are as follows [14]:

Two GANs each contain a discriminator and share two generators, so their loss function can be represented as [15]:

estimated by the above method. Therefore, the loss function of the CycleGAN model evaluator and generator are rewritten as formulas (6) to (16).

$$\begin{aligned} L_D &= E_{x_r \sim P} [\log(\text{sigmoid}(C(xr)))] \\ &\quad - E_{x_f \sim Q} [\log(1 - \text{sigmoid}(C(xf)))], \end{aligned} \quad (6)$$

$$L_G = -E_{x_r \sim Q} [\log(\text{sigmoid}(C(xf)))], \quad (7)$$

$$L_D^{\text{RGAN}} = -E_{(x_r, x_f) \sim (P, Q)} [\log(\text{sigmoid}(C(xr) - C(xf)))], \quad (8)$$

$$L_G^{\text{RGAN}} = -E_{(x_r, x_f) \sim (P, Q)} [\log(\text{sigmoid}(C(xf) - C(xr)))]. \quad (9)$$

In the formulas, x_r and P represent real data and their data sets, respectively; x_f and Q , respectively, represent generated data and its set. $C(x)$ is the output of the discriminator without transformation layer.

In addition, to make the identifiers of the relativistic discriminator play a role in the initial definition, this paper proposes an average relativistic discriminator, as shown in formulas (10) and (11) [18]:

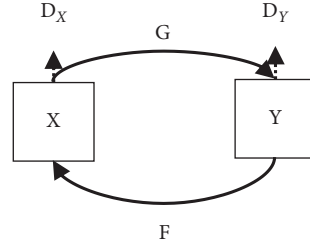


FIGURE 1: Schematic diagram of the CycleGAN model structure.

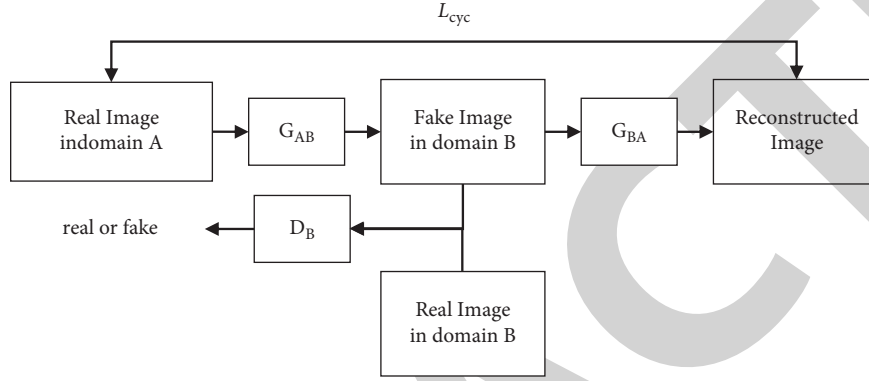


FIGURE 2: CycleGAN model structure.

$$L_D^{\text{RaGAN}} = -E_{x_r \sim p} [\log(\bar{D}(x_r))] - E_{x_f \sim Q} [\log(1 - \bar{D}(x_f))], \quad (10)$$

$$L_G^{\text{RaGAN}} = -E_{x_f \sim Q} [\log(\bar{D}(x_f))] - E_{x_r \sim p} [\log(1 - \bar{D}(x_r))], \quad (11)$$

$$\bar{D}(x_r) = \text{sigmoid}(C(x_r) - E_{x_f \sim Q} C(x_f)), \quad (12)$$

$$\bar{D}(x_f) = \text{sigmoid}(C(x_f)). \quad (13)$$

2.2.2. Improvement of Generator. Generator is a significant part of the CycleGAN model, which is related to the final transfer result of the model. The CycleGAN model generator loss function includes saturated loss function and unsaturated loss function. In practical applications, the saturated loss function is very unstable, which causes the failure of the CycleGAN model to reach the optimal state, and the problem of gradient disappearance is prone to occur when the learning rate is high [19]. Therefore, to solve this

problem, this paper improves the model from two aspects: generator and generating adversarial loss function.

(1) *Generator Improvement.* The CycleGAN model generator is usually composed of residual networks, and its basic model structure is shown in Figure 2 [20], including two downsampling convolution layers with 2 steps, two upsampling convolution layers with 1/2 step, and nine residual modules. It achieves the transfer of image style by downsampling the image, changing the image characteristics through the network conversion, and finally restoring the image through upsampling. The texture features reflecting ink painting features are added as additional conditions to the generator under the original input conditions, so that the CycleGAN model generator is improved. The improved model structure is shown in Figure 3 [21].

(2) *Improvement of Generating Adversarial Loss Function.* L2 is employed as the adversarial loss, and the average relativistic discriminator loss is used [22]. The loss of modified discriminator and the adversarial loss are shown as follows:

$$L_D = E_{(x \sim p_{\text{data}}(x))} [(D(X) - E_{y \sim p_{\text{data}}(y)} [D(G(Y))] - 1)^2] + E_{y \sim p_{\text{data}}(y)} [(D(G(Y)) - E_{x \sim p_{\text{data}}(x)} [D(X)] + 1)^2]$$

$$L_{\text{GAN}}(G, D_Y, X, Y) = E_{y \sim p_{\text{data}}(y)} [(D_Y(G(Y)) - E_{x \sim p_{\text{data}}(x)} [D_Y(X)] - 1)^2] + E_{x \sim p_{\text{data}}(x)} [(D_Y(X) - E_{y \sim p_{\text{data}}(y)} [D_Y(G(X))] + 1)^2]. \quad (14)$$

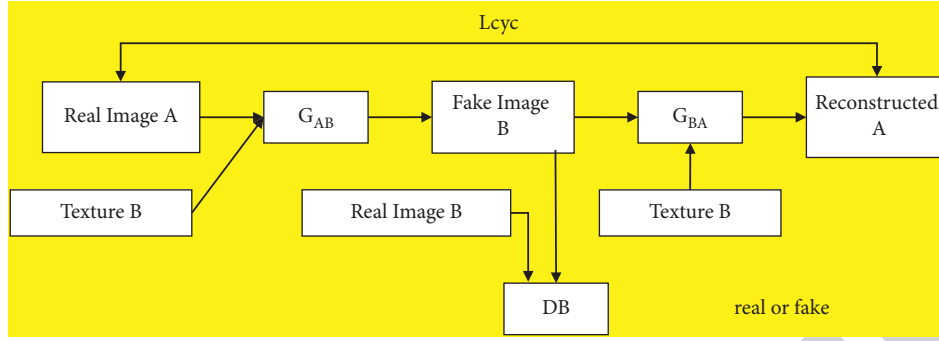


FIGURE 3: Improved CycleGAN model structure.

In the formula, L_{cyc} and L_{idt} keep unchanged, then the model's total loss is

$$L_{GAN}(G, F, D_X, D_Y) = L_{GAN}(G, D_Y, X, Y) L_{GAN}(F, D_X, X, Y) + \lambda_1 L_{cyc}(G, F) + \lambda_2 L_{idt}(G, F). \quad (15)$$

3. The Style Transfer Method of Art Works based on the Improved CycleGAN Model

3.1. Feature Extraction. Feature extraction has a great influence on the construction of style transfer of art works based on the improved CycleGAN model. Therefore, before the style transfer of art works, this paper extracted the art features that can reflect the style of art works at first. Feature extraction includes line feature extraction and texture feature extraction [18]. Among them, line feature extraction is the main manifestation of emotional features in traditional Chinese paintings, and the fluidity of lines is usually expressed by curvature, as in formula (16) [23]:

$$F_{line} = \frac{(1 + f_x^2)f_{yy} + (1 + f_y^2)f_{xx} - 2f_x f_y f_{xy}}{(1 + f_x^2 + f_y^2)^{3/2}}. \quad (16)$$

In the formula, x and y represent the coordinates of a certain pixel in the image, respectively, and $f(x, y)$ represents the pixel's grey level. $f_x, f_y, f_{xy}, f_{xx},$ and f_{yy} , respectively, represent the first-order, second-order, and mixed partial derivatives of $f(x, y)$, and F_{line} represents the Gaussian curvature of the pixel.

In this paper, the LBP method is adopted to extract texture features, as shown in formula (17) [24]:

$$LBP(x_c, y_c) = \sum_{p=0}^{p-1} 2^p s(i_p - i_c). \quad (17)$$

In the formula, (x_c, y_c) indicates the central element of the $3 * 3$ area, and its pixel value i_p, i_c indicates other pixel values in the area. $S(x)$ indicates a symbolic function, and its basic definition is shown as follows [25]:

$$S(x) = \begin{cases} 1, & \text{if } x \geq 0, \\ 0, & \text{else.} \end{cases} \quad (18)$$

By referring to relevant literature and the characteristics of Chinese ink painting, texture features that can best reflect ink painting are selected as the main features and extracted in this paper.

3.2. Ink Painting Transfer Process based on Improved CycleGAN. Based on the improved CycleGAN model, this paper takes ink painting as the research object and designs the style transfer process of art works as Figure 4. The specific steps are as follows:

The specific steps are as follows:

- (1) Image data collection and sorting: all the image data are unified in specification and size and divided them into training and test data set in a certain proportion;
- (2) Feature extraction: the LBP method is used to extract texture features from images and input them into the CycleGAN model generator as additional conditions;
- (3) Model training: the initial learning rate, batch size, epoch, and other parameters of the CycleGAN model are initialized, and the model is trained. The model is saved as it met the termination conditions;
- (4) Input the test data set into the saved CycleGAN model and output the image transfer results.

4. Simulation Experiment

4.1. Experimental Environment Construction. This experiment is simulated on a 64-bit Windows 10 with Intel Core i7-7800K CPU, and the GPU is NVIDIA GeForce RTX2070. The memory is 16G, the open-source depth framework is pytorch, and the programming language is python.

4.2. Data Sources and Preprocessing. In this paper, 300 natural landscape pictures and 360 Chinese ink paintings are taken from the Internet by crawler technology as experimental data sets, and the part of the data is shown in Figure 5. Considering the small number of data sets, to expand the data set, data enhancement technology is adopted to enlarge the natural landscape pictures and Chinese ink paintings to twice the original size in this paper. In addition, due to the different sizes of each image, all

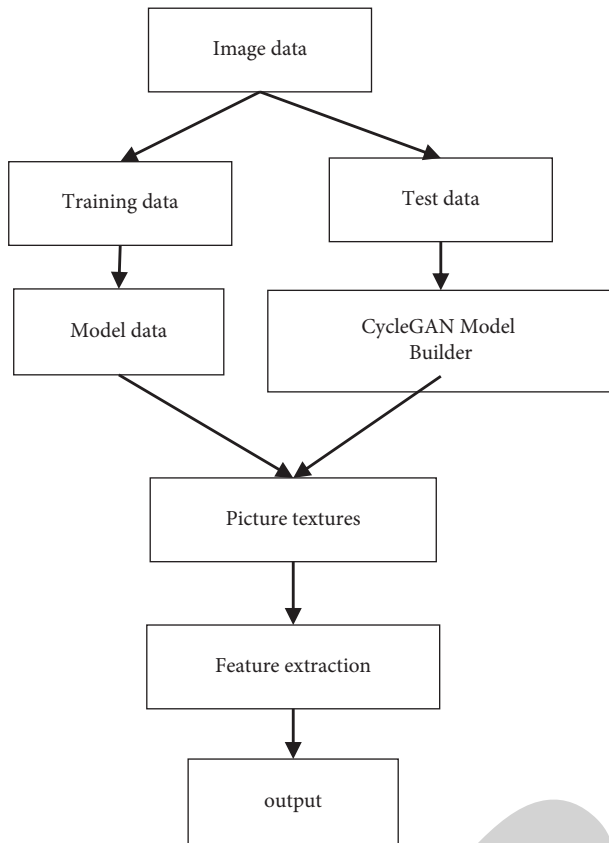


FIGURE 4: Art Work Style transfer process based on the improved CycleGAN model.

images are unified to $256 * 256$ pixels before training to meet the model input requirements [26].

4.3. Evaluation Indicators. At present, there is no unified evaluation indicator for the study of art works style transfer, which makes it difficult to objectively evaluate the transfer results. Through consulting relevant references, this paper finds that manual evaluation test and GAN train/test can basically evaluate the art works style transfer [23, 27–29]. Therefore, the above two indicators are selected as the evaluation criteria for the transfer effect of the proposed method. Among them, manual evaluation test reflects subjective evaluation results, while the GAN train/test reflects objective evaluation of image transfer effect to a certain extent by classifying images and evaluating the quality of generated images according to classification accuracy. The GAN train/test includes two indicators, GAN train and GAN test. When the GAN train is closer to the classification accuracy GAN base, it indicates that the diversity of generated samples is closer to the real sample, that is, the better the GAN model is; when the GAN test is close to GAN base, it indicates that the higher the quality of the image generated by the GAN model.

4.4. Parameter Setting. The model proposed in this experiment uses Adam as the optimizer. The original learning rate



FIGURE 5: Example of experimental data set.

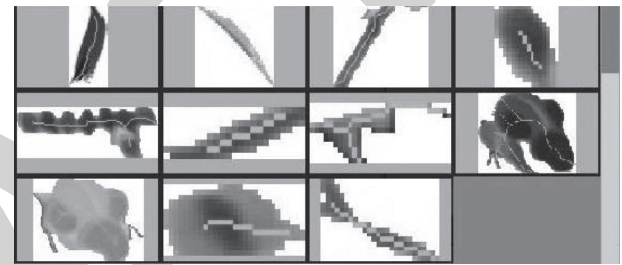


FIGURE 6: Extraction results of texture features.

is $2e - 3$, the batch size is 2, and the epoch is 200. The number of iterations of each epoch is consistent with that of the larger total pictures in the training data set. The training parameters of the compared model CycleGAN are configured with default parameters, and the epoch is also 200.

4.5. Experimental Results

4.5.1. Feature Extraction Results. The LBP method is adopted to extract texture features of works as shown in Figure 6. It shows that the proposed method can well extract texture features of ink painting works, laying a foundation for subsequent style transfer of ink painting works.

4.5.2. Qualitative Experimental Results. The verification of the proposed method for its effectiveness was conducted. The proposed model and CycleGAN model were used to transfer experimental data under the same parameter settings, and the transfer results of the two models were compared. The overall and partial comparisons are shown in Figures 7 and 8. In the figures, the first column is the initial image, and the second and third are, respectively, the transferred images of the compared model and the model in this paper. It can be seen from the figures that compared with the transferred images of the unimproved CycleGAN model, transferred images of the model proposed in this paper are more suitable for the characteristics of Chinese ink painting. The CycleGAN model only reduced the contrast of the original input image to transfer images, making the

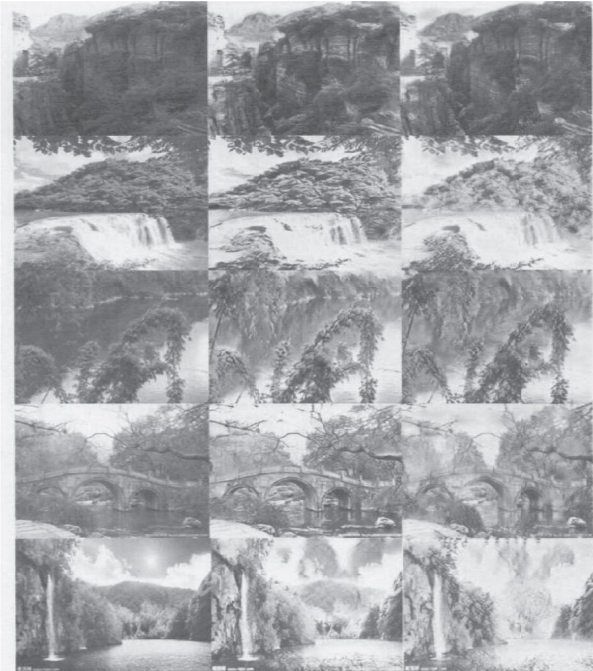


FIGURE 7: Comparison of transferred images of different models on the whole.

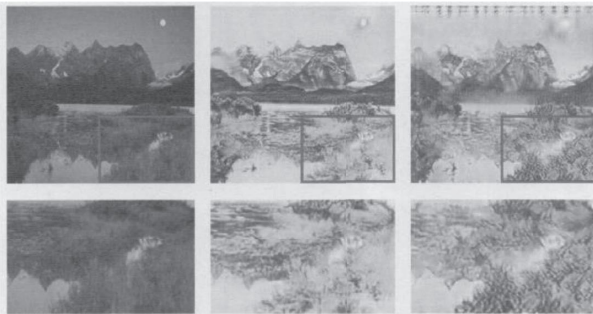


FIGURE 8: Comparison of transferred images of different models in part.

overall image style looks closer to the input images. The transferred images generated by the model proposed in this paper are closer to the average of all style and Chinese ink painting style by the average relativistic discriminator. Therefore, the improvements of CycleGAN model in this paper are effective, and the improved model can generate images with Chinese ink painting style.

Since both the proposed model and the CycleGAN model need to realize self-reconstruction, Figure 9 is the reconstruction result of the experimental data set on the proposed model. In the figure, the first column is the original input image, including a picture of natural landscape and ink painting style; the second column is the transferred image corresponding to the first column; the reconstructed image of the second column is shown in the third column. As the figure shows, the generated transfer image retains the original image content, while the landscape painting style is changed to ink painting style with Chinese characteristics,

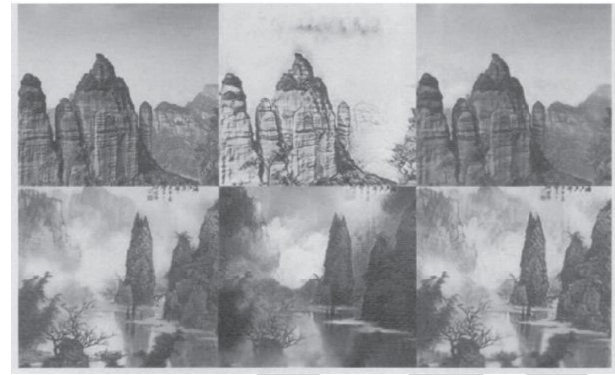


FIGURE 9: Image style transfer and reconstruction results.

and the ink painting image is changed to a more realistic landscape image. The reconstructed image can be reconstructed well through two generators that are opposite to each other. Therefore, the model proposed in this paper can realize image style transfer, which proves the effectiveness and feasibility of it.

4.5.3. Quantitative Analysis Results. To quantitatively analyze the validity of the proposed model, the GAN train/test indicators are used to evaluate the model. Considering that the data set for training is small, the classifier in this paper adopts the ResNet-50 model, and the outcomes of the proposed model and the unimproved CycleGAN model are obtained. The results are shown in Table 1. As the table shows, in comparison with the CycleGAN model, the GAN base of the proposed model is 94.3%, and it performs better in the GAN train and GAN test indicators. It indicates that the model proposed in this article has a certain effectiveness in the style transfer of art works.

As the style of art works is an abstract concept and its style transfer has a certain degree of subjectivity, this paper sets manual evaluation test indicators to further analyze the experimental results. Firstly, image sets A and B are generated by inputting 100 natural landscape images to the model proposed in this paper and the CycleGAN model, and the images in the A and B sets are disarranged. Then, 10 art students were selected to judge each image to see whether it looked like a Chinese ink painting or not. Secondly, the images that resemble ink paintings are counted, and their proportions are calculated as the pass rate. Finally, the average pass rate is taken as the final evaluation result, as shown in Table 2. From the table, compared with the CycleGAN model, the average pass rate of the proposed model is higher, with an increase of nearly 10%. This shows that the proposed model is effective in improving the CycleGAN model and can obtain images that are more suitable for Chinese ink painting style.

In order to verify the running time and space consumption of the proposed model, the running time and graphics card usage of model training with 1 epoch and 50 epochs were recorded, respectively. Also, compared them with that of the CycleGAN model under the same conditions, the results can be seen in Table 3. The table shows that

TABLE 1: Comparison of GAN train/test of different models.

Model	GAN train (%)	GAN test (%)
The original CycleGAN	61.86	61.02
The proposed model	67.03	70.37

TABLE 2: Comparison of manual evaluation test results of different models.

Model	Average pass rate (%)
The original CycleGAN	52.76
The proposed model	62.37

TABLE 3: Comparison of model running time and graphics card usage.

Model	1 epoch (s)	50 epoch	Graphics card usage (MB)
The original CycleGAN	117	1 h 40 min	6703
The proposed model	129	1 h 48 min	7137

in contrast with the CycleGAN model, the model proposed in this paper has no significant change in running time, which can be basically ignored. In terms of graphics card usage, the model proposed in this article has an increase of around 6.4% compared to the CycleGAN model. The reason is that additional information has been added to the generator. In general, it is feasible and valuable to improve model performance with less computing resources. Therefore, the method proposed in this paper has certain effectiveness and practical application value.

5. Conclusion

To sum up, the style transfer model of art works based on deep learning proposed in this paper utilizes the obvious texture features of Chinese ink paintings as the input of CycleGAN model generator, and utilizes relativistic discriminator to improve the loss function and adversarial loss function of CycleGAN model discriminator, improving the CycleGAN model generator. On the basis of the improved CycleGAN model, this paper studies the transfer of ink painting style. Compared with the unimproved CycleGAN model, the model proposed in this paper can generate images with more Chinese ink painting flavor. The accuracy of GAN base in the verification set Sv is 94.3%, and the performance of GAN train and GAN test is better, with the average pass rate increased by nearly 10%. The innovation of this study is to realize the transfer of artistic style by using the deep learning algorithm so as to provide an information-based way for the transformation of different styles in art.

Data Availability

The experimental data used to support the findings of this study are available from the corresponding author upon request.

Conflicts of Interest

The author declares that there are no conflicts of interest regarding this work.

References

- [1] U. Hahn and B. Pauwke, "Visualizing climate change: an exploratory study of the effectiveness of artistic information visualizations," *World Art*, vol. 11, no. 1, pp. 95–119, 2021.
- [2] G. Anna, M. Caccia, L. Bonizzoni et al., "Deep inside the colour: how optical microscopy contributes to the elemental characterization of a painting," *Microchemical Journal*, vol. 155, pp. 104730–104732, 2020.
- [3] D. Wang, D. Wang, and C. Yan, "Calculation and application of Xin'an painting school art style model," *Journal of Physics: Conference Series*, vol. 1651, no. 1, pp. 012033–012051, 2020.
- [4] E. Gardini, M. J. Ferrarotti, A. Cavalli, and S. Decherchi, "Using principal paths to walk through music and visual art style spaces induced by convolutional neural networks," *Cognitive Computation*, vol. 13, pp. 1–13, 2021.
- [5] Z. Yang, "Classification of picture art style based on VGGNET," *Journal of Physics: Conference Series*, vol. 1774, no. 1, pp. 012043–012056, 2021.
- [6] D. A. Ghani and N. M. B. Md Azahar, "Fusion art style of Malaysian & Japanese anime," *International Journal of Innovative Technology and Exploring Engineering*, vol. 8, no. 11s2, pp. 210–218, 2019.
- [7] H. Chen, H. Chen, and Y. Luo, "The artistic style transfer from Shanghai modern landmark buildings images to Xiao Jiaochang New Year pictures based on deep learning," *Journal of Physics: Conference Series*, vol. 1678, no. 1, pp. 012083–012092, 2020.
- [8] Y. Daniel, "Doubled visions: reflexivity, intermediality and co-creation in Clouzot's;and von Trier's and Leth's," *New Review of Film and Television Studies*, vol. 18, no. 4, pp. 452–479, 2020.
- [9] D. Kang, F. Tian, and S. Seo, "Perceptually inspired real-time artistic style transfer for video stream," *Journal of Real-Time Image Processing*, vol. 13, no. 3, pp. 581–589, 2017.
- [10] M. Ruder, A. Dosovitskiy, and T. Brox, "Artistic style transfer for videos and spherical images," *International Journal of Computer Vision*, vol. 126, no. 11, pp. 1199–1219, 2018.
- [11] C. Zhu, W. Yan, X. Cai, S. Liu, T. H. Li, and G. Li, "Neural saliency algorithm guide bi-directional visual perception style transfer," *CAAI Transactions on Intelligence Technology*, vol. 5, no. 1, pp. 1–8, 2020.
- [12] J. Cui, Y. Q. Liu, H. J. Lu et al., "PortraitNET: photo-realistic portrait cartoon style transfer with self-supervised semantic supervision," *Neurocomputing*, vol. 465, pp. 114–127, 2021.
- [13] V. Saman, W. Skalli, A. Bonnet-Lebrun, and M. Khalifé, "A novel dataset and deep learning-based approach for markerless motion capture during gait," *Gait & Posture*, vol. 86, pp. 70–76, 2021.
- [14] J. Plesters, A. Roy, and D. Bomford, "Interpretation of the magnified image of paint surfaces and samples in terms of condition and appearance of the picture," *Studies in Conservation*, vol. 27, no. sup1, pp. 3–176, 2013.
- [15] L. Liliana Vargas Murcia, "Painters in the splendor of tunja: naming unrecognized artists to bring them out of anonymity (XVI and XVII centuries)," *Historia y Memoria*, vol. 15, pp. 49–72, 2017.

Retraction

Retracted: Research on Urban Traffic Industrial Management under Big Data: Taking Traffic Congestion as an Example

Journal of Advanced Transportation

Received 23 January 2024; Accepted 23 January 2024; Published 24 January 2024

Copyright © 2024 Journal of Advanced Transportation. This is an open access article distributed under the Creative Commons Attribution License, which permits unrestricted use, distribution, and reproduction in any medium, provided the original work is properly cited.

This article has been retracted by Hindawi following an investigation undertaken by the publisher [1]. This investigation has uncovered evidence of one or more of the following indicators of systematic manipulation of the publication process:

- (1) Discrepancies in scope
- (2) Discrepancies in the description of the research reported
- (3) Discrepancies between the availability of data and the research described
- (4) Inappropriate citations
- (5) Incoherent, meaningless and/or irrelevant content included in the article
- (6) Manipulated or compromised peer review

The presence of these indicators undermines our confidence in the integrity of the article's content and we cannot, therefore, vouch for its reliability. Please note that this notice is intended solely to alert readers that the content of this article is unreliable. We have not investigated whether authors were aware of or involved in the systematic manipulation of the publication process.

Wiley and Hindawi regrets that the usual quality checks did not identify these issues before publication and have since put additional measures in place to safeguard research integrity.

We wish to credit our own Research Integrity and Research Publishing teams and anonymous and named external researchers and research integrity experts for contributing to this investigation.

The corresponding author, as the representative of all authors, has been given the opportunity to register their agreement or disagreement to this retraction. We have kept a record of any response received.

References

- [1] Y. Zhang, S. Yang, and H. Zhang, "Research on Urban Traffic Industrial Management under Big Data: Taking Traffic Congestion as an Example," *Journal of Advanced Transportation*, vol. 2022, Article ID 1615482, 8 pages, 2022.

Research Article

Research on Urban Traffic Industrial Management under Big Data: Taking Traffic Congestion as an Example

Yi Zhang ^{1,2}, Shuwang Yang,¹ and Hang Zhang³

¹School of Economics and Management, China University of Geosciences, Wuhan 430074, Hubei, China

²Principal's Office, China University of Geosciences, Wuhan 430074, Hubei, China

³Administration for Market Regulation of Henan Province, Zhengzhou 450018, Henan, China

Correspondence should be addressed to Yi Zhang; cughzb@cug.edu.cn

Received 8 April 2022; Accepted 26 May 2022; Published 11 June 2022

Academic Editor: Lingwei Xu

Copyright © 2022 Yi Zhang et al. This is an open access article distributed under the Creative Commons Attribution License, which permits unrestricted use, distribution, and reproduction in any medium, provided the original work is properly cited.

This paper establishes a prediction model of traffic flow, where three cycle dependent components are used to model three characteristics of traffic data, respectively. CNN is used to extract spatial features, and the combination of LSTM and attention mechanism is used to dynamically capture the influence of historical period on target period. Finally, the results are obtained by weighted integration of each component. Its prediction result is more accurate, which can provide reference for governance of urban transportation industry under the background of big data.

1. Introduction

Road congestion has always been the key problem of traffic industry structure governance [1, 2]. Under smart traffic, predicting road conditions can effectively alleviate the urban traffic pressure and promote the transportation industry to upgrade the construction of an intelligent transportation system, which needs the support of a large amount of data [3, 4]. Only in this way can we ensure the stable operation of intelligent transportation system and bring better traffic experience to users. In the early years, urban traffic relied on manual management, which could only implement manual traffic control according to past data [5]. However, with the increasing number of vehicles, traffic problems can no longer be solved by manual management. The emergence of big data has become the development and application of “timely rain,” which accelerates the collection speed of traffic data and also improves the accuracy and efficiency of data processing. Therefore, applying big data technology to urban smart traffic system is the need of urban transportation development and traffic management [6].

The urban smart traffic management system is still in the initial stage of development in China, and the traffic systems in many cities are moving closer to this direction, gradually

realizing intelligence, abandoning the traditional manual control mode [7], and can better and more scientifically solve the traffic congestion problem. The urban smart traffic system relies on computer artificial intelligence to deal with complex traffic problems, which is a combination of automatic control and computer technology. In the face of real traffic problems, it can obtain the traffic situation in real time and provide data support for traffic management. In addition, in the development of China's urban smart traffic system, the traditional traffic management system has not been completely abandoned, but integrated with it, and on the basis of China's urban development road construction work, the problem of urban traffic has been scientifically dealt with [8]. However, when the system is applied, it needs to be analyzed and calculated based on the massive data of local urban traffic conditions. In order to select the best traffic improvement scheme, we can not only reduce the manpower and material resources consumed by the urban traffic system [9] but also reduce energy consumption through rational planning routes and improve the current and future urban environmental quality in China.

This paper establishes a traffic flow prediction model for traffic congestion prediction of vehicles under big data,

aiming to provide reference for urban traffic industry governance under the background of big data.

2. Urban Intelligent Traffic Detection System under Big Data

2.1. Intelligent Traffic Control. Intelligent traffic control system relies on integrated management and command and dispatch system to control road traffic conditions. The intelligent traffic control system collects the traffic information from the front devices installed at the intersection and sends the collected information back to the central management system of the control center for comprehensive management, and directly reflects the traffic information on the GIS ground through the integrated information platform of the base GIS. At the same time, traffic controllers control devices through GIS platform to divert road traffic.

It is built around intelligent transportation system (ITS), which integrates advanced information technology, computer processing technology, sensor technology, data communication technology, and electronic automatic control into the traditional transportation system. A real-time, efficient, and accurate comprehensive transportation management system [10] is established by organically combining the environment of pedestrians and vehicles, which can alleviate urban traffic congestion and reduce traffic accidents.

2.2. Intelligent Traffic Congestion Control. Traffic congestion is considered as any event which combines low vehicle speed and long queues of these slow-moving cars [11].

The detection of traffic congestion is to detect all kinds of traffic incidents and accidents in a timely, rapid, and comprehensive manner, improve the response time to deal with emergencies, grasp the real situation on the scene in a timely and accurate manner, implement the right measures at the first time, and avoid the occurrence of second incidents. The architecture of the traffic event detection system is shown in Figure 1. Its functions include: real-time monitoring of traffic conditions on accident-prone sections; realize real-time monitoring of traffic condition of main and auxiliary road sections of diverging and merging; realize real-time monitoring of traffic condition of main road. The traffic event detection system combines camera and detection control unit to collect traffic event information through video camera or electromagnetic induction, and transmits the collected traffic event information to the control center in real time through the cable network. In some places that are not conducive to camera installation, the video detector cannot be used for spot placement, and the induction system such as circular coil/geomagnetic infrared can be used.

3. Shortcomings and Development of Intelligent Traffic Detection System

The above-mentioned intelligent detection system mainly sends the connected information to the application server through the vehicle, and then the application server forwards

all the information to the cluster, which belongs to the high-frequency track road condition prediction. Therefore, whether it is the traditional statistical method or the single machine learning method, the prediction accuracy of these models is low and the applicability of these models is poor [12].

Forecasting short-term traffic passenger flow is a complex nonlinear problem, which greatly increases the difficulty of passenger flow forecasting because of its characteristics such as nonstationarity, randomness, and sudden change, especially the short-term passenger flow changes too fast and there are too many random influencing factors, resulting in less obvious regularity. Therefore, it is more difficult to predict [13]. Therefore, scholars at home and abroad have also carried out related research. Among all the methods for short-term traffic flow prediction, the neural network model is popular because of its superiority in processing multidimensional data, flexibility of model structure, adaptability to fresh samples, and learning ability.

With the increasing capacity of computer and the iterative upgrade of neural network algorithm, there are more and more research studies on short-term traffic flow prediction by the neural network [14]. Among them, the recurrent neural network (RNN), the convolutional neural network (CNN), and the long and short-term memory network (LSTM) are considered as more appropriate methods to capture the spatiotemporal characteristics of traffic flow [15].

4. Prediction Model of Road Condition

With the development of computer technology, target detection technology is widely used in real-time detection of objects, including target location and identification [16]. Real-time target detection is widely used in intelligent transportation. For example, real-time vehicle location and other current vehicle detection methods are mainly divided into two categories [17]: traditional methods based on machine learning and methods based on deep learning. The traditional methods of basic machine learning generally include two links: feature extraction and classification according to features. In addition, support vector machine (SVM) or AdaBoost is used to classify the extracted histogram gradient features or Harr features, while the methods based on deep learning mainly include R-CNN, Fast R-CNN, Faster R-CNN, MaskR-CNN, YOLO, YOLOV2, YOLOV3 SSD. The feature extraction ability of the convolutional neural network is used to extract the vehicle feature information, and then the features are classified by a classifier.

4.1. Overview of Neural Network

4.1.1. Concept and Development. Artificial neural network refers to a kind of empirical model composed of multiple neurons that can imitate the actions of biological neural units, and similar to biological neural units, one neural unit can not only receive a single stimulus input signal but also receive multiple segments of stimulus input signals at the same time, and the connection between two neurons can

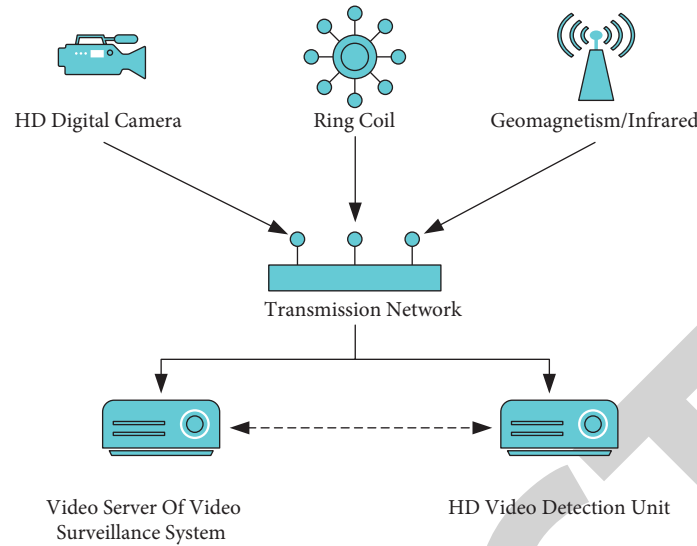


FIGURE 1: Architecture of traffic congestion detection system.

send signals to the output port. Of course, the relationship between input and output is not linear. Therefore, this neural network can be used to simulate all kinds of chaotic signal relationships to realize the original design intention. Through the development of neural network, the neural network model will have more complicated structures and richer parameters with the increase of layers. Therefore, it possesses stronger fitting ability when dealing with major data problems.

4.1.2. Long and Short-Term Memory Network. LSTM is a variant of RNN network. The change lies in that it adds memory characteristics on the basis of RNN, which can endow neural network with long-term memory ability and make the model have good applicability to long-term series.

Generally, it is only necessary to set up a four-layer structure to build the LSTM model, as shown in Figure 2.

- (1) Input layer, where one-dimensional time series data is usually input
- (2) LSTM layer, it is also the feature of the LSTM neural network. Three gating units in neurons are the obvious features of LSTM which are different from the traditional circular neural network. They are the input gate forgetting gate and the output gate. Because of the addition of gating units, the problems of gradient disappearance and long-distance dependence have been effectively alleviated.
- (3) Fully connected layer, the role of fully connected layer in the LSTM model is to transform the data from high dimension to low latitude, which increases the complexity of the model while retaining useful information.
- (4) Output layer is mainly responsible for outputting the results of neural network model operation, and there are many prediction scenarios.

The internal structure of LSTM is shown in Figure 3. The gate unit is expanded on the basis of RNN, and the complexity of the hidden layer is improved. The gate unit includes input gate, output gate, memory gate, and forget gate:

- (1) Input gate: filter from input to decide whether to save the information
- (2) Forget gate: determine whether the state information of the current neuron should be discarded
- (3) Output gate: it determines whether the information state of the current neuron should be output
- (4) Memory gate: the new input is filtered to determine which information can be preserved. Through the cooperation of different gate units in the hidden layer, the information is no longer updated indefinitely, but is filtered and removed in an orderly manner, which effectively solves the problem of gradient disappearance and realizes the preservation of long-time series data memory.

Because LSTM introduces the structure of three gates, especially the forget gate that determines whether the current neuron state information should be discarded, LSTM has a better performance than RNN when dealing with time series problems with long intervals and delays. LSTM can control the convergence of gradient during training; thus, the problem of gradient disappearance or explosion can be alleviated. At present, there are two algorithms used to train the LSTM model, namely, back propagation through time (BPTT) and real-time recursive learning algorithm (RTRL). In this paper, the BPTT algorithm is used to build the network model for that it is simpler and clearer in concept, and it can calculate data faster. Except for the prediction of time series data, LSTM has made great achievements in the fields of speech processing machine, image interpretation, handwriting generation, image generation, and so on.

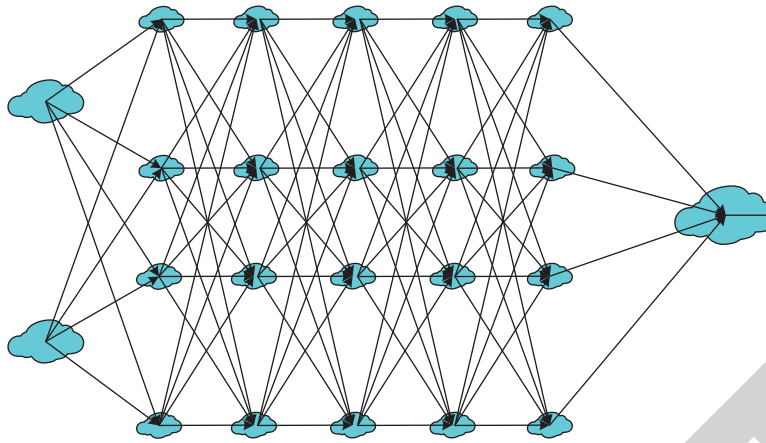


FIGURE 2: Diagram of LSTM structure.

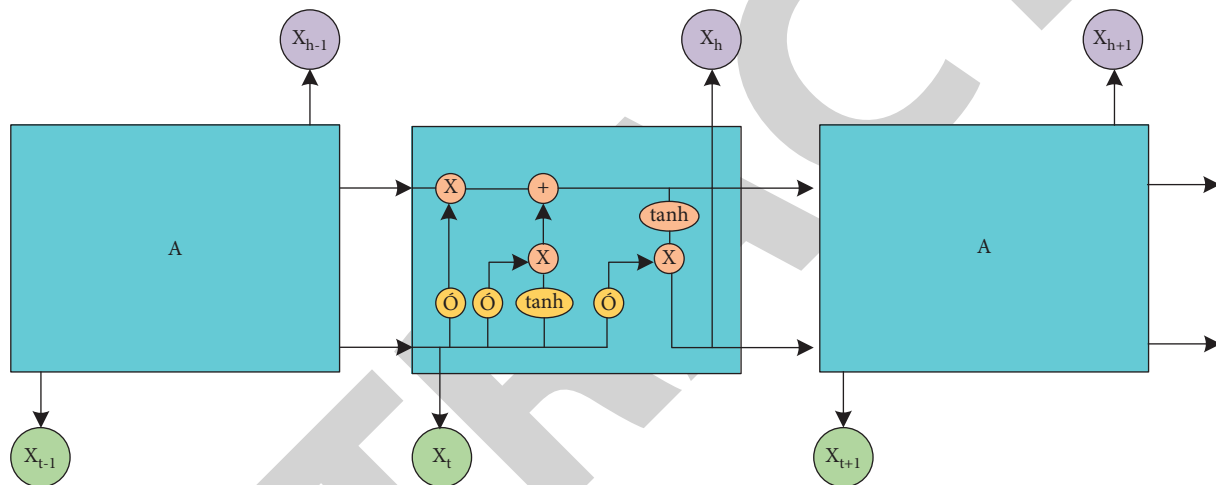


FIGURE 3: Internal structure diagram of LSTM.

4.1.3. Convolutional Neural Network. Convolutional neural network is abbreviated as “CNN,” and its network structure generally consists of three parts, namely, convolution layer, pool layer, and fully connected layer for this type of input of pictures. A single convolution layer can realize simple extraction of data features, and more layers of networks can extract more complex features from basic features through iterative training. Multilayer network can extract more deep features from data and improve the effect of the model. CNN has a relatively simple structure and generally takes the BPTT algorithm for training, which makes it a very classic deep neural network model. Convolutional neural network generally consists of input layer, convolution layer, pooling layer, fully connected layer, and output layer, as shown in Figure 4.

The core of CNN lies in convolution layer and pooling layer, which needs to cooperate with other layers to complete the construction of neural network model.

- (1) Input layer: it is the window of data input, and the input of convolutional neural network is a two-dimensional matrix, which is usually a picture.

- (2) Convolution layer is composed of multiple convolution kernels, and the local high-dimensional features of samples are extracted layer by layer through convolution calculation.
- (3) Pooling layer, which realizes downsampling by pooling function, it reduces the dimension of data, improves the computational efficiency of CNN, and at the same time, retains important information in sample data.
- (4) Fully connected layer, which performs full connection operation on related information after convolution and pooling for many times, increasing the complexity of convolutional neural network.
- (5) Output layer is used to calculate the previous sample data and output the calculation result.

Compared with the traditional neural network, the convolutional neural network has the feature of small-scale local convolution weight sharing pooling and dimension reduction. Unlike the feature extracted by the traditional neural network, which is the overall feature, the small-scale

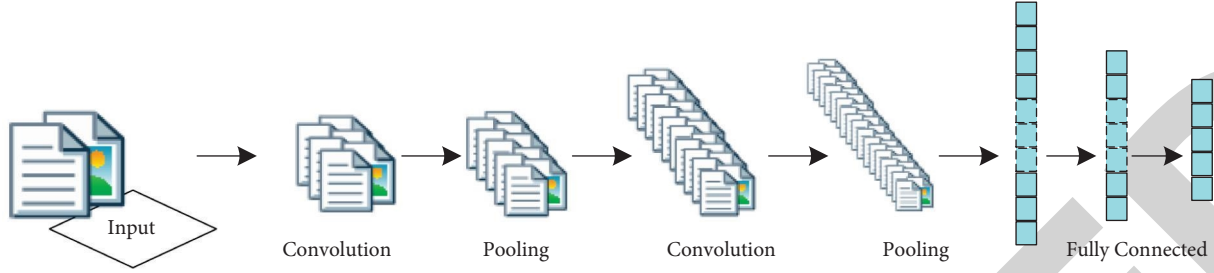


FIGURE 4: CNN network model.

local convolution of the convolutional neural network can be used to convolve the sample matrix data through the convolution kernel in the convolution layer. Each time, only a small part of the matrix data is covered, and then multiple convolution kernels are used to operate so that the high-dimensional local features of the matrix can be obtained, which is more conducive to extracting the local features of the data.

4.2. The Establishment of Prediction Model on Traffic Flow

4.2.1. Definition of Traffic Flow. Traffic flow is random, which is a complex problem and will be affected by many factors. In the spatial dimension, for continuous road sections, the traffic situation of the previous road section will affect the traffic situation of the next road section. For example, the traffic jam in the previous road section will affect the traffic flow of the next section. In this paper, the traffic flow data of continuous road sections are used as input, and the idea of forecasting the traffic flow at the end time is studied.

On the road section i , use total n periods of traffic flow in the past $[t - n + 1, t]$ under the upstream and downstream sections $[i - m, i + m]$ so as to forecast traffic of $t + 1$ time period.

Make the historical traffic flow in the form of space-time matrix, as shown in formula (1). This spatiotemporal input matrix includes all traffic information of the target road section and adjacent road sections in time and space. Each row in the matrix represents the traffic flow of n periods in the same section with time interval of $[t - n + 1, t]$; each column represents $2m + 1$ road section traffic flow on road section range $[i - m, i + m]$ at a certain moment.

$$X_{i,t} = \begin{bmatrix} x_{i-m,t-n+1} & x_{i-m,t-n+2} & L & x_{i-m,t} \\ M & M & L & M \\ x_{i-1,t-n+1} & x_{i-1,t-n+2} & L & x_{i-1,t} \\ x_{i,t-n+1} & x_{i,t-n+2} & L & x_{i,t} \\ x_{i+1,t-n+1} & x_{i+1,t-n+2} & L & x_{i+1,t} \\ M & M & L & M \\ x_{i+m,t-n+1} & x_{i+m,t-n+2} & L & x_{i+m,t} \end{bmatrix}, \quad (1)$$

where $x_{i,t}$ represents the traffic flow at section i , time t .

$X_{i,t}$ can also be expressed as n column vectors in chronological order, as shown in formulas (2) and (3):

$$X_{i,t} = [T_{i,1} \ T_{i,2} \ L \ T_{i,t} \ T_{i,n}], \quad (2)$$

$$T_{i,t} = [x_{i-m,t} \ K \ x_{i-1,t} \ x_{i,t} \ x_{i+1,t} \ L \ x_{i+m,t}]^T, \quad (3)$$

where $T_{i,t}$ is the vector composed of traffic flow of target road section i and upstream and downstream road section at time t .

4.2.2. CNN Model. The traffic state changes of the upstream and downstream sections are related, and the traffic flows between sections will influence each other. For example, traffic congestion caused by an accident in the upstream section will reduce the traffic flow in the downstream section. In order to reflect the correlation between such traffic sections, CNN can be used to capture its spatial characteristics.

Input the scaled time series into the CNN to learn the spatial characteristics. Input convolution layer K into $X_{i,t}$. The convolution formula is calculated as follows:

$$Y_{i,t}^{(K^*)} = \text{Relu}(W_k * X + b_k), \quad (4)$$

where K represents the number of convolution layers; the symbol $*$ represents the convolution operation; ReLU is the activation function; W_k and b_k are two sets of parameters in the K -th convolution layer.

At this time, the spatial features of the three time-dependent features are as follows: short-time dependent component spatial feature $y_{i,t}$, daily period-dependent component spatial feature $y_{i,t}^p$, and weekly period-dependent component spatial feature $y_{i,t}^w$, which are taken as the input of LSTM.

4.2.3. LSTM Model. LSTM is used to capture the dependence in time series, and attention mechanism is incorporated to dynamically capture the influence of historical period on target period.

In this paper, the data of the first W weeks and the first P days are input, and the traffic data of time period $[t - q, t + q]$ are extracted from each first P day and input into the daily cycle component to solve the problem of daily cycle dependence, and the traffic data of time period $[t - q, t + q]$ is extracted from each first W week and input into the weekly cycle component to solve the problem of cycle dependence.

LSTM is used to extract time information of different scales as shown in formulas (5) and (6):

$$h_{i,t}^{p,q} = LSTM(y_{i,t}^p, h_{i,t}^{p,q-1}), \quad (5)$$

$$h_{i,t}^{w,q} = LSTM(y_{i,t}^w, h_{i,t}^{w,q-1}), \quad (6)$$

where $h_{i,t}^{p,q}$ is the representation of section i in the middle period q of the P -th day; $h_{i,t}^{w,q}$ is the representation of section i in the middle period q of the w -th week; $y_{i,t}^p$ and $y_{i,t}^w$ are the spatial features.

At this time, the influence of traffic in different historical periods on the future forecast target is different. Therefore, attention mechanism is introduced to dynamically adjust the influence of different historical periods on the future forecast results.

The importance value $\alpha_{i,t}^{p,q}$ at different time of day is obtained by comparing the temporal and spatial features $h_{i,t}$ learned by the short-time component with the hidden state $h_{i,t}^{p,q}$. The importance values $\alpha_{i,t}^{w,q}$ at different times of the week can be obtained similarly. The calculation of significance α uses the attention mechanism, as shown in formulas (7) and (8):

$$\alpha_{i,t}^{p,q} = \frac{\exp(\text{score}(h_{i,t}^{p,q}, h_{i,t}))}{\sum_{p \in P} \exp(\text{score}(h_{i,t}^{p,q}, h_{i,t}))}, \quad (7)$$

$$\alpha_{i,t}^{w,q} = \frac{\exp(\text{score}(h_{i,t}^{w,q}, h_{i,t}))}{\sum_{w \in W} \exp(\text{score}(h_{i,t}^{w,q}, h_{i,t}))}. \quad (8)$$

The scoring function used in this paper is additive model, such as formulas (9) and (10):

$$\text{score}(h_{i,t}^{p,q}, h_i) = v^{T1} \tanh(W_{H1} h_{i,t}^{p,q} + W_{X1} h_i + b_{X1}), \quad (9)$$

$$\text{score}(h_{i,t}^{w,q}, h_4) = v^{T2} \tanh(W_{H2} h_{i,t}^{w,q} + W_{X2} h_4 + b_{X2}), \quad (10)$$

where $W_{H1}, W_{X1}, b_{X1}, v^{T1}, W_{H2}, W_{X2}, b_{X2}$, and v^{T2} are all parameters learned through training, and v^T represents the transposition of v .

The weighted sum of each time interval q on day P is expressed as $h_{i,t}^p$. The weighted sum $h_{i,t}^w$ of the corresponding period of the previous w week is calculated as formulas (11) and (12):

$$h_{i,t}^p = \sum_{q \in Q} \alpha_{i,t}^{p,q} h_{i,t}^{p,q}, \quad (11)$$

$$h_{i,t}^w = \sum_{q \in Q} \alpha_{i,t}^{w,q} h_{i,t}^{w,q}, \quad (12)$$

where $\alpha_{i,t}^{p,q}$ represents the importance of the time interval q in the P -th day; $\alpha_{i,t}^{w,q}$ represents the importance of the time interval q in the w -th week.

Use an LSTM to save these cycle dependency information, and the dynamic dependencies of the daily cycle component and the weekly cycle component of the final output are as follows:

$$\begin{aligned} \mathcal{S}_{i,t}^W &= LSTM(h_{i,t}^p, h_{i,t}^{p-1}), \\ \mathcal{H}_{i,t}^w &= LSTM(h_{i,t}^w, h_{i,t}^{w-1}). \end{aligned} \quad (13)$$

4.2.4. Combined Model. $h_{i,t}^c$ is obtained by weighted fusion of short-term dependence, daily cycle dependence, and weekly cycle dependence, while the time dependence of the predicted road section is retained. The calculation is as shown in formula (14):

$$h_{i,t}^c = W_{\theta 1} \circ \hat{h}_{i,t}^p + W_{\theta 2} \circ \hat{h}_{i,t}^w + W_{\theta 3} \circ h_{i,t}, \quad (14)$$

where $W_{\theta 1}, W_{\theta 2}, W_{\theta 3}$ are the learned parameters; \circ is the Hadamard product. Input $h_{i,t}^c$ to the fully connected layer and activate it with tanh function. The final prediction result is output y , which is calculated as follows:

$$y = \tanh(W_{\beta} h_{i,t}^c + b_{\beta}), \quad (15)$$

where W_{β} and b_{β} are all parameters learned through training.

The output forecast result of is saved in the file with suffix "pickle," and the predicted traffic flow range is between $[0, 1]$. In order to facilitate the analysis, the result data should be played back to the same range of the original data according to the same proportion so that the evaluation index can be calculated later.

5. Test Analysis

5.1. Parameter Setting. In the establishment of the neural network, parameters in the model should be set. The convolution layer K of the convolutional neural network is set as 3, the convolution kernel is set as 64 with a size of 3×3 , the convolution step is set as 1, and the activation function is ReLU. MAE and RMSE are used for all evaluation indexes. Simulation parameters are shown in Table 1.

5.2. Analysis of Results. CNN-LSTM model was used to predict the traffic flow, and the change of the loss function of the model with the increase of training times on working days was studied, as shown in Figure 5. As can be seen from the trend diagram, the loss function of the CNN-LSTM model during weekday training decreases with the increase of the number of training iterations, and rapidly declines in the first 50 iterations, after which the curve gradually flattens out. When the training iteration reaches 600 times, the loss function of CNN-LSTM model is in a stable state.

When the training iteration was 600 times, the loss function of the model on the rest day test set was in a relatively stable state. After 600 training sessions, even if the number of iterations is increased, the loss function does not change significantly but increases the complexity of model calculation and the risk of overfitting. Therefore, the selection of 600 iterations is appropriate, which verifies the rationality of the grid search algorithm.

Figure 6 shows the predicted value curve and real value curve of traffic flow of the CNN-LSTM model in a certain working day time area. It can be seen from the figure that the CNN-LSTM model can accurately predict the change of traffic flow on weekdays, and the predicted value has a good fitting degree with the real value. Compared with the LSTM prediction model, the CNN-LSTM model extracted the

TABLE 1: Simulation parameters.

Parameters	Value
Daily and weekly components	$w=1, P=3,$ and $q=5$
Dimension of hidden layer in LSTM	128
Batch	64
Learning rates	0.001
Dropout	0.5

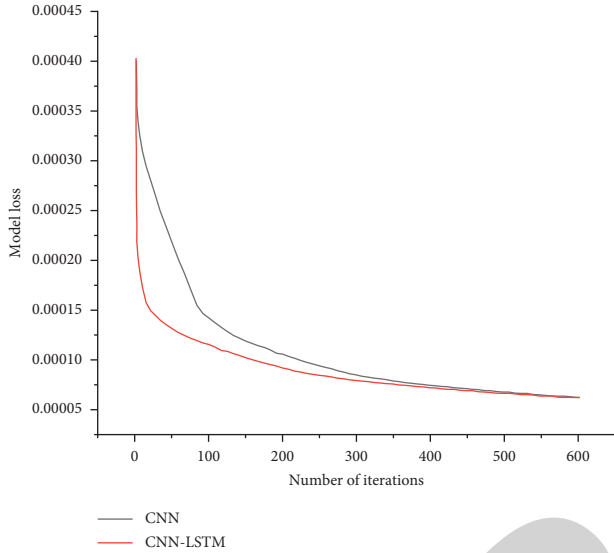


FIGURE 5: Model loss l under 600 iterations.

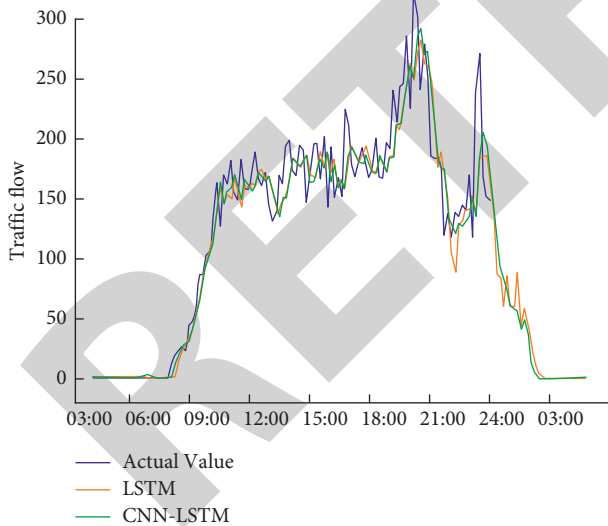


FIGURE 6: Traffic flow prediction under CNN-LSTM model.

TABLE 2: Analysis of experimental results.

Model	Running time (second)	MAE	RMSE
LSTM	121.03	21.07	28.94
CNN	98.71	20.41	28.22
LSTM + CNN	69.20	18.75	24.87
LSTM + CNN + ATTENTION	45.22	15.61	21.52

characteristics of passenger flow between stations and predicted the subway passenger flow from the time and space dimensions. The fitting of the model has better accuracy. In addition, the forecast curve of passenger flow on weekends is smoother, which is caused by the randomness of passenger flow on weekends.

The performance results of short-term traffic flow forecast are shown in Table 2. By using different methods to experiment on the same data set, comparing MAE and RMSE of each model, it is found that the model proposed in this paper has the best effect. According to the results in the table, if only CNN is adopted, the model only considers spatial correlation and ignores temporal information, while LSTM only considers temporal correlation and ignores spatial information. Although the CNN + LSTM model extracts time and spatial correlation at the same time, it does not dynamically consider the influence of each historical period on the target period.

From the experimental results, the running time of LSTM + CNN + ATTENTION is smaller than the LSTM and CNN. The smaller the MAE and RMSE index values are, the smaller the model error is and the better the prediction effect is. In contrast, the combined model proposed in this paper based on CNN, LSTM, and attention mechanism is better than the other three models, and its MAE and RMSE values are 15.61 and 21.52, which improves 25.91% and 25.64%, respectively, which shows that this model can accurately predict the traffic flow in different time series, thus effectively reducing traffic jams.

6. Conclusion

Traffic flow prediction is one of the key technologies of the intelligent transportation system, which can effectively solve the traffic jam problem. In this paper, three-time characteristic components are used to predict the traffic flow in the future where CNN is used to extract spatial features, LSTM and attention mechanism are used to dynamically extract temporal features, and finally, test of traffic prediction is implemented. The results show that, compared with the other three traffic flow forecasting models, the combined model proposed in this paper based on CNN, LSTM, and attention mechanism has better effect, and its MAE and RMSE values are 15.61 and 21.52, respectively, which shows that this model can accurately forecast traffic flows in different time series, thus effectively reducing traffic jams.

Data Availability

The dataset can be accessed upon request.

Conflicts of Interest

The authors declare that they have no conflicts of interest.

References

- [1] I. Goodfellow, Y. Bengio, and A. Courville, *Deep Learning*, MIT Press, Cambridge, MA, 2016.

Retraction

Retracted: Integration and Application of Online Sports Resources Based on Multidimensional Intelligent Technology and Resource Optimization Architecture

Journal of Advanced Transportation

Received 8 August 2023; Accepted 8 August 2023; Published 9 August 2023

Copyright © 2023 Journal of Advanced Transportation. This is an open access article distributed under the Creative Commons Attribution License, which permits unrestricted use, distribution, and reproduction in any medium, provided the original work is properly cited.

This article has been retracted by Hindawi following an investigation undertaken by the publisher [1]. This investigation has uncovered evidence of one or more of the following indicators of systematic manipulation of the publication process:

- (1) Discrepancies in scope
- (2) Discrepancies in the description of the research reported
- (3) Discrepancies between the availability of data and the research described
- (4) Inappropriate citations
- (5) Incoherent, meaningless and/or irrelevant content included in the article
- (6) Peer-review manipulation

The presence of these indicators undermines our confidence in the integrity of the article's content and we cannot, therefore, vouch for its reliability. Please note that this notice is intended solely to alert readers that the content of this article is unreliable. We have not investigated whether authors were aware of or involved in the systematic manipulation of the publication process.

Wiley and Hindawi regrets that the usual quality checks did not identify these issues before publication and have since put additional measures in place to safeguard research integrity.

We wish to credit our own Research Integrity and Research Publishing teams and anonymous and named external researchers and research integrity experts for contributing to this investigation.

The corresponding author, as the representative of all authors, has been given the opportunity to register their agreement or disagreement to this retraction. We have kept a record of any response received.

References

- [1] T. Chu, "Integration and Application of Online Sports Resources Based on Multidimensional Intelligent Technology and Resource Optimization Architecture," *Journal of Advanced Transportation*, vol. 2022, Article ID 2333497, 9 pages, 2022.

Research Article

Integration and Application of Online Sports Resources Based on Multidimensional Intelligent Technology and Resource Optimization Architecture

Ting Chu ^{1,2}

¹Haikou University of Economics New Silk Road Fashion Sports Institute, Haikou 571127, China

²Shanxi Vocational University of Engineering Science and Technology, Jinzhong 030619, China

Correspondence should be addressed to Ting Chu; chuting@sxgkd.edu.cn

Received 25 April 2022; Accepted 13 May 2022; Published 3 June 2022

Academic Editor: Lingwei Xu

Copyright © 2022 Ting Chu. This is an open access article distributed under the Creative Commons Attribution License, which permits unrestricted use, distribution, and reproduction in any medium, provided the original work is properly cited.

Share the relevant factors of the overall structure of the sports network in colleges and universities, and divide the overall structure of its operation system. In view of the unequal division of educational resources, this paper proposes the construction content of the college sports network education resource sharing mechanism: the construction of college sports network education resources, the college sports network education resource sharing platform, and the management and coordination of college network education resources sharing. In the guidance of cybernetics based on the basic characteristics of network education resources, the sharing of sports network education resources is realized, so as to effectively build a scientific evaluation index system.

1. Introduction

With the development of computer technology and network communication technology, the network has become the main channel for most people to obtain information in their study and life, and network teaching has gradually become a modern education tool that responds to the development of the times and society [1]. Based on the powerful information dissemination ability, excellent resource sharing performance, advanced two-way interaction and multimedia technology of computer network, modern distance education can provide rich teaching resources and flexible teaching forms for teaching, improve students' learning initiative and flexibility, and facilitate individualized teaching and learning [2]. In view of the contradiction of physical education courses in terms of space and learning and training, the reform of physical education in colleges and universities should make full use of the advantages of modern distance education, integrate course resources, expand teaching time and space, and enrich teaching methods, so that physical education can meet the requirements of social development.

Modern distance education refers to the form of education in which students and teachers, and students and educational institutions are linked by distance education system teaching and communication mainly using multiple media means [3]. It is a new form of education that occurs with the development of modern information technology and is the main means of constructing people's lifelong learning system in the era of knowledge economy [4]. In China, there have been traditional one-way distance education teaching forms such as television video teaching, electric university, and correspondence course, which have limited learning time and space, and the teaching media are used as presentation tools rather than cognitive tools and cannot realize interactive and independent learning [5]. Modern distance education is a new two-way interactive education mode formed with the development of multimedia technology, network, and communication technology, which is the main means to build people's lifelong learning system in the era of knowledge economy, with the adaptability of time and space and the openness and interactivity of education way and enriches the teaching content, increases students' interest in learning and self-

motivation, expands the knowledge, can cultivate students' ability to work in science and technology, can provide timely feedback, and to a large extent solves the problem of optimal combination of cross-regional teacher distribution [6, 7]. It takes advantage of the advanced communication network to transmit information, it can realize interactive and independent learning across time and space [8]. Modern distance education is a major project to make full use of and optimize China's educational resources, popularize and improve the quality of education, form an open education network, and build a lifelong learning system [9].

Modern distance education can disseminate information in large capacity, high speed, and wide range, and with the help of multimedia technology, it can build rich teaching resources, break the time and space limitation of students' learning, and improve students' autonomy and enthusiasm of learning [10]. For physical education courses, learners can learn various theoretical knowledge and sports skills from the Internet at any time and place, overcoming the influence of venue, time, or climate [11]. At the same time, the problems of difficulty in explaining, understanding, and repeating various body movement techniques involved in physical education can also be solved by collecting the standard movements of sports stars in large sports events through multimedia videos, animations, or websites [12]. The problem can also be solved by using multimedia videos, animations, or websites to collect standard movements of sports stars in major sports events to assist teaching [13].

Network course teaching is the specific embodiment of applying computer network technology to teaching, which is a new teaching mode based on multimedia, computer network, and international Internet, and is teaching that extends the classroom to the campus network and the Internet, so that the resources can be shared throughout the school or even nationwide and globally [14, 15]. If sports distance education can be carried out on the basis of existing sports network course resources, this can solve the learning problem of many people who want to learn but cannot study at school (rural primary and secondary school physical education teachers, social sports workers, athletes, and coaches), and at the same time, the tuition fees of distance education can be used for the subsequent development of the curriculum, thus making the network course resources sustainable [16].

This paper proposes the construction content of the sharing mechanism of college sports network education resources: the construction of college sports network education resources, the sharing platform of college sports network education resources, and the management and coordination of college network education resources sharing.

2. Related Work

Although a large number of educational information resources already exist on the Internet, these resources are in a disorganized state, and therefore, suggestions are made to increase the construction of online educational information resources [17]. In the information-based society, online

education is gaining more and more recognition and advantages with its unique mode and distance education has formed a global trend, while online education cooperation and international competition are being strengthened [18]. Some famous distance education systems have already implemented global teaching, and 90% of the colleges and universities in the United States, which is the largest country in the network distance education model, have carried out network program education with the Internet as the main means, and about 3,000 network courses are open to people of different levels, and more than 7,000 people have obtained the corresponding degrees through network courses.

In order to better implement the spirit of the above-mentioned documents, the national school sports workers face the modern information environment, the development and integration of college physical education curriculum resources, physical education teaching methods and models of innovation and physical education network teaching and other aspects of active attempts and exploration [19]. Most of the existing national and provincial and municipal fine sports resources have been networked to a certain extent, but by visiting the national fine course resource network and obtaining the national and provincial fine sports courses included in it, we found that the number of sports professional courses is more than that of university sports courses, and the teaching resources of national fine courses are more networked than that of provincial fine courses [20]. The network is larger than that of provincial and municipal level. The network platform construction for physical education in some national key universities has been paid attention to by universities, and more than 50% of the physical education courses in 211 universities have adopted network teaching to some extent, while few physical education courses in general undergraduate institutions have adopted network teaching. Compared with other disciplines, the level of university physical education network platform is still low, just reaching the level of network-assisted teaching.

3. Definition of Related Concepts

3.1. Educational Resources. Educational resources include the sum of educational knowledge, educational experience, educational skills, educational assets, educational costs, institutions, educational brands, educational personalities, educational concepts, educational facilities, and interpersonal relationships inside and outside the educational field, which have been created and accumulated by human society through the long evolution of civilization and educational practices since the beginning of educational activities and educational history. According to the available information, educational resources were first defined in China as "the financial, human and material resources provided by society for education."

3.2. College Sports Network Education Resources. The concept of college sports network education resources is the core concept of this paper. People usually call the combination of network resources and college education applications as

college network education resources. College network educational resources are also usually expressed as educational information resources, and in daily research, college network educational resources and educational information resources are usually used in place of each other. The definition of college sports network resources in this study refers to the college sports network resources that belong to the category of educational information resources in a narrow sense, that is, the college network educational information resources in the classification of college network education resources proposed by [12]. According to the requirements of the scope of this paper and their use and existence in physical education, college sports network education resources are roughly divided into nine types, such as physical education media materials, physical education audiovisual teaching materials, physical education multimedia courseware, physical education reading materials, physical education college network courses and high-quality courses, physical education teaching resource library, physical education websites, and college physical education network teaching resource management application platform types.

4. Constructing the Operation System of College Sports Network Education Resources Sharing

The ultimate goal of sharing college sports network education resources is to achieve the sharing of valuable sports network education resources. Through the coordination among all elements, a scientific and reasonable regional college sports network education resources sharing operation system is built to realize the effective operation of the college sports network education resources sharing mechanism in the region.

4.1. Element Composition. The regional university sports network education resource sharing mechanism is a multidisciplinary, complex and open system involving many factors, so it is necessary to establish the main position of users in the sharing from a holistic perspective to meet the users' needs for sports. In order to establish the main position of users in the operation of the sharing mechanism, it is necessary to understand the real needs of users and to build a management and coordination institution with macroscopic control to carry out macroscopic overall planning and coordinated development. The sharing platform, technology, talents, funds, and policies are the guarantee support for sharing. Without support, even the best educational resources and the best management and coordination service mechanism cannot be realized. Therefore, the real demand, sharing platform, management and coordination, guarantee mechanism, and the most basic college sports network education resources constitute the elements of the regional education resources sharing system. Under the guidance of sharing concept, as a complete system, each element is mutually supportive and collaborative and is an indispensable system as a whole. The relationship of each element is shown in Figure 1.

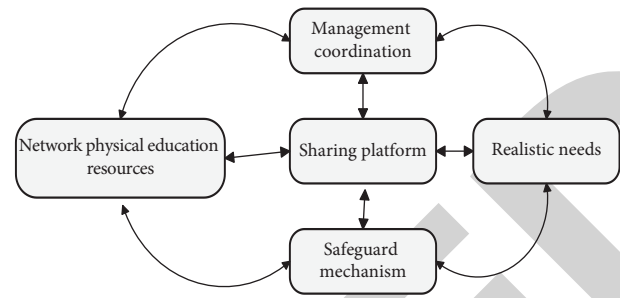


FIGURE 1: Elements of the operation system of regional university sports network education resource sharing.

4.2. Framework of Operation System. The fundamental purpose of constructing the operation system of regional university sports network education resources sharing is to make full use of the Internet to establish an effective operation mechanism for regional university sports network education resources sharing and to improve the user's ability to know and obtain university sports network education resources.

Based on the purpose of building the sharing operation system, the framework of the sharing operation system must be guided by scientific concepts and provide nontechnical support for other sharing work. The construction of college sports network education resources, which is the object of college sports network education resources sharing, is the focus of the system and the guarantee for the effective operation of the college sports network education resources sharing mechanism. The construction of college sports network education resources platform provides technical support for regional college sports network education resources sharing. At the same time, the management and coordination mechanism is used as an auxiliary tool to manage the construction and sharing process of education resources [21, 22]. The sharing guarantee system is divided into technical support, sharing method, institutional guarantee, sharing mechanism, and sharing price, which provide technical and nontechnical guarantee for effective sharing of resources. The effective incentive mechanism and the effective sharing incentive mechanism as a promotion as shown in Figure 2.

4.3. Architecture Design of Education Resource Library. The college sports network education resource library is mainly a resource library system that provides teaching support for college sports network teaching and promotes teachers' teaching and students' learning and exercise of basic sports knowledge and skills. It is constructed in accordance with the unified technical specifications and the inner logical relationship of the curriculum in accordance with international standards, is composed of excellent digital sports media materials, knowledge materials, and exemplary teaching cases and other basic materials for sports teaching, and is an entity carrying sports education resources and an open sports network teaching support system that can be expanded continuously. Its basic position is to build a network education and database that can meet the needs of

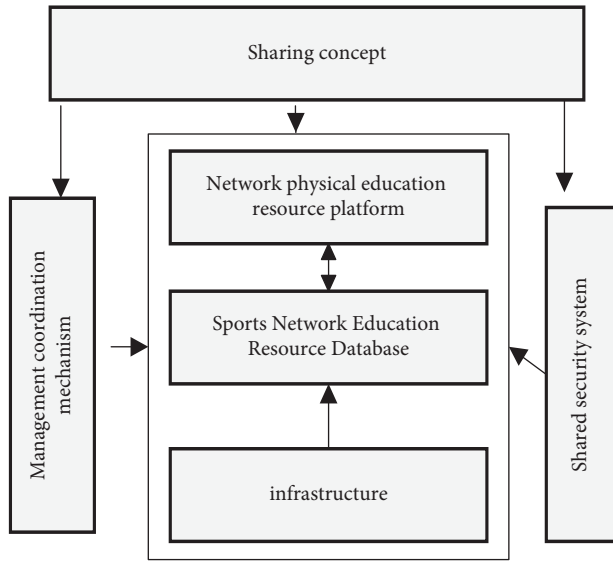


FIGURE 2: Framework of regional Korakan sports network education resource sharing system.

physical education teaching, scientific research, technology development, and teaching management in colleges and universities, to build a knowledge network and knowledge service network, and to provide core physical education network education resources for the physical education network education platform [23]. Its functions include physical education resource collection, resource verification and storage, resource retrieval, and resource browsing and downloading. Based on the basic positioning of the university sports network education resource library and its functions, the architecture structure is shown in Figure 3.

The physical education network education resource management system in colleges and universities is a functional facility for managing, maintaining, and updating the physical education resources stored in the resource library media and is the support system of the network teaching resource library. The resource library management platform realizes scientific and reasonable composition and management of physical education network teaching resource library, which is conducive to the advantages of physical education network teaching resource library and thus to the teaching and learning of physical education in colleges and universities. The teaching and learning management support platform provides a flexible, scalable, interactive teaching and learning support environment suitable for multiple levels, multiple objects, and multiple network environments and supports various teaching modes such as synchronous teaching, asynchronous teaching, teacher-led learning, and students' independent learning and practice [24, 25].

4.4. Education Resource Sharing Platform. The regional university sports network education resources sharing platform is a comprehensive information sharing platform to realize the common construction and sharing of regional university sports network education resources, so as to

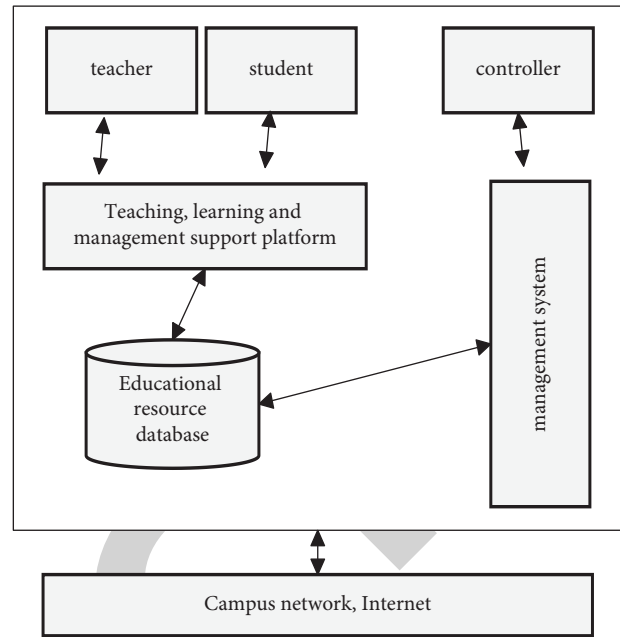


FIGURE 3: The architecture of university sports network education resources.

promote the unified management of regional sports network education resources, make modern education technology and sports humanities highly combined, and finally realize the regional university sports network education resources. On the basis of full sharing, this platform also has the characteristics of networking, intelligence, and multimedia, and the most applied educational technology is mostly inclined to technology, with less embodiment of human personality, so the platform should follow reasonable design specifications and follow the principles of scalability, practicality, unity, security, and reliability.

The sports network education resource sharing platform is an open platform for human-computer interaction using computers as tools to handle sports venues, sports equipment, sports teaching, and sports library materials. Its most important feature is remote, two-way, real-time, and interactive. The web-based network teaching platform is relatively mature, and according to the requirements followed by the platform development and design, the sports network teaching platform is technically based on a three-layer B/S architecture that combines the ASP-based B/S module structure system with the web database system 3 (Figure 4).

Teaching resource platform, courseware platform, interaction platform, and management platform are the four subsystems of the sports network education resource sharing platform, and each module has its submodules.

- (1) Teaching resource platform: it mainly provides a self-help platform for learners to collect, organize, browse, and edit physical education resources, and students can improve physical education resources by themselves through this platform.

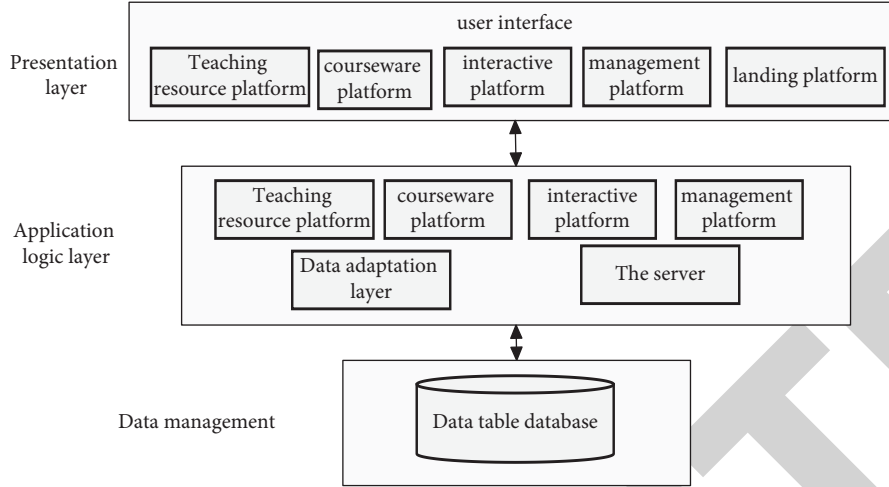


FIGURE 4: System structure of university sports network education resource sharing platform.

It includes self-help system of general physical education resources, self-help system of multimedia physical education resources, and mutual evaluation system of physical education resources.

- (2) Courseware platform: the courseware platform module contains sports network course management system, video system, and examination system. The module completes the setting of the curriculum and the release of the examination of motor skills mastery.
- (3) Interactive platform: it includes two parts: online communication system and question-answer system. Solve the problem of students learning motor skills in the process of interactive platform.
- (4) Management platform includes user management system and database management system. The main function of the subsystem is to set up the system as a whole and analyze the data management platform including user management system and database management system.

4.5. Machine Learning Algorithm: Support Vector Machine. Compared with neural networks and other traditional machine learning algorithms, support vector machines have fewer constraints and no “overfitting” defects, which are very suitable for modeling and prediction of small-sample, nonlinear college sports performance.

Let the sample set of college sports performance be $X = \{(x_1, y_1), (x_2, y_2), \dots, (x_n, y_n)\}, i = 1, 2, \dots, n$, and the support vector machine regression is specified as

$$f(x) = w \cdot \phi(x) + b, \quad (1)$$

where w, b are the parameters of the support vector machine.

To build a college sports performance prediction model, the most reasonable values of w, b must be found, and for this purpose, based on the principle of minimizing structural risk, they are transformed into the following form:

$$\min \frac{1}{2} \|w\|^2 + C \frac{1}{k} \sum_{i=1}^k \varepsilon (f(x_i) - y_i),$$

$$\text{s.t. } \varepsilon (f(x_i) - y_i), \quad (2)$$

$$= \begin{cases} |f(x_i) - y_i| - \varepsilon, & |w \cdot \phi(x) + b - y_i| \geq \varepsilon, \\ 0, & |w \cdot \phi(x) + b - y_i| < \varepsilon, \end{cases}$$

where ε is the regression error; C is the penalty parameter of the error.

In order to simplify the solution process and reduce the computational complexity of modeling, the relaxation factors $\varepsilon, \varepsilon^*$ are introduced, and the quadratic programming form is obtained as

$$\min_{w, b, \varepsilon, \varepsilon^*} \frac{1}{2} \|w\|^2 + C \sum_{i=1}^l (\xi_i + \xi_i^*),$$

$$\text{s.t. } \begin{cases} y_i - w \cdot \phi(x) - b \leq \varepsilon + \xi_i, & \xi_i \geq 0; i = 1, 2, \dots, n, \\ w \cdot \phi(x) + b - y_i \leq \varepsilon + \xi_i^*, & \xi_i^* \geq 0; i = 1, 2, \dots, n. \end{cases} \quad a_i^* \quad (3)$$

Using Lagrange multipliers a_i^*, a_i to further transform (3), we obtain

$$\min_{a_i^* \in \mathbb{R}^2} \frac{1}{2} \sum_{i,j=1}^n (a_i^* - a_i)(a_j^* - a_j) k(x_i, x_j) + \varepsilon \sum_{i=1}^n (a_i^* + a_i)$$

$$- \sum_{i=1}^n y_i (a_i^* - a_i), \quad (4)$$

where $k(x_i, x_j)$ denotes the kernel function.

The regression function of the support vector machine can be described as

$$f(x) = \sum_{i=1}^n (a_i - a_i^*) (\phi(X_i), \phi(X)) + b. \quad (5)$$

The RBF function is chosen as the kernel function, which is defined as

$$k(x_i, x_j) = \exp\left(-\frac{\|x_i - x_j\|^2}{2\sigma^2}\right), \quad (6)$$

where σ denotes the parameter of RBF.

4.6. Particle Swarm Algorithm. The current optimal solution of the particle swarm algorithm is $pbest$, the current optimal solution of the population is $gbest$, and the fitness function describing the degree of superiority and inferiority of individual particles is constructed as

$$\text{fitness} = \frac{1}{2N} \sum_{i=1}^N \sum_{j=1}^D (y_{ij} - t_{ij})^2. \quad (7)$$

x_{id}^k, v_{id}^k are the velocity and position of particle i at the k th iteration, and they are updated by

$$\begin{aligned} v_{id}^{k+1} &= \omega v_{id}^k + c_1 \text{Rand}(p_{id} - x_{id}^k) \\ &\quad + c_2 \text{Rand}(p_{\text{pbest}} - x_{id}^k), \\ x_{id}^{k+1} &= x_{id}^k + v_{id}^k, \end{aligned} \quad (8)$$

where c_1, c_2 are learning factors; Rand are random numbers; ω are inertia weights.

5. Simulation Verification

In the sports network education resource sharing platform, the information of entities directly related to the user's application logic, such as teacher information, sports network course information, sports competition information, and student information, needs to be stored in a database. Therefore, in the process of designing a sports network education resource sharing platform, database design plays a crucial role. A scientific and reasonable design can improve throughput speed and reduce network burden while ensuring data integrity. All information systems have a database management system to support them, and the university sports network education sharing platform is no exception, as shown in Figure 5.

There are many ways to access IoT educational resources, and due to the lack of unified standards, many IoT device providers use private protocols to connect with the Internet, so it is theoretically unrealistic to develop a program to support the access of various heterogeneous IoT resources. For this reason, we have adopted two ways to complete the access of various types of IoT educational resources. For IoT devices that can use HTTP protocol for transmission, we provide access to two standard data formats, JSON and XML. The data sender can send the conforming IoT resource packets to the server through HTTP-POST method, and the server then completes the data preservation through the

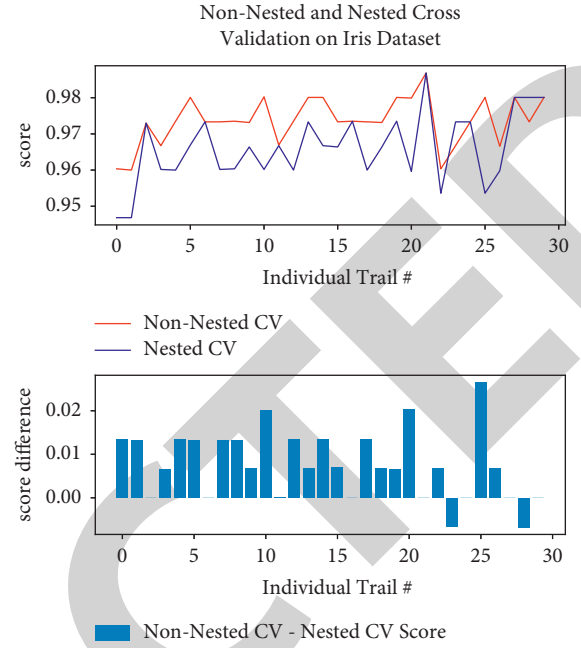


FIGURE 5: Platform test results.

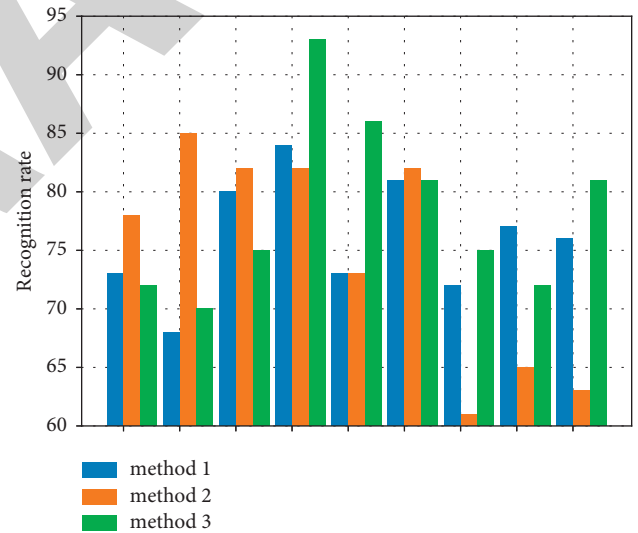


FIGURE 6: Recognition rate of different network actions.

following stages with different network recognition rates as shown in Figure 6.

For the data that cannot realize HTTP protocol by itself, we adopt the model of base SDK + specific access type developed separately. The reason why this approach is used is because I found that, no matter what kind of IoT resources are used to access the IoT educational resource library, the work to be done and its steps are the same. All need to go through the following stages: data reading: how to make the computer can get IoT data; this process may require the computer to take the initiative to get, and there may be a passive computer to receive. After the data reading is completed, the IoT data exists in the computer. IoT data

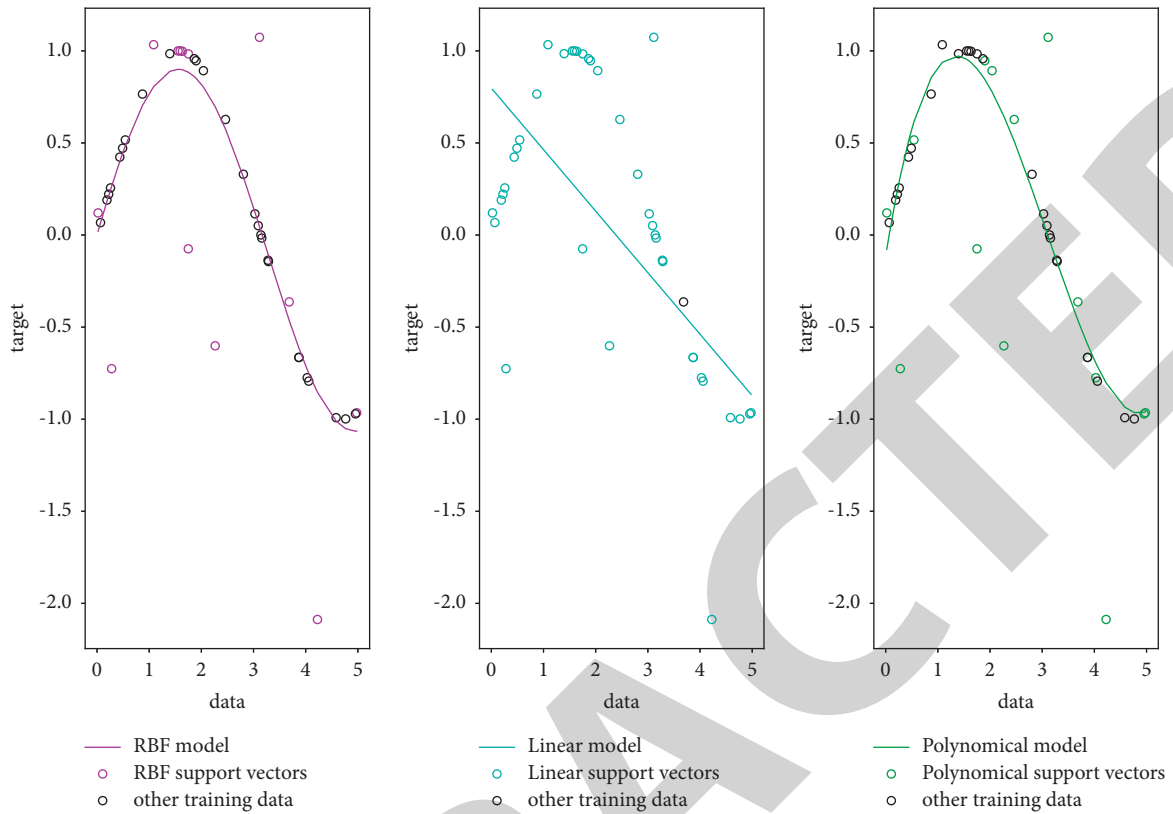


FIGURE 7: Data acceptance categorization effect.

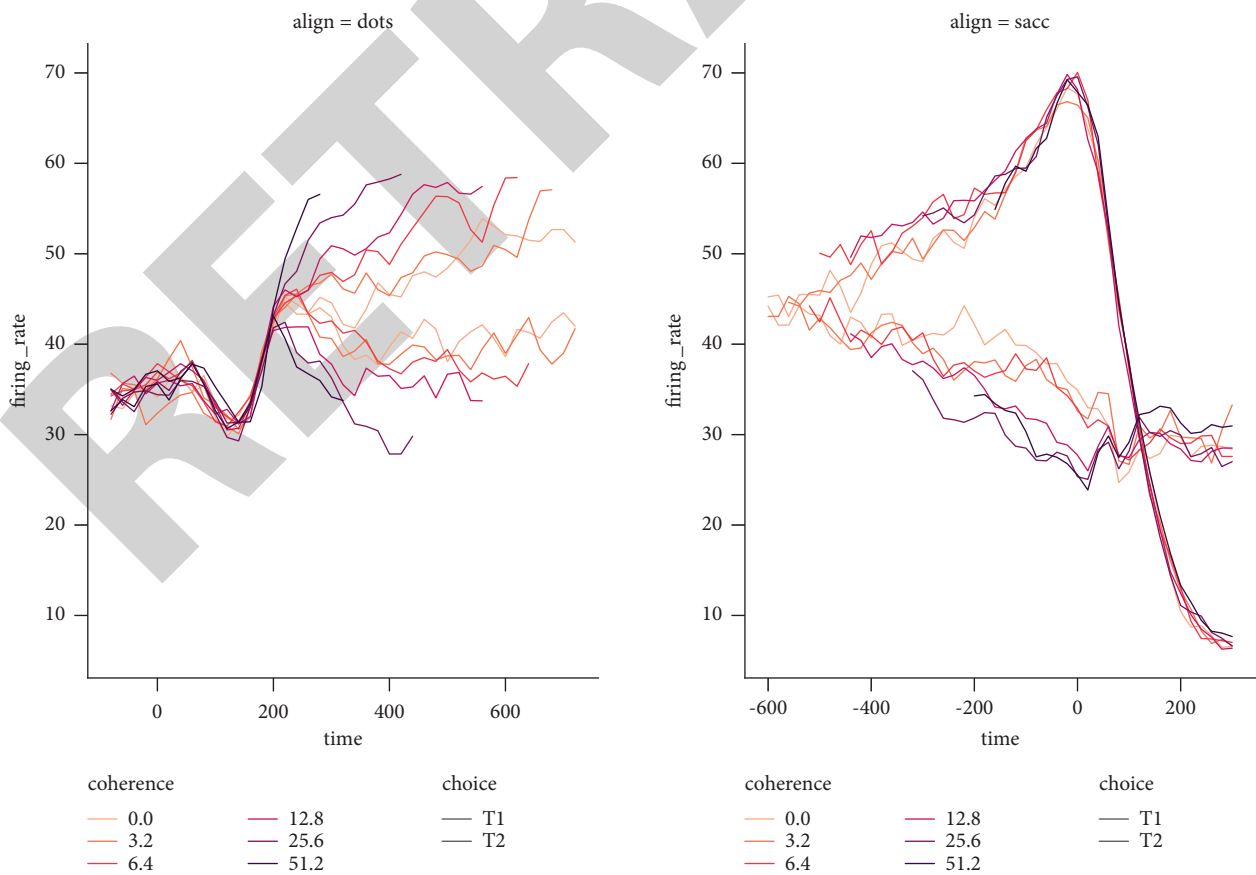


FIGURE 8: Effect of integration of different sports resources.

TABLE 1: The proportion of students at each category from 2016 to 2019.

Year	Excellent category (%)	Good class (%)	Pass (%)	Failing category (%)
2019	0.88	15.89	74.97	8.55
2018	1.05	16.77	72.32	9.99
2017	1.36	20.32	67.82	10.63
2016	0.97	19.87	69.22	10.15

TABLE 2: Algorithm performance comparison table.

Evaluating indicator	Literature 13	Literature 16	Literature 17	Our algorithm
AUC	0.707	0.712	0.762	0.854
Running time (s)	0.995	0.874	1.23	1.854

exists in the computer, accepting the data categorization effect as shown in Figure 7.

The data entering the computer may be meaningless binary, two bytes of which represents temperature information and two bytes represents humidity information, so we must get the parsed data with the help of parsing rules. The parsed data, though representing a certain physical quantity, is not necessarily understood by the user, so it needs to be converted into data that can be understood by the user through the corresponding data and formula. Considering the technical characteristics of IoT, it is often that the same data is read several times or wrong data is read, and the application must filter out invalid data as much as possible; of course, complete filtering is impossible. The effect of sports resource integration is shown in Figure 8.

As can be seen from Figure 8, only the data reading work is related to the IoT access method, so we encapsulate other functions into the SDK way. Users can carry out a small amount of development and can complete a certain type of IoT resources access; of course, the system has come with a variety of IoT resources access, such as the common RTU way and serial port way. At the same time, the resource library provides open data query interface, and users can request through HTTP-POST, so that the resource library to return to the IoT education resources data is presented in JSON or XML format. The proportion of the number of students in each category was calculated for each year to observe the overall distribution of students' physical fitness in the school, as shown in Table 1.

As shown in Table 1, only 1% of the students were classified as "Proficient" each year. The percentage of students in the "Failing" category found that 10% of students did not reach the pass mark in recent years. The percentage of students in the "Good" category was nearly 20%. In contrast, the percentage of students in the "Excellent" and "Good" categories increased significantly in 2017 compared to 2016, and the percentage of students in the "Excellent" category was the highest in recent years. In the "Good" category, the percentage of students in 2017 is still the highest. In the "Pass" category, 2019 has the highest percentage of students and it is clear that the passing rate of students in 2019 has increased, while the percentage of "Failing" category has decreased by 1.54%. The physical quality of these two categories of students is significantly

lower than the normal level of health, if not timely adjustment, will have a great impact on their lives and studies. To reduce the failure rate and to improve the physical quality of students are the original intention of every university and every physical education teacher to carry out teaching.

The performance comparison of different methods is shown in Table 2.

6. Conclusion

In this paper, the construction contents of college sports network education resources sharing mechanism are proposed: the construction of college sports network education resources, the sharing platform of college sports network education resources, and the management and coordination of college sports network education resources sharing. The guarantee of the sharing of Koranic sports Koranic network education resource was guided by control theory. The development prospect of the sharing mechanism of college sports network education resources was also analyzed.

Data Availability

The experimental data used to support the findings of this study are available from the corresponding author upon request.

Conflicts of Interest

The author declares no conflicts of interest regarding this work.

References

- [1] A. MacPhail and J. Halbert, "We had to do intelligent thinking during recent PE": students' and teachers' experiences of assessment for learning in post-primary physical education," *Assessment in Education: Principles, Policy & Practice*, vol. 17, no. 1, pp. 23–39, 2010.
- [2] A. E. Staiano and S. L. Calvert, "Exergames for physical education courses: physical, social, and cognitive benefits," *Child development perspectives*, vol. 5, no. 2, pp. 93–98, 2011.
- [3] A. M. Trad, K. A. Richards, and W. J. Wilson, "Strategies to increase self-, student, and discipline advocacy in adapted physical education," *Teaching Exceptional Children*, vol. 54, no. 1, pp. 52–62, 2021.

Retraction

Retracted: Power Allocation Intelligent Optimization for Mobile NOMA Communication System

Journal of Advanced Transportation

Received 8 August 2023; Accepted 8 August 2023; Published 9 August 2023

Copyright © 2023 Journal of Advanced Transportation. This is an open access article distributed under the Creative Commons Attribution License, which permits unrestricted use, distribution, and reproduction in any medium, provided the original work is properly cited.

This article has been retracted by Hindawi following an investigation undertaken by the publisher [1]. This investigation has uncovered evidence of one or more of the following indicators of systematic manipulation of the publication process:

- (1) Discrepancies in scope
- (2) Discrepancies in the description of the research reported
- (3) Discrepancies between the availability of data and the research described
- (4) Inappropriate citations
- (5) Incoherent, meaningless and/or irrelevant content included in the article
- (6) Peer-review manipulation

The presence of these indicators undermines our confidence in the integrity of the article's content and we cannot, therefore, vouch for its reliability. Please note that this notice is intended solely to alert readers that the content of this article is unreliable. We have not investigated whether authors were aware of or involved in the systematic manipulation of the publication process.

Wiley and Hindawi regrets that the usual quality checks did not identify these issues before publication and have since put additional measures in place to safeguard research integrity.

We wish to credit our own Research Integrity and Research Publishing teams and anonymous and named external researchers and research integrity experts for contributing to this investigation.

The corresponding author, as the representative of all authors, has been given the opportunity to register their agreement or disagreement to this retraction. We have kept a record of any response received.

References

- [1] X. Fu, Z. Tang, and P. Xiao, "Power Allocation Intelligent Optimization for Mobile NOMA Communication System," *Journal of Advanced Transportation*, vol. 2022, Article ID 5838186, 6 pages, 2022.

Research Article

Power Allocation Intelligent Optimization for Mobile NOMA Communication System

Xiaobin Fu , Zhen Tang , and Pingping Xiao 

College of Physical Science and Engineering, Yichun University, Yichun 336000, Jiangxi, China

Correspondence should be addressed to Xiaobin Fu; fxb8508457@163.com

Received 16 March 2022; Revised 17 April 2022; Accepted 26 April 2022; Published 10 May 2022

Academic Editor: Li Feng

Copyright © 2022 Xiaobin Fu et al. This is an open access article distributed under the Creative Commons Attribution License, which permits unrestricted use, distribution, and reproduction in any medium, provided the original work is properly cited.

Non-orthogonal multiple access (NOMA) technology can greatly improve user access and spectral efficiency. This paper considers the power allocation optimization problem of a two-user mobile NOMA communication system. Firstly, a mobile NOMA communication system model is established. Then, we analyze the outage probability (OP) of mobile NOMA communication system and the relationship between OP performance and user power allocation coefficient. Finally, the optimization objective function is established, and a power allocation optimization algorithm employing monarch butterfly optimization (MBO) is proposed. Compared with firefly algorithm and artificial fish swarm algorithm, the efficiency of MBO algorithm is increased by 20.7%, which can better improve the OP performance.

1. Introduction

Recently, the number of mobile users has increased rapidly. With the rapid growth of wireless communication data, the available spectrum becomes more and more crowded, and the space in the electromagnetic spectrum will become more and more scarce [1]. To meet the high-quality communication and large-scale user access, 5G mobile communication technology has attracted extensive attention [2]. 5G mobile communication technology has been rapidly popularized with ultrahigh bandwidth, ultralarge capacity, ultralow delay, and ultraslow energy consumption, which has brought far-reaching impact and change to people's life, work, and national economic development [3, 4].

Non-orthogonal multiple access (NOMA) technology has good fairness and considerable spectral efficiency, and it is regarded as a key technology of 5G mobile communication [5–7]. A novel deep learning method was proposed to cut down the computation complexity of NOMA multiuser detection in [8]. In [9], a multiagent deep learning method was proposed to solve the complex NOMA optimization problem, which considered user fairness and decoding complexity. The authors in [10] proposed a trusted NOMA model and maximized the secure rate at the near user by

using KKT conditions. To improve the NOMA system performance, the authors in [11] proposed a joint queue-aware and channel-aware scheduling to reduce traffic delay.

Power allocation can improve the NOMA performance in [12–14]. The authors in [15] constructed a multicarrier NOMA system and proposed a power allocation algorithm to reduce computational complexity. In [16], considering an unmanned aerial vehicle (UAV)-assisted NOMA system, user grouping and power allocation were used to reduce the relative distance between users and UAV. The authors in [17] obtained the error probability to fairly allocate power to different users of the NOMA system. Considering vehicle mobility, the authors in [18] proposed a sequence-based power allocation algorithm for NOMA UAV-aided vehicular platooning. However, there are some problems in these schemes, such as large amount of calculation, poor energy efficiency performance, insufficient power utilization, and unable to balance the fairness and service quality of users.

In order to obtain the best power allocation coefficient, the swarm intelligence optimization algorithm has been widely used in [19, 20]. In [21], artificial fish swarm algorithm (AFSA) optimized a wireless sensor network coverage problem, which can reduce the energy consumption. With simplified propagation and firefly algorithm (FA), an

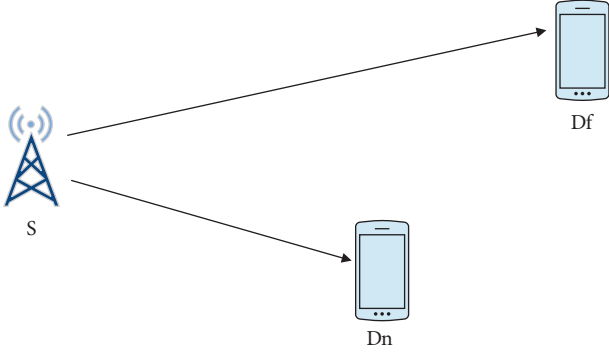


FIGURE 1: System model.

improved power point tracking algorithm was proposed in [22]. An improved cuckoo search algorithm was proposed to optimize the mobile outage probability (OP) prediction in [23]. However, these algorithms still have some shortcomings, such as low discovery rate, slow solution speed, and low solution accuracy.

Therefore, we investigate the mobile power allocation optimization. The main contributions of this paper are as follows:

- (1) A mobile NOMA communication system model is established. For ideal communication conditions, we derive the exact expressions for OP and analyze the relationship between OP and power allocation coefficient.
- (2) Considering the system efficiency and user fairness, we have established the optimization objective function. Employing monarch butterfly optimization (MBO), an intelligent optimization algorithm is proposed. MBO can reduce the computing parameters. The power allocation optimization algorithm employing MBO has good convergence performance and optimization performance.
- (3) Compared with FA and AFSA, the MBO algorithm can obtain the shortest time, which is 18.7063s, while AFSA is 48.9128s, and FA is 23.6096s. The efficiency of MBO is increased by 20.7%, which can better improve the OP performance of the mobile NOMA system.

2. System Model

Figure 1 is the mobile NOMA communication system. The system is composed of a source S, a far user Df, and a near user Dn. h_i represents the channel gains of $S \rightarrow Df$ and $S \rightarrow Dn$, $i = \{S Dn, S Df\}$. h_i is expressed as follows [24]:

$$h = \prod_{t=1}^N a_t, \quad (1)$$

where a_i is a Nakagami variable.

S transmits $\sqrt{a_1 P_s} x_1 + \sqrt{a_2 P_s} x_2$ to Df and Dn. P_s is the transmission power. a_1 and a_2 are power allocation coefficients of Df and Dn, respectively. $a_1 + a_2 = 1$, and $a_1 > a_2$.

The signals received at Df and Dn are as follows [25, 26]:

$$\begin{aligned} y_{Df} &= h_{SDf} (\sqrt{a_1 P_s} x_1 + \sqrt{a_2 P_s} x_2 + \eta_{SDf}) + v_{SDf}, \\ y_{Dn} &= h_{SDn} (\sqrt{a_1 P_s} x_1 + \sqrt{a_2 P_s} x_2 + \eta_{SDn}) + v_{SDn}, \end{aligned} \quad (2)$$

where v_{SDf} and v_{SDn} are AWGN of Df and Dn, respectively, and η_{SDf} and η_{SDn} are the distortion noise from the transmitter.

The signal-to-interference noise ratios of Df and Dn are as follows [25, 26]:

$$\begin{aligned} \gamma_{SDn} &= \frac{|h_{SDn}|^2 a_2 \gamma}{|h_{SDn}|^2 \gamma + \gamma + 1}, \\ \gamma_{SDf} &= \frac{|h_{SDf}|^2 a_1 \gamma}{|h_{SDf}|^2 a_2 \gamma + \gamma + 1}, \\ \gamma_{SDf} &= \frac{|h_{SDf}|^2 a_1 \gamma}{|h_{SDf}|^2 a_2 \gamma + \gamma + 1}, \end{aligned} \quad (3)$$

where $\gamma = P_s/N_0$ is the transmit signal-to-noise (SNR) ratio at S.

3. OP Performance Analysis

3.1. *OP of Df.* The OP of Df is expressed as

$$\begin{aligned} \text{OP}_{Df} &= \Pr(\gamma_{SDf} < \gamma_{\text{thf}}) \\ &= \Pr\left(\frac{|h_{SDf}|^2 a_1 \gamma}{|h_{SDf}|^2 a_2 \gamma + \gamma + 1} < \gamma_{\text{thf}}\right) \\ &= \Pr\left(|h_{SDf}|^2 < \frac{[\gamma + 1]\gamma_{\text{thf}}}{a_1 \gamma - a_2 \gamma \gamma_{\text{thf}}}\right) \\ &= \int_0^{[\gamma+1]\gamma_{\text{thf}}/a_1\gamma - a_2\gamma\gamma_{\text{thf}}} f_{|h_{SDf}|^2}(y) dy \\ &= F_{|h_{SDf}|^2}(y) \Big|_0^{[\gamma+1]\gamma_{\text{thf}}/a_1\gamma - a_2\gamma\gamma_{\text{thf}}} \\ &= G_{1,3}^{2,1}\left[\frac{[\gamma + 1]\gamma_{\text{thf}}}{a_1 \gamma - a_2 \gamma \gamma_{\text{thf}}} \Big|_{1, \dots, 1, 0}\right], \end{aligned} \quad (4)$$

where γ_{thf} is the interrupt threshold of Df.

3.2. *OP of Dn.* The OP of Dn is given as

$$\begin{aligned} \text{OP}_{Dn} &= \Pr(\gamma_{SDf} \rightarrow n < \gamma_{\text{thf}}, \gamma_{SDn} < \gamma_{\text{thn}}) \\ &= \Pr\left(|h_{SDn}|^2 < \frac{[\gamma + 1]\gamma_{\text{thf}}}{a_1 \gamma - a_2 \gamma \gamma_{\text{thf}}}, |h_{SDn}|^2 < \frac{[\gamma + 1]\gamma_{\text{thn}}}{a_2 \gamma - \gamma \gamma_{\text{thn}}}\right), \end{aligned} \quad (5)$$

where γ_{thn} is the interrupt threshold of Dn.

To simplify the integration process, we define the following variables:

$$\begin{aligned}\tau_1 &= \frac{[\gamma + 1]\gamma_{\text{thf}}}{a_1\gamma - a_2\gamma\gamma_{\text{thf}}}, \\ \tau_2 &= \frac{[\gamma + 1]\gamma_{\text{thn}}}{a_2\gamma - \gamma\gamma_{\text{thn}}}, \\ \tau &= \max(\tau_1, \tau_2).\end{aligned}\quad (6)$$

Bringing the above variables into (11), we obtain that

$$\begin{aligned}\text{OP}_{\text{Dn}} &= \Pr(|h_{\text{SDn}}|^2 < \tau_1, |h_{\text{SDn}}|^2 < \tau_2) \\ &= \Pr(|h_{\text{SDn}}|^2 < \max(\tau_1, \tau_2)) \\ &= \Pr(|h_{\text{SDn}}|^2 < \tau) \\ &= F_{|h_{\text{SDn}}|^2}(\tau)|_0^r \\ &= G_{1,3}^{2,1}[\tau_{1,\dots,1,0}^1].\end{aligned}\quad (7)$$

4. Intelligent Power Allocation Optimization Employing MBO Algorithm

Here, we employ the MBO algorithm to optimize the mobile power allocation.

4.1. Optimization Objective Function. To achieve high efficiency and user fairness, we should ensure $\min|\text{OP}_{\text{Df}} + \text{OP}_{\text{Dn}}|$ and $\min|\text{OP}_{\text{Df}} - \text{OP}_{\text{Dn}}|$. Therefore, the optimization objective function is

$$\min \left(\begin{array}{l} G_{1,3}^{2,1} \left[\frac{(\gamma+1)\gamma_{\text{thf}}}{a_1\gamma - a_2\gamma\gamma_{\text{thf}}} \right]_{1,\dots,1,0}^1 + G_{1,3}^{2,1}[\tau_{1,\dots,1,0}^1] + \\ \left| G_{1,3}^{2,1} \left[\frac{(\gamma+1)\gamma_{\text{thf}}}{a_1\gamma - a_2\gamma\gamma_{\text{thf}}} \right]_{1,\dots,1,0}^1 - G_{1,3}^{2,1}[\tau_{1,\dots,1,0}^1] \right| \end{array} \right). \quad (8)$$

4.2. MBO Intelligent Optimization Algorithm. Therefore, employing the MBO algorithm, an intelligent power allocation optimization algorithm is proposed. In [27], it presents the MBO algorithm.

4.2.1. Population Initialization. The number of the monarch butterfly population is N . The number of iterations is MaxGen , and the adjustment rate is BAR .

4.2.2. Fitness Evaluation. The fitness value of each monarch butterfly individual is calculated and sorted. The sorted population is divided into two subpopulations NP_1 and NP_2 , respectively. They have N_1 and N_2 individuals, respectively.

4.2.3. New Subpopulation Generation. At the current iteration t , the NP_1 and NP_2 generate two new subpopulations, respectively. For NP_1 , it uses the migration operator to generate a new subpopulation, which is expressed as follows:

TABLE 1: Simulation parameters.

Parameter	Value
K	0
σ	0
M	1, 2, 3, 4
N	1, 2, 3, 4

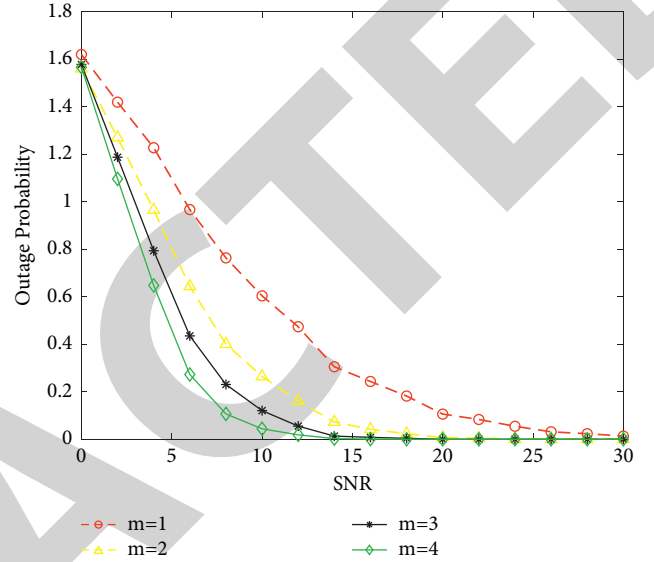


FIGURE 2: The OP performance with different (m).

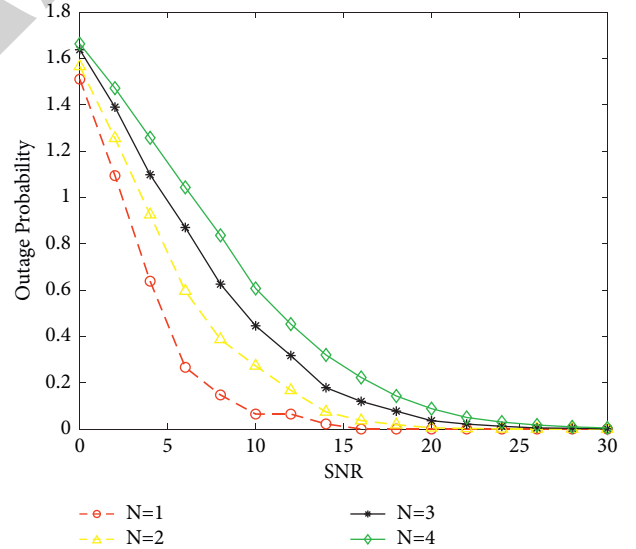


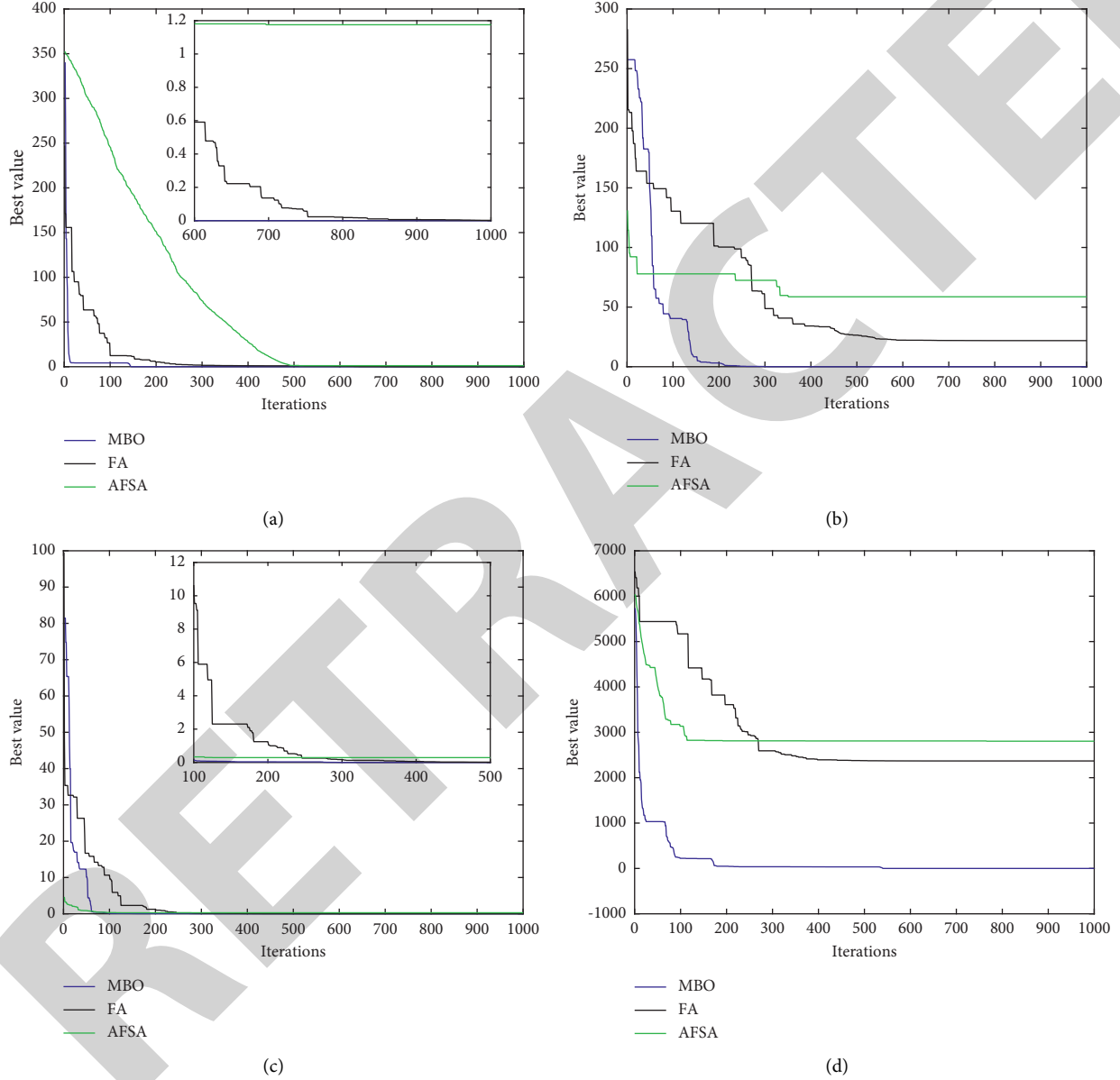
FIGURE 3: The OP performance with different (N).

$$\begin{cases} x_{i,k}^{t+1} = x_{r_1,k}^t, & r \leq p, \\ x_{i,k}^{t+1} = x_{r_2,k}^t, & \text{else,} \end{cases} \quad (9)$$

where x_{r_1} and x_{r_2} represent the k th element of r_1 and r_2 that is the newly generated position of r_1 and r_2 , respectively. r_1 and r_2 are randomly selected from NP_1 and NP_2 , respectively. r is a random number.

TABLE 2: Four test functions.

	Function	Ranges	Dimension
Griewank	$F1 = \sum_{i=1}^d x_i^2/4000 - \prod_{i=1}^d \cos(x_i/\sqrt{i}) + 1$	[-600, 600]	20
Rastrigin	$F2 = 10d + \sum_{i=1}^d [x_i^2 - 10 \cos(2\pi x_i)]$	[-5.12, 5.12]	20
Sphere	$F3 = \sum_{i=1}^d x_i^2$	[-500, 500]	20
Schwefel	$F4 = 418.9828d - \sum_{i=1}^d x_i \sin(\sqrt{ x_i })$	[-500, 500]	20

FIGURE 4: The convergence performance of different algorithms on F_1 - F_4 . (a) F_1 . (b) F_2 . (c) F_3 . (d) F_4 .

For NP_2 , it uses the adjustment operator to generate a new subpopulation, which is expressed as follows:

$$\begin{cases} x_{i,k}^{t+1} = x_{\text{best},k}^t, & r \leq p, \\ x_{i,k}^{t+1} = x_{r_3,k}^t, & \text{else,} \end{cases} \quad (10)$$

where x_{best} represents the position of the globally optimal individual and x_{r_3} represents the location of r_3 , which is randomly selected from NP_2 .

$rand$ is between $[0, 1]$. If $rand > BAR$, NP_2 updates $x_{i,k}^{t+1}$ again. The process is as follows:

$$\begin{cases} x_{i,k}^{t+1} = x_{i,k}^t + \beta * (dx_k - 0.5), \\ dx = \text{Levy}(x_i^{t+1}), \end{cases} \quad (11)$$

where β is the weight factor and dx represents the step size which is calculated by the Levy function.

TABLE 3: Simulation parameters for power allocation.

Parameter	Value
Iteration	1000
Population number	100
Dimension	1
Range	[0.5, 0.9]

TABLE 4: Power allocation optimization comparison.

	Optimal power allocation coefficient	Time (s)
MBO	0.56768	18.7063
FA	0.56768	23.6096
AFSA	0.56768	48.9128

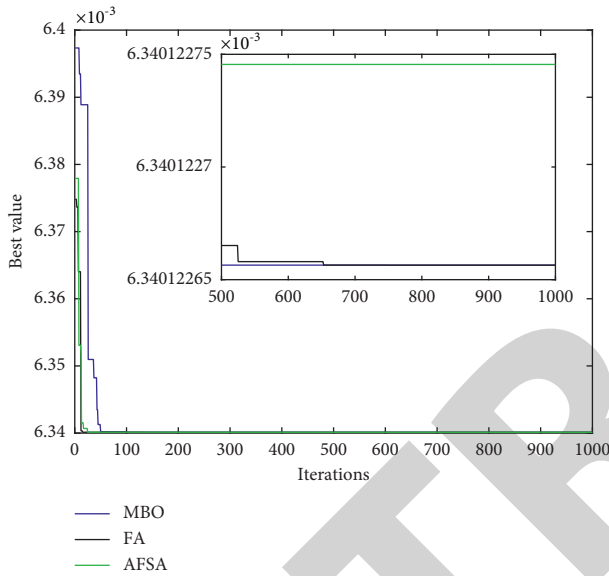


FIGURE 5: The iterative optimization process of the three algorithms.

4.2.4. New Subpopulation Merge. It merges the two newly generated subpopulations and calculates the fitness of the new population. Repeat above process, and when the number of iterations reaches $MaxGen$, the best solution is obtained.

5. Performance Analysis

This section will analyze the OP performance and optimize the power allocation using MBO, AFSA, and FA algorithms.

Table 1 gives the simulation parameters. For the ideal case, the residual hardware impairment $k=0$, and the incomplete channel state information $\sigma=0$. Figure 2 shows the OP performance with different m . From Figure 2, when the power allocation coefficient is constant, the system OP performance becomes better with the increase in SNR and m . The OP performance with different N is shown in Figure 3. As N is decreased, it can minimize the system OP.

We select four test functions, which are shown in Table 2. Figure 4 shows the convergence performance of different algorithms. For F_1 – F_4 functions, the MBO is the best.

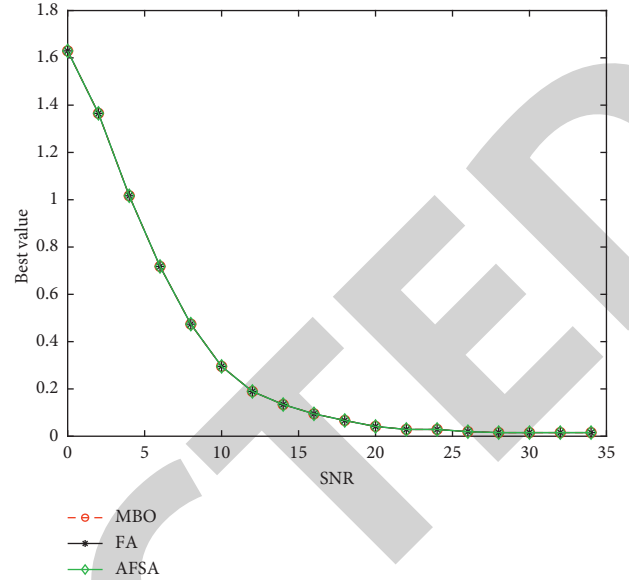


FIGURE 6: System performance comparison of the three algorithms.

Next, the power allocation will be optimized by MBO, FA, and AFSA. Table 3 shows the simulation parameters for power allocation. Table 4 shows the power allocation optimization comparison of MBO, FA, and AFSA algorithms. Compared with FA, MBO has a 20.7% decrease. The iterative optimization process of the MBO, FA, and AFSA algorithms is shown in Figure 5.

The system performance comparison of the MBO, FA, and AFSA algorithms is shown in Figure 6. From Figure 6, the performance of the MBO algorithm is good, which is the same as FA and AFSA algorithms. However, the MBO algorithm has a low complexity.

6. Conclusion

This paper studies the power allocation optimization for the mobile NOMA communication system. Firstly, the mobile NOMA model is built, and the OP expressions for D_f and D_n are derived. Then, the optimization objective function is established, and a power allocation optimization algorithm is proposed. Finally, it can obtain the best power allocation coefficient. The efficiency of the MBO algorithm is improved by 20.7%.

Data Availability

The data used to support the findings of this study are available from the corresponding author upon reasonable request and with permission of funders.

Conflicts of Interest

The authors declare that they have no conflicts of interest.

Acknowledgments

This project was supported by the National Natural Science Foundation of China (No. 11664043).